THE INTERACTION OF HELIUM METASTABLE ATOMS WITH METAL SURFACES

by

P. D. JOHNSON B.Sc.

A Thesis
Submitted for the Degree of
Doctor of Philosophy
of the
University of Warwick

March 1978

MEMORANDUM

The work reported in this Thesis was performed by myself, except where specifically acknowledged as otherwise in the text, in the Department of Physics of the University of Warwick. Parts of Chapter 3 have been published in J. Phys. E 10, 431 (1977) and it is intended to publish much of the contents of the final chapters shortly. For convenience, the references cited in each chapter have been listed at the end of each chapter rather than at the end of the Thesis.

[redacted]

PETER D. JOHNSON

ACKNOWLEDGEMENTS

I would like to express my thanks to my supervisor Dr. T. A. Delchar for introducing me to the subject of metastable atoms and for his interest during the course of the work. I would also like to thank Professor A. J. Forty for the provision of facilities within the Department of Physics.

I am particularly indebted to Dr. D.P. Woodruff both for valuable discussions on the subject of metal surfaces in general and for his patience and understanding during the latter half of this work. I must also acknowledge the help of the many members of the Surface Physics Group, past and present, but in particular Drs. L. McDonnell and M. A. Byrne for their advice on experimental matters. I should also like to thank the many physicists, both in the Warwick Department and elsewhere who have given their time to discuss the problems described in this Thesis. Dr. H. D. Hagstrum is thanked for many stimulating discussions and his comments on the conclusions of this Thesis. In addition, I am indebted to Mr. O. S. Simpson for his excellent technical support and encouragement.

The provision of a maintenance grant by the Science Research Council during the period of this work is also gratefully acknowledged.

I would like to thank Val Mason for her careful typing of this Thesis. Finally I would like thank my parents for their continued support and Julia for her encouragement and invaluable advice in the proof reading of this Thesis.

ABSTRACT

An investigation has been made of the interaction of helium metastable atoms (2^3S and 2^1S) with metal surfaces in different degrees of contamination. In order to carry out this investigation, an ultra-high vacuum chamber has been constructed enabling the operator to clean the metal surfaces in situ, monitor the state of cleanliness of the surfaces with Auger electron spectroscopy and then perform experiments with a beam of metastable atoms. A new metastable atom source has been built to produce a reasonably intense beam of atoms in the metastable states.

Experiments have been performed on a clean Ni (100) surface and this surface with adsorbed sulphur and oxygen. Further experiments have been performed on a polycrystalline tungsten surface both in the clean state and with adsorbed carbon monoxide. Secondary electron energy distributions resulting from the impact of excited atoms on these surfaces show little agreement with the results to be expected on the basis of presently accepted theories. It is found that, in general, the total yield of secondary electrons increases linearly with coverage.

Extensive comparisons have been made between the experiments reported in this thesis and the results from INS and other experiments with metastable atoms. These comparisons lead to the conclusion that the interaction of an ion and that of an excited atom with metal surfaces are two different processes. A new model for the de-excitation of the excited atom has been suggested and the results to be expected from such a de-excitation mechanism examined.

CONTENTS

INTRODUCTION

The last two decades have seen a vast increase in the amount of research devoted to the study of solid surfaces. Such an increase is clearly justified, since such problems as heterogeneous catalysis and corrosion, the workings of many solid state electronic devices and certain biological systems will only be grasped in a fundamental way if basic surface phenomena are understood.

Following the development of improved vacuum techniques many new experimental tools have been devised for the investigation of surface phenomena. To characterize a surface it is necessary to specify (i) the chemical identity of the atoms present, (ii) the geometrical or structural arrangement of the atoms, and (iii) the energy structure of their outermost or valence electrons. The principal means for the chemical identification of the surface atoms now in use is Auger Electron Spectroscopy (AES). This method makes use of the fact that electrons are ejected from the surface as the atoms relax following ionization of their core electrons. These ejected electrons have characteristic energies dependent on core level energies and thus on chemical identity. The symmetry of surface structures is determined from the symmetry of diffracted electron beams observed by the technique of Low Energy Electron Diffraction (LEED). Specific atom positions were first determined by detailed examination of the variation of the intensity of diffracted electron beams with the

energy or wavelength of the incident electrons. However, a better understanding of other experimental techniques is now adding to the accumulated information in this area. The third basic characterization, the energy level structure of the electrons in the surface atoms, is currently the subject of three experimental methods.

These three electron spectroscopies all rely on the measurement of the kinetic energy distributions of electrons ejected from the surface as a result of some emission process. The energy of the emitted electrons determines the final state energy of the transition by means of which the electron was excited; further, surface specificity is enhanced by limitations on the mean free path of the unscattered electrons. Energy level diagrams characterizing these spectroscopies are shown in fig. 1. The first is Field Emission Spectroscopy where the electrons are made to tunnel from the filled band of the solid through a peaked barrier into the vacuum. The barrier is produced by the application of a strong electric field at the surface of the specimen which is in the form of a sharp point. This spectroscopy is extremely surface sensitive as all observed electrons must tunnel through the surface. Resonances in the density of states resulting from adsorption of various atoms on the surface have been shown to have a strong effect on the tunnelling probability as a function of energy, and consequently the method has been used to study several adsorption systems. However the

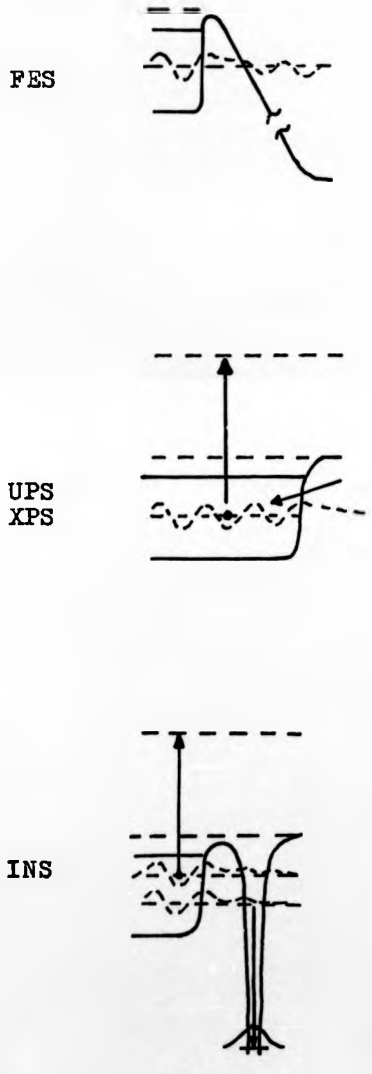

FIG. 1

Energy level diagrams of three electron spectroscopies applied to the determination of energy level structure at solid surfaces.

major disadvantage of this technique is that it is possible to examine the density of states only to a level approximately 3eV below the Fermi level.

The second spectroscopy is based on the photoemission process. A photon is absorbed by an electron which is excited to a higher energy level, escaping from the solid if it is produced sufficiently close to the surface. If the photon is in the ultraviolet frequency range the Spectroscopy is called Ultraviolet Photoelectron Spectroscopy (UPS); if in the x-ray range, X-ray Photoelectron Spectroscopy (XPS) or Electron Spectroscopy for chemical analysis (ESCA). With XPS it is possible to explore the core energy levels as well as the valence levels. The photoemission spectroscopies have the advantage of ease of use, and further, the increasing use of Synchrotron radiation as the source of photons is leading to a fully tunable source, enabling excitation from a wide range of energy states. Recent years have seen a large amount of effort devoted to gaining an understanding of the angular distribution of the emitted photoelectrons and this is now adding to the amount of information to be obtained from this technique.

The final electron spectroscopy is based on the neutralization of slow ions incident on the surface and as such is referred to as Ion Neutralization Spectroscopy (INS). Unlike the previous spectroscopies INS is based on an electronic transition in which two electrons participate. One electron from the solid tunnels through

the barrier between surface and ion and drops into the ground atomic state. In a radiationless process of the Auger type, a second electron accepts the energy released in this downward transition and may escape from the solid if properly directed. The two-electron character of this neutralization process causes the measured kinetic energy distribution of the ejected electrons to reflect the integral self-convolution of the local density of states function, a feature which leads to complications in the data reduction. However whilst INS presents considerable deconvolution problems it is known to be extremely surface sensitive and by using helium ions it is possible to explore the density of states to a depth of 10eV below the Fermi level.

The object of the work described in this thesis was to explore the possibility of developing an electron spectroscopy based on the interaction with metal surfaces of the metastable excited states of helium. In developing his theory of INS (discussed in chapter 1) Hagstrum postulated that there should be essentially no difference between electron ejection as a result of incident ions and ejection resulting from incident metastable atoms. The use of metastable atoms with thermal energies should have the advantage of giving less broadening in the resulting energy distribution of the ejected electrons, this being a problem encountered in INS.

Accordingly an ultra high vacuum system was constructed enabling an examination of the interaction of

metastable atoms with metal surfaces. This necessitated the design and construction of a source providing a high intensity of helium atoms excited to the 2^1S and 2^3S states. The vacuum system and source will be described in chapters 2 and 3. Experiments performed on clean surfaces and on the same surfaces following controlled contamination are described in chapters 4 and 5. In chapter 6 the results of these experiments are compared with the predictions of various different theories.

CHAPTER ONE

THE INTERACTION OF IONS AND EXCITED ATOMS WITH SOLID SURFACES

1.1 Introduction

In 1924 Webb[1] established that metastable atoms incident on a metal surface may eject secondary electrons by virtue of their potential energy. His work using metastable mercury atoms was extended by Coulliette[2] and later by Sonkin[3]; the latter author demonstrating that the nature of the surface played an important part in the ejection process. Oliphant[4] was the first to observe electron ejection from a metal surface by helium metastable atoms. He examined the effect of surface cleanliness and also the variation in the total yield of secondary electrons with the incident kinetic energy of the metastable atoms. However the poor vacuum conditions used in his experiments cast doubt on the validity of his results. Further work using helium metastable atoms was done by Greene[5], who also included incident neon and argon metastable atoms. Stebbings[6] measured the total electron yield resulting from helium metastable atoms striking a chemically cleaned gold surface. He concluded that his value of 0.29 electrons/atom was the yield for the triplet 2^3S metastable state. Hasted[7] measured yields for helium metastable atoms incident on tungsten, molybdenum and tantalum surfaces flashed to 1700°C. The latter author estimated his values by extrapolating the total yield, as a function of time after flashing the specimen, back to the yield from the hot surface. For all three

surfaces he found that the yield was higher when the surface was contaminated. This is in contrast to the later work of Maclennan[8], who measured the secondary emission coefficients for He (2^1S), He (2^3S) and Ne ($^3P_{0,2}$) metastable atoms incident on an atomically clean tungsten surface.

Maclennan and Delchar[9] extended Maclennan's earlier work by examining the role of the metal surface's work function in the ejection process. They also investigated the effect of adsorption of different gases on the metal surface. In a series of papers Dunning, Smith et al[10, 11, 12] have recently remeasured various secondary yields and also examined the energy and angular distributions of the ejected electrons. In their experiments they found that the yield of electrons was less from a cleaner surface.

Early theoretical treatments of the ejection of electrons by positive ions or metastable atoms considered several processes. Massey[13], Shekhter[14] and Cobas and Lamb[15] considered the electron ejection as Auger de-excitation of the excited atom. They further suggested that a positive ion would first be resonance neutralized forming an excited atom which would then de-excite with electron ejection. Shekhter also proposed and investigated theoretically the single stage Auger neutralization of an incident positive ion. Hagstrum [16, 17, 18] found a number of results which existing theory did not explain. In attempting to explain such results Hagstrum[19] developed a semi-quantitative theory and one of his conclusions was

that on an atomically clean surface slow rare gas metastable atoms and ions should exhibit the same electron yield.

1.2 Electronic Transitions for Ions and Excited Atoms Incident on a Surface.

Two reasonably distinct mechanisms exist for the ejection of electrons from a metal surface as a result of ion bombardment. At energies above an ill-defined threshold of several hundred eV, ions eject electrons by virtue of their kinetic energy. Momentum is transferred from the ion to the lattice atoms and subsequently to bound electrons. This ejection process is strongly dependent on the incident kinetic energy of the ion, in contrast to the mechanism for electron ejection at lower incident energies. For ions of lower kinetic energy and for excited atoms incident on a solid, four basic electronic transitions may be distinguished for electron ejection from the surface. These transitions are dependent on the potential energy of the incident particle and are

(1) Auger neutralization of an ion,

(2) Auger de-excitation of an excited atom,

(3) Resonance neutralization of an ion, and

(4) Resonance ionization of an atom.

It is also possible that the neutralization of an ion near a surface is accompanied by a radiative process. However Shekhter[14] demonstrated that the probability for such a process is very low (approximately 5×10^{-7}) as the characteristic radiative lifetimes, 10^{-8} sec, by far exceed the time spent by the ion in the vicinity of the surface, approximately 10^{-14} sec.

1.3 Auger Neutralization

In developing his theory of Ion Neutralization Spectroscopy Hagstrum[19] demonstrated that whilst a two-stage ejection process, resonance neutralization followed by Auger de-excitation, played a small part for slow incident noble gas ions of kinetic energy above 10eV, for ions of energy below 10eV Auger neutralization accounted for all ejected electrons. The electronic transition involved in the Auger neutralization process is shown schematically in fig. 1.1. It involves two electrons from the valence band of the metal; one electron neutralizes the incident ion directly to the ground state and a second electron absorbs the energy released in this transition. The second electron may then escape from the metal as a true secondary electron if it has sufficient energy to overcome the surface barrier. Theoretical treatments of this problem have been considered by Hagstrum[19] and by Propst[20], both using perturbative approaches and by Wenaas and Howsmon[21] who use quantum scattering theory.

Propst[20] considers the radiation field set up by the first electron as it falls to the ground state of the atom as the perturbation that excites the second metal electron. Hagstrum uses the Coulomb interaction of the two participating metal electrons as the perturbation. In the following discussion of the perturbative approach the more comprehensive treatment of Hagstrum will be followed.

Reference to fig.1.1 will show that the limiting kinetic energies of the emitted secondary electrons are

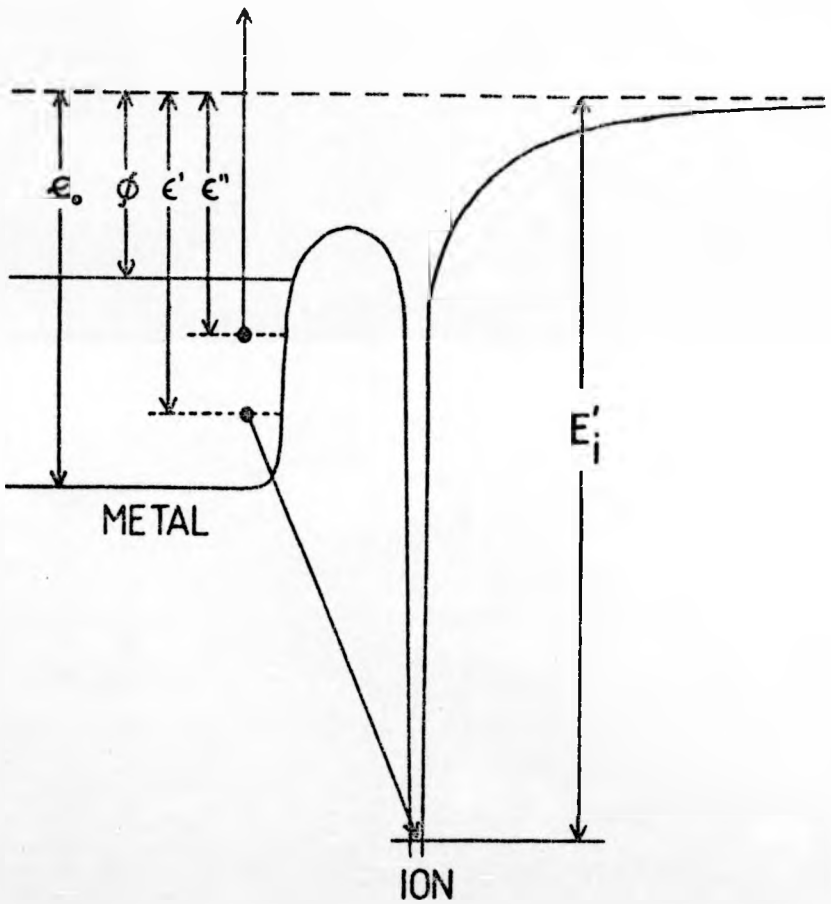

FIG. 1.1

AUGER NEUTRALIZATION

$$E(e^-)_{max} = E_i' - 2\phi$$
$$E(e^-)_{min} = E_i' - 2\epsilon_o \qquad (1)$$
$$= 0 \text{ if } E_i' < 2\epsilon_o$$

E_i' is the effective ionization energy of the incident ion near the surface, ϕ is the work function of the metal and ϵ_o is the energy difference between the vacuum level and the bottom of the valence band. It should be noted that $E_i' > 2\phi$ is necessary for the production of an external secondary electron. The energy of any secondary electron will be given by

$$E(e^-) = E_i' - \epsilon' - \epsilon'' \qquad (2)$$

where ϵ' and ϵ'' are the energies of the participating electrons with respect to the vacuum level.

The transition rate or transition probability per unit time for this process, which occurs when the ion is at a distance s from the surface and which results in an excited metal electron of energy ϵ_k with velocity vector lying in the element of solid angle $d\Omega$ is given by

$$P_x(s)d\Omega = \frac{2\pi}{\hbar} |H_{fi}|^2 \rho(E_t)d\Omega \qquad (3)$$

where $\rho(E_t)$ is the electron density of final states at total energy E_t and H_{fi} is the matrix element

$$H_{fi} = \iint U_f^*(\underline{r}_1)U_{He}^*(\underline{r}_2)\frac{e^2}{r_{12}}U_2(\underline{r}_2)U_1(\underline{r}_1)d\underline{r}_1 d\underline{r}_2 \qquad (4)$$

Here U_1 and U_2 are the initial state wavefunctions of the two electrons occupying bound states in the metal. The final state is one in which one of the electrons fills the vacant state U_{He} and the other is excited to a continuum state U_f. Both U_1 and U_2 extend into the

vacuum only to the extent that they have exponentially decaying tails. From physical considerations the helium ion is always constrained to remain in the vacuum. Thus the strength of the Auger decay depends on the overlap of the U_2 tail with U_{He}.

In their treatment Wenaas and Howsmon use quantum scattering theory and derive terms for the secondary electron energy distributions and total yield in terms of scattering matrix elements. The secondary electron energy distributions can be calculated using Fermi's Golden Rule of scattering theory; transition probabilities $|H_{fi}|^2$ are averaged over initial electron energy state densities and summed over final state densities

$$\eta_o(E_e, E_I) = \iiint \eta(E_m)\, \eta(E_m')\, |H_{fi}|^2\, \eta(E_e)\, \delta(E_f - E_i)\, dE_m\, dE_m'\, dE_e$$

In the above equation the integrals over electron and atom state energies are indicated while the integrals over direction are implied. $\eta_o(E_e, E_I)$ is the secondary electron energy distribution, $\eta(E_m)$ and $\eta(E_m')$ are the electron densities of occupied states, $\eta(E_e)$ is the electron density of unoccupied states and $\delta(E_f - E_i)$ contains terms for the unperturbed kinetic energies of the atom and ion as well as the two electrons.

The initial state energy which is evaluated when the ion and surface are widely separated is given by

$$E_i = E_I + E_m - \epsilon_o + E_{m'} - \epsilon_o + I \qquad (6)$$

where $E_m - \epsilon_o$ and $E_{m'} - \epsilon_o$ are the kinetic energies of the two electrons in the potential well ϵ_o of the metal (fig. 1.1), and E_I and I are respectively the kinetic

energy and ionization potential of the incident ion. The final state energy which is evaluated when the atom and surface are widely separated is given by

$$E_f = E_A + E_e \qquad (7)$$

where E_A is the kinetic energy of the reflected atom and E_e is the kinetic energy of the secondary electron. The total secondary yield is the integral of the distribution

$$\gamma = \int \eta(E_e, E_I) dE_e \qquad (8)$$

A typical secondary electron energy distribution from an ion neutralization experiment is shown in fig. 1.2. In this case it is that resulting from helium ions incident on a Ni(100) surface. In attempting to account for discrepancies between the theory and experiment, the shift and broadening of the secondary electron distribution, Hagstrum examined the effects of the image charge force, the energy level shifts of an atom or ion near a surface, and also the finite lifetimes of the initial and final states. To take account of the energy level shifts he introduced an effective ionization potential for the ion as it neared the surface. Hagstrum's conclusions that the image charge force and the energy level shifts play a direct role in the neutralization process are supported by Wenaas and Howsmon. However in the latter treatment the effects appear in the theory in a different way. The attraction of the ion is accompanied by shifts in the electronic structure of the ion and a difference in the kinetic energies of the incident and reflected particles. This change in the kinetic energy is thought to account for any shift or broadening in the resulting

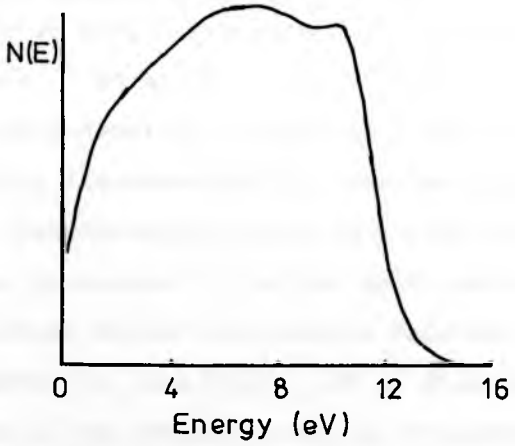

FIG. 1.2

Secondary electron energy distribution resulting from 5 eV helium ions incident on a Ni(100) surface.

secondary electron distribution. An alternative explanation for these effects is that of Propst, who suggests that a large number of low energy electrons are produced by inelastic electron collisions. However, the other authors argue that such a large amount of scattering would not be expected from a process as surface specific as Auger neutralization.

In order to obtain information about the density of states of the surface under observation, Hagstrum has developed a considerable mathematical procedure for analysing the secondary electron energy distributions of INS. His method involves two basic deconvolutions. First, a function $F(\epsilon)$, the final state transition density, is derived from an effective electron energy distribution for "zero velocity" ions obtained by "debroadening" measured energy distributions. This function is assumed to be the self convolution of the initial state transition density function $U(\epsilon)$ and is thus inverted to give $U(\epsilon)$. It is this function $U(\epsilon)$ which is to be compared with the transition density function of a one electron spectroscopy such as UPS.

1.4 Resonance Processes at Surfaces

The resonance processes are illustrated in fig. 1.3. If one considers the system comprising the incident ion A^+ and all of the metal electrons Ne_m^- the resonance neutralization process may be represented by

$$A^+ + Ne_m^- \rightarrow A^* + (N - 1)e_m^- \qquad (9)$$

where A^* is the excited atom formed and N is the total number of electrons in the metal. From fig. 1.3 it will

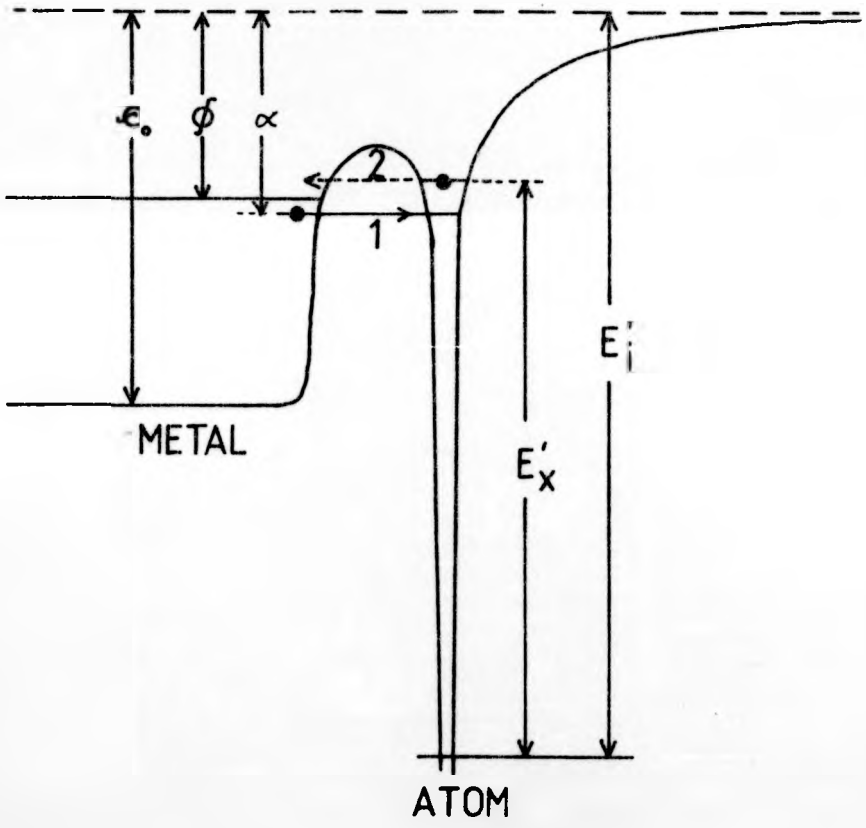

FIG. 1.3

The Resonance Processes

1) Neutralization
2) Ionization

be seen that the resonance neutralization process can occur only at energy levels which are filled inside the metal.

Resonance ionization may be represented by equation (9) reversed

$$A^* + Ne_m^- \rightarrow A^+ + (N+1)\, e_m^- \qquad (10)$$

This process will occur only at energy levels which are empty inside the metal.

In examining the energy level shifts for ions and atoms near a surface Hagstrum calculated the value of a parameter α where

$$\alpha = E_I' - E_x' \qquad (11)$$

at various distances from the surface. Here E_I' and E_x' are the effective ionization and excitation potentials of the atom near the surface. The results of his calculation for a He (2^3S) atom incident on a tungsten surface are shown in fig. 1.4. Examination of this figure shows that resonance ionization is possible only if

$$\alpha < \emptyset \text{ and } S < S_c$$

and resonance neutralization is possible only for

$$\alpha > \emptyset \text{ and } S > S_c$$

S_c is the critical distance from the surface at which $\alpha = \emptyset$. Consideration of the most probable distance from the surface at which the resonance processes are likely to occur led Hagstrum to conclude that a two-stage process for an ion, resonance neutralization followed by Auger de-excitation, is highly unlikely. An ion is therefore expected to undergo Auger neutralization.

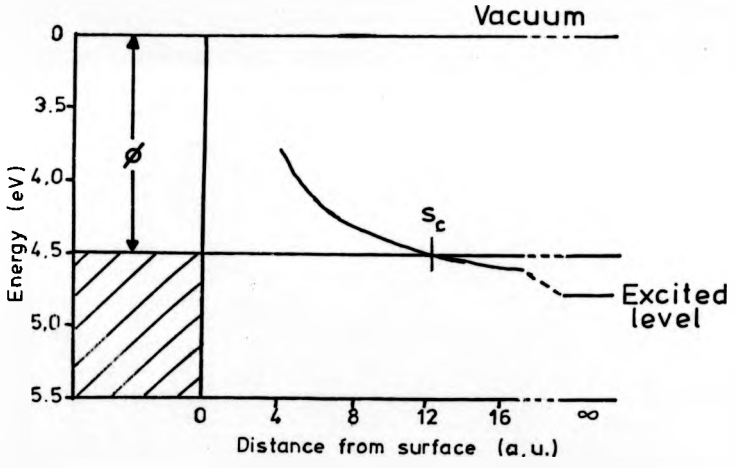

FIG. 1.4

Plot of the variation of the excited level of the helium metastable atom as a function of distance from a tungsten surface.

However using the same argument Hagstrum demonstrated that for an incident excited atom the two-stage process, resonance ionization followed by Auger neutralization, has a high probability of occurring..

1.5 Auger De-excitation

When an excited atom undergoes Auger de-excitation at a surface an electron falls from the Fermi sea to occupy the hole in the ground state level of the atom. The energy released in this transition is then transferred to the excited electron which may be released to the vacuum. This process and the alternative process, where there is no exchange of electron between metal and atom, are shown in fig. 1.5.

For both processes the energy of the ejected electron is given by

$$E(e^-) = E_x' - \epsilon \qquad (12)$$

where E_x' is the effective excitation potential of the atom near the surface and ϵ is the energy of the participating electron in the conduction band of the metal with respect to the vacuum level. Energy extrema will be given by

$$\begin{aligned} E(e^-)_{max} &= E_x' - \phi \\ \text{and } E(e^-)_{min} &= E_x' - \epsilon. \end{aligned} \qquad (13)$$

As in the case of Auger neutralization it is possible to formulate the matrix elements for the two processes

$$\begin{aligned} (H_{fi})_{exch} &= \iint U_f^*(\underline{r}_1) U_G^*(\underline{r}_2) \frac{e^2}{r_{12}} U_M(\underline{r}_2) U_E(\underline{r}_1) d\underline{r}_1 d\underline{r}_2 \\ (H_{fi})_{non-exch} &= \iint U_f^*(\underline{r}_2) U_G^*(\underline{r}_1) \frac{e^2}{r_{12}} U_M(\underline{r}_2) U_E(\underline{r}_1) d\underline{r}_1 d\underline{r}_2 \end{aligned} \qquad (14)$$

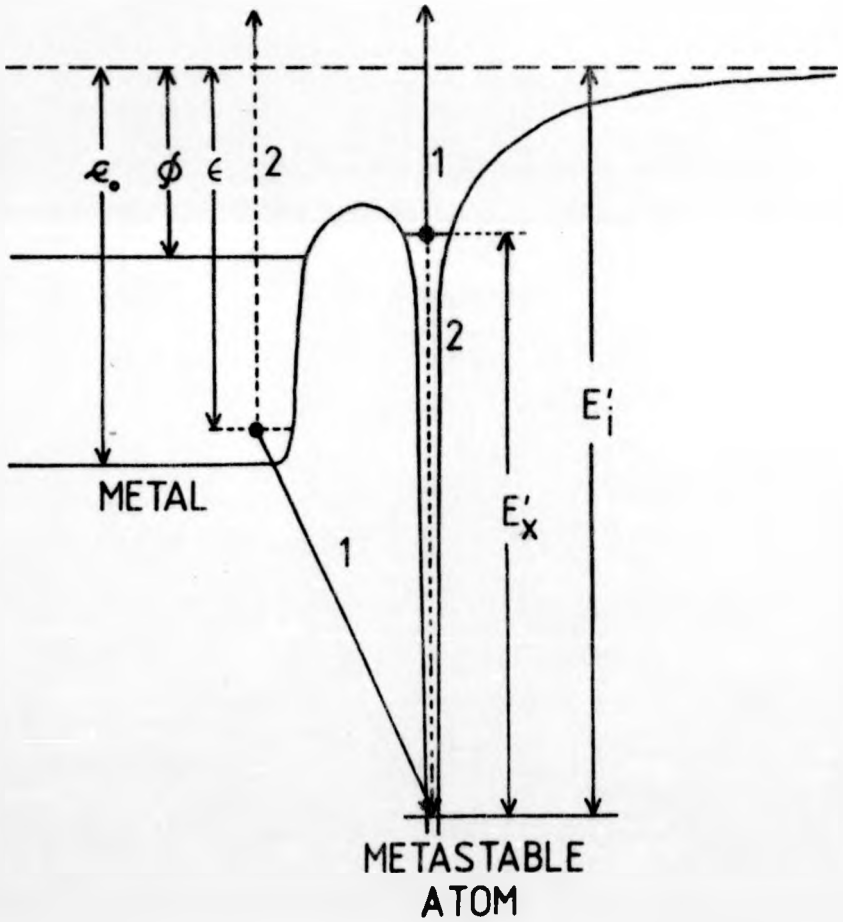

FIG. 1.5

AUGER DE-EXCITATION

Here U_f is the wavefunction of the free electron, U_G the wavefunction of the electron in the groundstate of the atom, U_E the electron in the excited state of the incident atom and U_M the electron from the metal. Once again it will be seen that the process depends on the overlap of the wavefunctions for U_M and U_G. The matrix element for the non-exchange process is zero if the states U_E and U_G have different spins and is small if U_E and U_G are both S states.

1.6 Experimental Observations for Metastable Atoms Incident on Metal Surfaces.

Investigating the interaction of metastable helium atoms with single crystal tungsten surfaces both in the clean state and with monolayer coverage of different gases Maclennan and Delchar[22] obtained results which seemed to support the ideas of Hagstrum. Their ejected electron energy spectra for helium metastable atoms incident on a clean tungsten (110) surface and the same surface with carbon monoxide monolayer coverage are shown in fig. 1.6 (a). They suggested a model, similar to Hagstrum's, whereby following ionization the resulting ion may be neutralized by an electron that originates from the chemisorbed atom and the excess energy then given either to an electron in the surface or one in the adatom. This model is represented in fig. 1.6 (b).

Varney[23] examined the interaction of metastable argon and xenon atoms and metastable nitrogen and hydrogen molecules with a polycrystalline tungsten surface. With the use of suitable adsorbates he was able to raise or

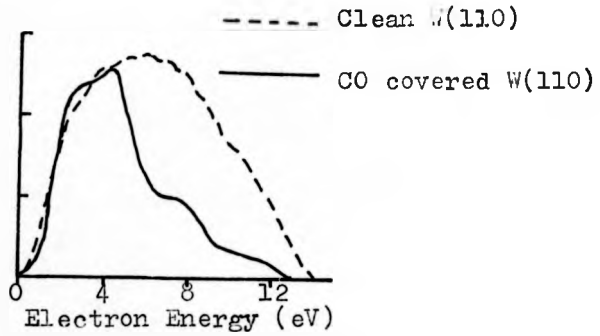

(a) Electron energy distributions.

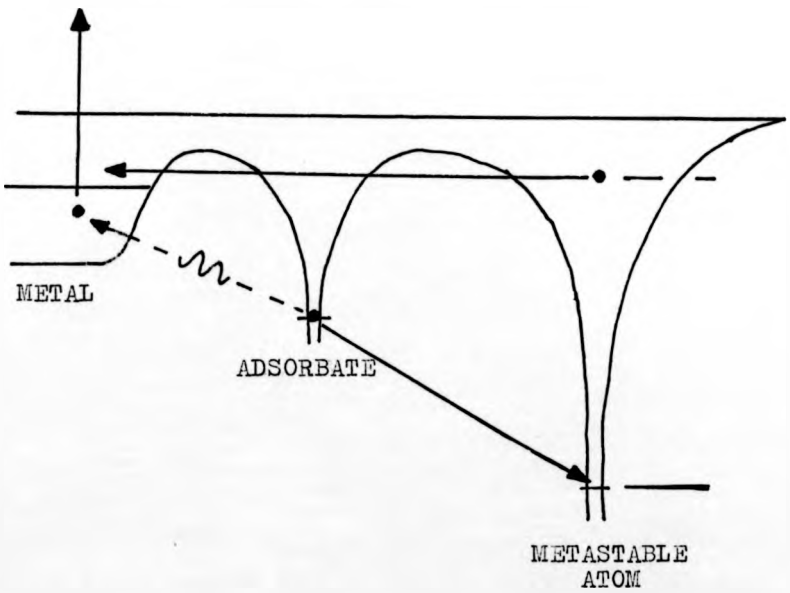

(b) MacLENNAN/DELCHAR MODEL

FIG. 1.6

lower the work function of the metal surface and measure the resulting variation in the total yields of secondary electrons, positive ions and photons. He concluded that his results were in agreement with the theory of Hagstrum.

The results of more recent experiments have led to a different model being proposed. These experiments include metastable helium, neon, and argon atoms incident on polycrystalline tungsten, metastable helium atoms incident on a stainless steel surface and metastable argon and krypton atoms incident on a naphthacene surface. The experiments on naphthacene were performed by Shibata et al[24] and the other experiments by Allison et al[12]. These latter authors have proposed a model by which the incident metastable atom interacts with one of the adsorbed atoms or molecules in a collision that is analagous to gas phase Penning Ionization. The ion formed in this process may subsequently be Auger neutralized with the release of an electron from the metal. However in their experiments the surfaces under investigation were in a contaminated state and the authors suggested that the energy levels associated with such a surface would be more discrete in nature than the continuum of levels of the atomically clean surface. They further suggested that such conditions would favour Penning ionization more than resonance ionization. This suggestion was given support by experiments which looked for spin conservation in the electrons ejected from surfaces following the impact of metastable atoms[25, 26]. In such experiments, spin conservation between the ejected electron and the electron in the

excited state of the incident atom was of the order of 60%. This led to the conclusion that the electron in the excited state of the atom plays a more direct role in the ejection process than it would if the two-stage process took place.

1.7 Penning Ionization

Penning ionization occurs with almost unity probability when an excited atom, typically a metastable helium atom, collides with an atom whose ionization potential is lower than the excitation potential of the excited atom. The excited atom is de-excited and the other atom ionized with the release of an electron having as kinetic energy any excess energy from the process. Such an interaction may be represented by

$$A^* + B = B^+ + e^- + A \qquad (15)$$

Hotop and Niehaus[27] have suggested that Penning ionization in the gas phase is an exchange process. Born-Oppenheimer type potential curves for their model are depicted in fig. 1.7 For a transition occurring at a separation R the energy of the ejected electron is simply

$$E(e^-) = V^*(R) - V^+(R)$$

where $V^*(R)$ and $V^+(R)$ refer to the potential energies of the A^*/B and A/B^+ systems respectively. Extreme possible values of the electron energy distribution are

$$E(e^-)_{max} = E_o + E_k^*(R=\infty) + \epsilon'$$
$$\text{and} \quad E(e^-)_{min} = E_o - \epsilon^* + \epsilon'' \qquad (16)$$

with quantities defined as in the figure. Hotop and Niehaus have also suggested that the transition probability for the process varies as an exponential with R, that is $w(R) \sim e^{-\chi R}$ where χ has the values consistent with

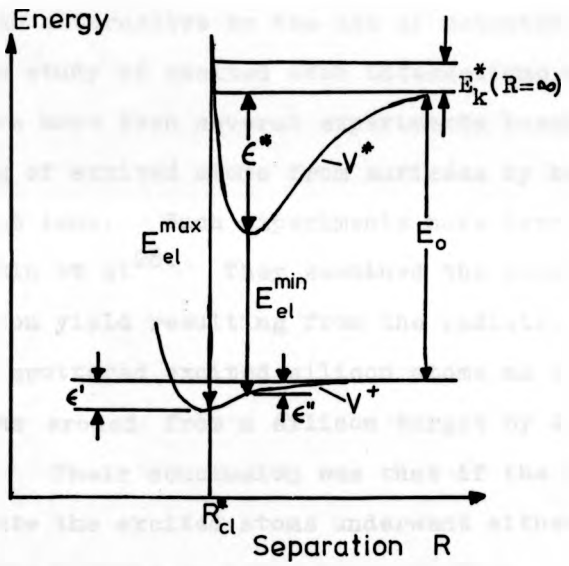

FIG. 1.7

Potential curve model of Penning ionization. $E_k^*(R=\infty)$ is the collision energy and E_o is the difference in the potential energy of the two systems at infinity.

the exchange mechanism

$$A^*(1) + B(2) \rightarrow A(2) + B^+ + e^-(1) \qquad (17)$$

The numbers (1) and (2) in equation (17) designate the excited electron initially bound to A and one of the outer shell electrons initially bound to B.

1.8 Alternative Techniques for the Study of the Interaction of Excited Atoms with Surfaces

As an alternative to the use of metastable atom probes for the study of excited atom interactions with surfaces, there have been several experiments based on the sputtering of excited atoms from surfaces by high energy incident ions. Such experiments have been performed by Martin et al[28]. They examined the change in the total photon yield resulting from the radiative de-excitation of sputtered excited silicon atoms as an oxide layer was eroded from a silicon target by 45 keV Argon ions. Their conclusion was that if the conditions were appropriate the excited atoms underwent either a double resonance process or Auger de-excitation.

Another technique was that of Thomas et al[29], who examined the de-excitation of excited helium atoms produced by the collision of 30 keV helium ions with metal surfaces. These authors studied the Doppler-broadened spectral lines emitted in the radiative decay of the scattered excited atoms: the broadening was characteristic of the velocity distribution of the reflected particles. The primary conclusion of this study was that the excited atoms recoiling from the target have a high probability of radiationless decay.

They further concluded that their results were consistent with the prediction of Cobas and Lamb for Auger de-excitation of excited atoms.

Summary

In this chapter an outline has been given of existing theories for the de-excitation of excited atoms at solid surfaces. It has been shown that whilst the theory seems to be well developed, the evidence from different experiments has often been conflicting. Direct support for a two-stage process, resonance ionization and subsequent Auger neutralization, has been found in only a limited number of experiments. Other studies have indicated alternative mechanisms, possibly Penning Ionization or its equivalent, Auger de-excitation. Thus, from this outline, it will be seen that there existed a need for further study as has been attempted in the present set of experiments.

References

1. H. W. Webb, Phys. Rev. 24, 113 (1924).
2. H. J. Coulliette, Phys. Rev. 32, 636 (1928).
3. S. Sonkin, Phys. Rev. 43, 788 (1933).
4. M.L.E. Oliphant, Proc. Roy. Soc. (London) A124, 228 (1929).
5. D. Greene, Proc. Phys. Soc. 63, 876 (1950).
6. R.F. Stebbings, Proc. Roy. Soc. (London) A241, 270 (1957).
7. J. B. Hasted, J. Appl. Phys. 30, 23 (1959).
8. D. A. Maclennan, Phys. Rev. 148, 218 (1966).
9. D. A. Maclennan and T. A. Delchar, J. Chem. Phys. 50, 1772 (1969).
10. F. B. Dunning, A.C.H. Smith and R.F. Stebbings, J. Phys. B: Atom molec. Phys 4, 1683 (1971).
11. F.B. Dunning and A.C.H. Smith, J. Phys. B: Atom. molec. Phys. 4, 1696 (1971).
12. W. Allison, F.B. Dunning and A.C.H. Smith, J. Phys. B: Atom molec. Phys. 5, 1175 (1972).
13. H.S.W. Massey, Proc. Cambridge Phil. Soc. 26, 386 (1930); 27, 469 (1931).
14. S. S. Shekhter, J. Exptl. Theoret. Phys. (U.S.S.R.) 7, 750 (1937).
15. A. Cobas and W.E. Lamb, Jr., Phys. Rev. 65, 327 (1944).
16. H. D. Hagstrum, Phys. Rev. 89, 244 (1953).
17. H. D. Hagstrum, Phys. Rev. 91, 336 (1954).
18. H. D. Hagstrum, Phys. Rev. 96, 325 (1954).
19. H. D. Hagstrum, Phys. Rev. 96, 336 (1954).
20. F. M. Propst, Phys. Rev. 129, 7 (1963).
21. E.P. Wenaas and A.J. Howsmon, in The Structure and Chemistry of Solid Surfaces, G. Somorjai, Ed. (John Wiley & Sons, Inc., New York, 1969).
22. T.A. Delchar, D.A. Maclennan and A.M. Landers, J. Chem. Phys. 50, 1779 (1969).

23. R. N. Varney, Phys. Rev. 175, 98 (1968).

24. T. Shibata, T. Hirooka and K. Kuchitsu, Chem. Phys. Lett., 30, 241 (1975).

25. B.L. Donnally, R. Faber, J. Gates and C. Volk, Bull. Am. Phys. Soc., 18, 141 (1973).

26. P. J. Keliher, F.B. Dunning, M.R. O'Neill, R.D. Rundel, and G. K. Walters, Phys. Rev. A, 11, 1271 (1975).

27. H. Hotop and A. Niehaus, Z. Physik 238, 452 (1970).

28. P. J. Martin, A.R. Bayly, R.J. Macdonald, N.H. Tolk, G. J. Clark and J. C. Kelly, Surf. Sci. 60, 349 (1976).

29. W. E. Baird, M. Zivitz, J. Larsen and E.W. Thomas, Phys. Rev. A 10, 2063 (1974).

CHAPTER TWO

THE EXPERIMENTAL SYSTEM

2.1 Introduction

In designing an experimental system for surface sensitive work the consistent achievement of an ultra-high vacuum is a major consideration. The ultra-high vacuum allows data to be collected over a reasonably long period before well characterised surfaces are degraded through contamination by molecules from the ambient residual atmosphere. Having obtained a good vacuum, it should then be possible to clean the specimen in situ, and hopefully monitor the state of surface cleanliness. Besides these general considerations the present apparatus was designed to allow an intense flux of metastable atoms to strike the target.

2.2 Ultra-High Vacuum System

The ultra-high vacuum system was designed by the author and constructed in the engineering workshops of the Physics Department. It was fabricated from non-magnetic stainless steel, type EN58B, and consisted basically of three chambers; the helium source, the atom excitation region which served as a buffer chamber, and the target chamber. The buffer chamber and the target chamber were pumped by oil diffusion pumps whilst the helium source was pumped by a mercury diffusion pump. All three diffusion pumps were backed by rotary pumps. The target chamber was equipped with a high conductance liquid nitrogen cold trap; the buffer chamber was left untrapped since this arrangement allowed a higher pumping speed and thus the

production of a more intense beam of helium atoms. The oil diffusion pumps were filled with Santovac 5, a polyphenyl ether having a vapour pressure of better than 10^{-9} torr. These two pumps gave effective pumping speeds of 300 litres/sec and 250 litres/sec in the buffer chamber and target chamber respectively. The pumping speed in the source chamber was approximately 15 litres/sec. To reduce vibration, the vacuum system was mounted on anti-vibration pads and each rotary pump was connected via a flexible pipe. A schematic diagram of the equipment is shown in fig. 2.1 and a photograph in Plate 1.

Ultra-high vacuum was obtained by the following procedure:

1. The entire system was pumped down to a vacuum of 10^{-3} torr with the rotary pumps.
2. The diffusion pumps were switched on to take the system to better than 10^{-6} torr.
3. The chambers including the cold trap were baked in an oven at 200°C for at least 24 hours.
4. The oven was removed, the system allowed to cool, all filaments rigorously outgassed and finally liquid nitrogen was added to the target chamber cold trap.

Following this routine, vacua of the order of 10^{-10} torr were obtained in the target chamber and 5×10^{-9} torr in the buffer chamber. All pressures were measured with Bayard Alpert ion gauges, type VIG 10, and are the equivalent nitrogen pressures. Residual gas analysis

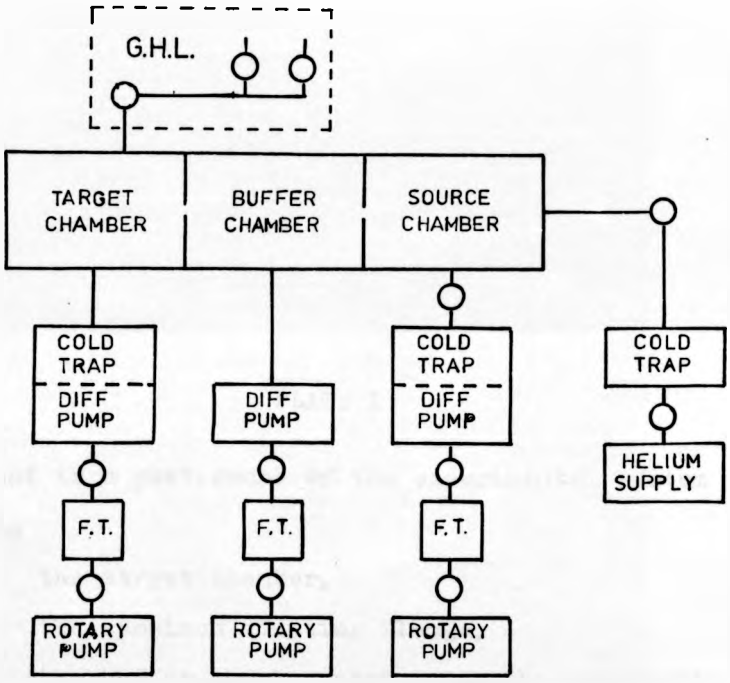

FIG. 2.1

Schematic diagram of the pumping system where F.T. and G.H.L. represent foreline traps and the gas handling line respectively.

PLATE 1

Overleaf is a photograph of the experimental system showing

A) the target chamber,

B) the specimen mounting flange,

C) the buffer chamber containing the metastable gun and ion deflector plates and,

D) the solenoid surrounding the metastable gun.

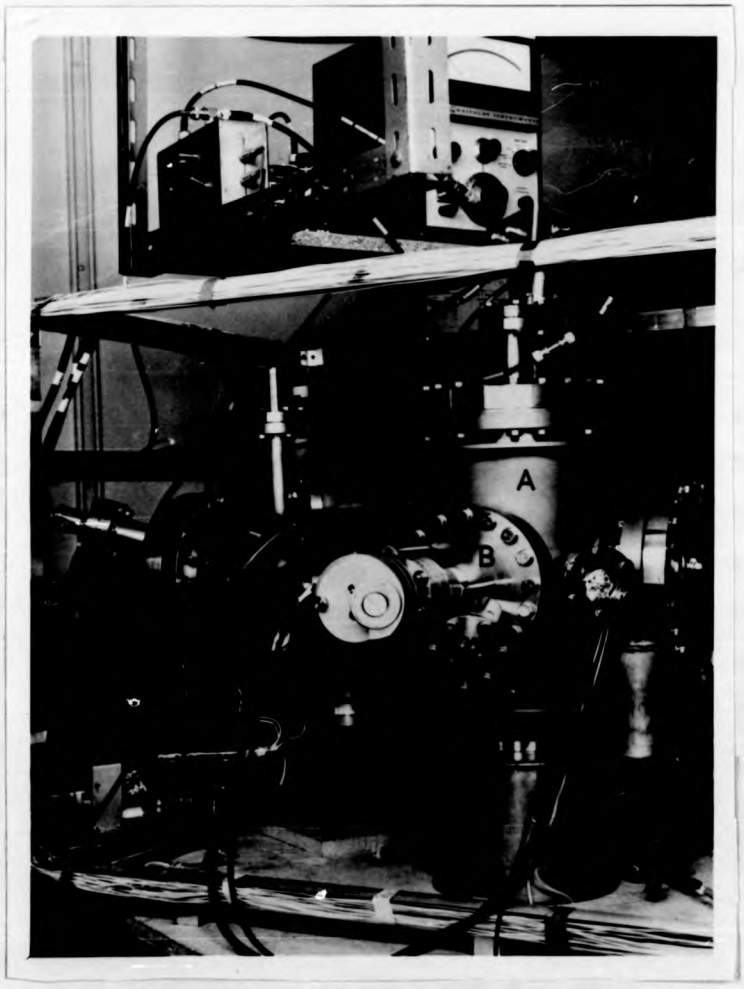
A
B

in the target chamber was carried out with a Micromass I mass spectrometer (V.G. Micromass Ltd.) A typical mass spectrum taken whilst the system was under ultra-high vacuum is shown in fig. 2.2.

2.3 Specimen Preparation

The specimen holder, described more fully in the next section, necessitated the preparation of specimens with a thin stem at one end. This was accomplished by turning single crystal rods, 6 mm. in diameter, on the electrolytic lathe shown in Plate 2. The single crystal rods, 5N purity from Metals Research Ltd., were held by two chucks and rotated above a wheel, the lower section of which was immersed in a caustic soda bath. With an electric motor turning the wheel and adjustment of the distance separating the crystal rod and wheel, it was possible to maintain a continuous thin film of caustic soda solution in contact with the rod. By then applying a suitable a.c. voltage between the rod and an electrode in the caustic soda bath, the centre of the crystal rod was gradually etched away electrolytically. This produced a dumb-bell shaped rod which was then spark cut through the centre to form the basis for two specimens.

As the crystals were supplied in a random orientation, they were orientated to within 1^{o} by X-ray Laue back reflection and then spark machined to expose the desired low-index crystal plane. Before mounting on the specimen stage, the crystal was mechanically polished and finally electropolished in an orthophosphoric acid solution. Finally, the entire assembly was vapour degreased with trichloroethylene before installation in

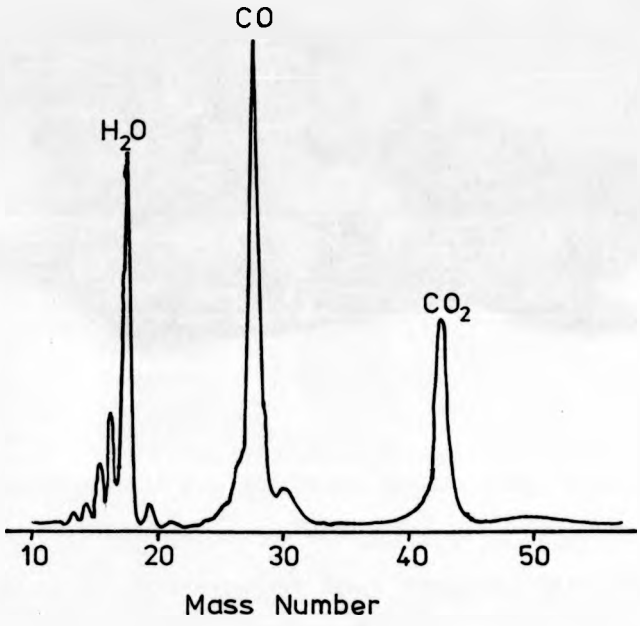

FIG. 2.2

Mass spectrum taken in U.H.V. conditions.

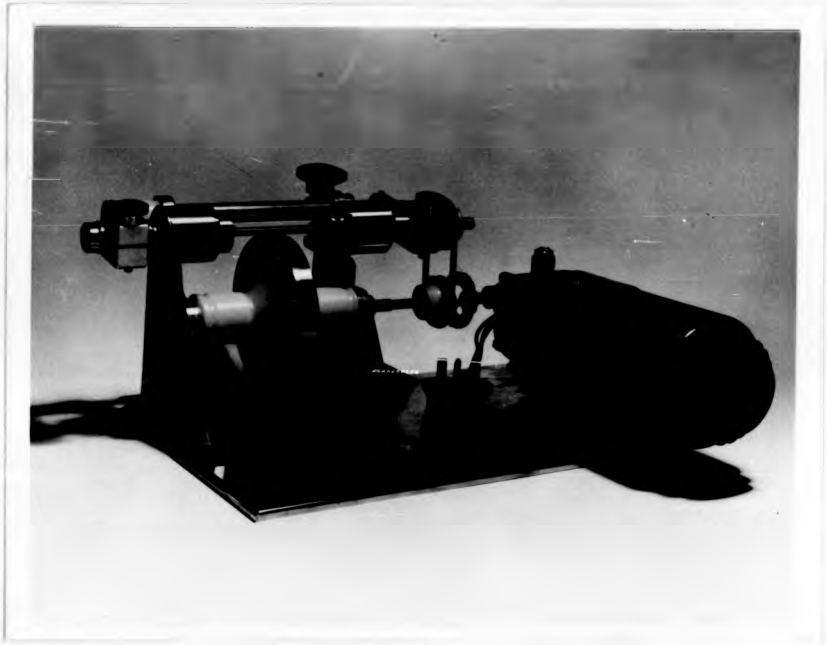

PLATE 2

The electrolytic lathe used in the specimen preparation.

the experimental chamber.

Facilities for cleaning the specimen inside the chamber included electron bombardment and argon ion bombardment using an ion gun which produced a poorly collimated beam. A gas handling line led directly into the side of the experimental chamber and was fitted with silver and palladium thimbles which allowed the introduction of pure oxygen and hydrogen respectively, in an easily controlled fashion. Carbon monoxide and argon (used for argon ion bombardment) were supplied from 1 litre flasks of spec pure quality gas obtained from B.O.C. Special Gas Dept.

2.4 Specimen Mounting

The specimen was mounted on the holder shown in Plate 3. This type of holder allowed the specimen to be heated to high temperatures by electron bombardment with minimal heat loss by conduction. The holder is best understood by reference to the diagram in fig. 2.3 The centre of a short length of thin tungsten wire was formed into a coil into which the thin stem of the specimen was pushed. The coil was then spot welded to the stem and the free ends of the tungsten wire spot welded to supports on the holder. During electron bombardment the specimen's potential was raised to 1 kV and this necessitated the use of ceramic insulators to isolate its supports from the rest of the holder. An extra plate was introduced onto the holder to prevent material evaporated from the high temperature region from being deposited onto these ceramics and degrading their insulation properties.

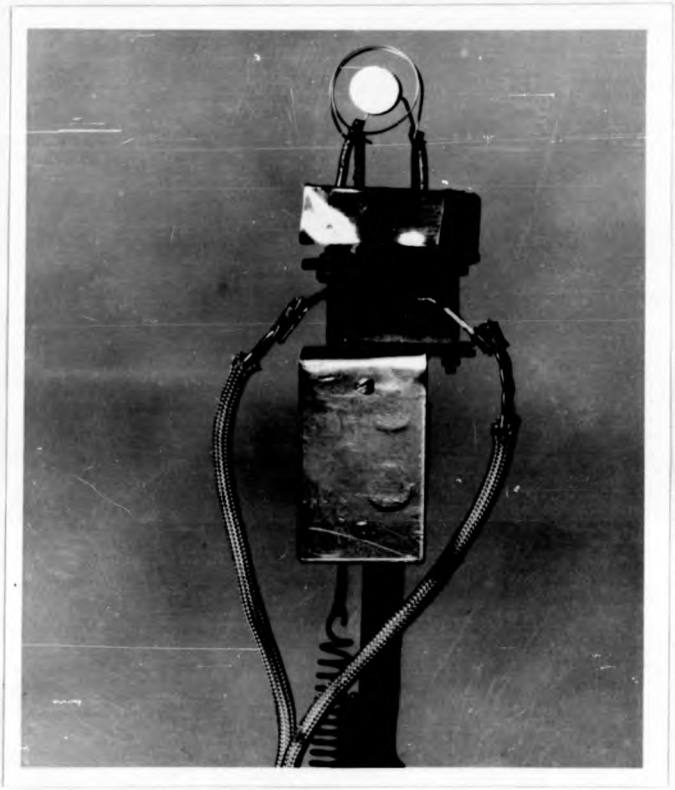

PLATE 3

The Specimen Holder.

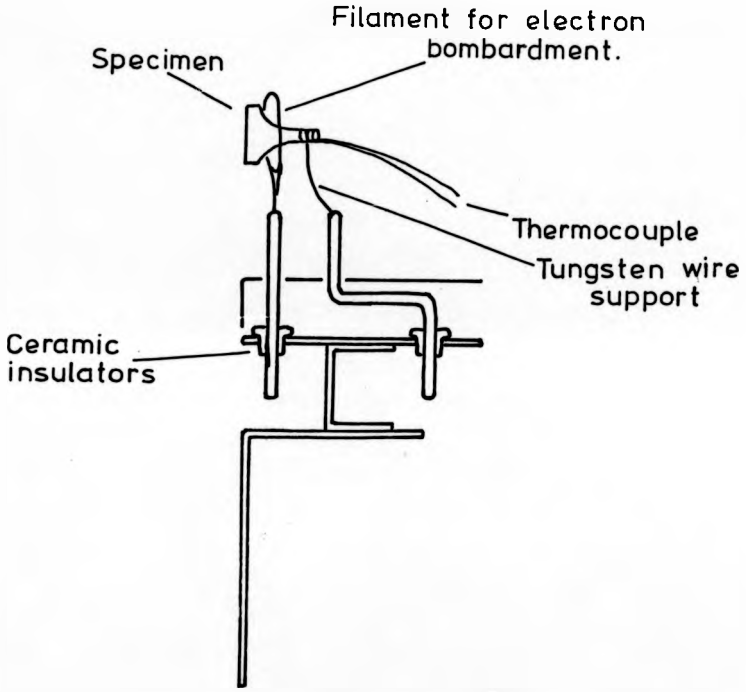

FIG. 2.3

The Specimen Holder

In the case of nickel, specimen temperatures could be measured with a chromel - alumel thermocouple spot welded to the stem. The holder was mounted on a simple rotary drive (RD1, Vacuum Generators Ltd.) which allowed rotation about an axis perpendicular to the metastable beam axis. Additional slight movement to allow for further alignment of the specimen was made possible by mounting the flange bearing the rotary drive on bellows. This flange could be clamped to three posts when the specimen had been positioned.

It was found necessary to surround the target with molybdenum heat shields during any annealing process as the temperature rise in the target chamber caused distortion of the grids in the electron spectrometer.

2.5 The Helium Atom Beam

As will be described in more detail in the next chapter, the flux of metastable atoms was obtained by causing electrons to collide with a beam of helium atoms. The helium beam was formed by allowing helium to flow from the source chamber into the buffer chamber via an array of seven stainless steel tubes. Each tube had an internal diameter of .21 mm and was approximately 5 mm in length. This array was brazed on to a plate which was welded to bellows to allow lateral movement and alignment with a final collimating aperture in the side of the target chamber. The array plate could be moved by adjusting three equispaced screws set radially around the plate. The use of an array of tubes gave a helium beam with a greater centre line intensity[1].

Alignment of the system was accomplished by directing a modulated laser beam (He - Ne laser) through a flat glass window behind the tubes to impinge on a photodiode placed behind the final collimating hole in the target chamber. The array of tubes was moved until the intensity detected by the photodiode was a maximum. The target was positioned by manipulating it until the laser light reflected centrally from its surface. Final adjustment was made when the metastable flux was passing through the system.

The array and collimating orifice were designed to give a beam 1 mm in diameter at the target. However in practice it was found that the beam was approximately 2 mm in diameter. It was felt that this was due to the placing of the excitation region between the array and the orifice. Collisions of the helium atoms with other helium atoms and also with electrons travelling in the opposite direction would tend to scatter the beam atoms through small angles. This would give the appearance of a source aperture with a larger diameter than that of the array.

Helium was supplied from a BOC cylinder for which the specification was 99.998% pure helium. Impurities were removed from the helium by allowing it to pass through a liquid nitrogen cooled trap containing activated alumina before arriving at the array of tubes. With the helium beam flowing through the system the pressures in the different chambers were 2.5×10^{-4} torr and 7.5×10^{-9} torr (equivalent nitrogen pressures) in

the buffer and target chambers respectively. The pressure in the source chamber was of the order of a few torr.

2.6 Data Collection

The same electron spectrometer, a retarding field analyser, was used for both Auger Electron Spectroscopy (AES) and for measurement of the energy distributions of the secondary electrons resulting from metastable atom impact. This analyser was of the conventional type, having three grids in front of a collector. The first grid was held at earth potential so that electrons leaving the specimen were in a field free region and a retard voltage was applied to the second and third grids electrically connected together. Whilst the use of three grids was not so convenient for the metastable atom work, Taylor[2] has shown that the use of twin retard grids is necessary for reasonable resolution in AES.

The grids were fabricated by stretching tungsten mesh over perspex forms and spot welding it to stainless steel retainer rings. The mesh had 100 mesh in^{-1} and was manufactured from 0.0008 inch tungsten wire. At this stage the grids were extremely flexible and it was necessary to chromium plate them to produce a certain rigidity. The details of this plating process may be found in Appendix II. Following the spark erosion of a $\frac{1}{4}$ inch diameter hole through the centre of each grid, they were photographed so that accurate measurements could be made of their radius from the prints. Ceramics were then cut so that the entire spectrometer could be assembled

with all grids and the collector being centred on the same point. The whole assembly was finally mounted in a metal can so that stray electric fields did not interfere with the performance of the spectrometer.

This spectrometer subtended an angle of approximately 100^{o} or π steradians at the specimen. Because of the low energy of the electrons to be collected, compensation for any magnetic fields in the region of the specimen was needed. Although the collection is over a fairly large solid angle, the presence of a magnetic field degrades resolution by producing non radial trajectories. Magnetic compensation was achieved by passing current through three mutually perpendicular pairs of rectangular coils. Some measure of the residual magnetic field strength was obtained using a search coil connected to a Keithley electrometer. Using this method the magnetic field strength in the specimen region appeared to have been reduced to approximately 5% of its value with no compensating fields present.

The specimen itself was screened from electric fields by the metallic body of the chamber. This "Faraday cage" was completed by positioning a transparent mesh behind the viewport in the target chamber. All the electrical connections to the inside of the system were made via V.G. Eft5 electrical feedthroughs.

2.7 The Electronic Configuration used for Auger Electron Spectroscopy.

A brief review of the technique of Auger Electron Spectroscopy is given in Appendix I. The electronic

arrangement used for Auger electron analyses is shown in fig. 2.4. The addition of a small sinusoidal modulation to the retard voltage and the use of a Lock-in amplifier allowed direct readings of either the energy distribution of the ejected electrons N(E) or its first derivative dN(E)/dE. The modulation applied to the transformer was taken from a Brookdeal Signal Source 452. Because of the proximity of the grids and collector there was a large in-phase signal passing through the load resistor due to capacitive linkage. To enable full use of the dynamic range of the detection system it was necessary to cancel this in-phase component by the application of a 180^{o} phase shifted signal to an adjustable neutralizing capacitor. This was simply achieved by applying the signal from one side of the transformer to the grids and the signal from the other side to the neutralizing capacitor. A potential of +180V was applied to the collector to suppress the emission of secondary electrons from its surfaces. The lock-in amplifier used was the Brookdeal system 40, which comprised a low noise amplifier with variable gain from 30 to 100 db, and a coherent filter and phase sensitive detector, both referenced by a signal from a reference unit.

Examination of the elastic peak in the secondary electron energy distribution, N(E) allowed the phase of the detector to be adjusted to maximise the level of detection. By then switching the system to the second harmonic of the modulation frequency w, second derivative curves, dN(E)/dE, were obtained as is usual in Auger electron analysis.

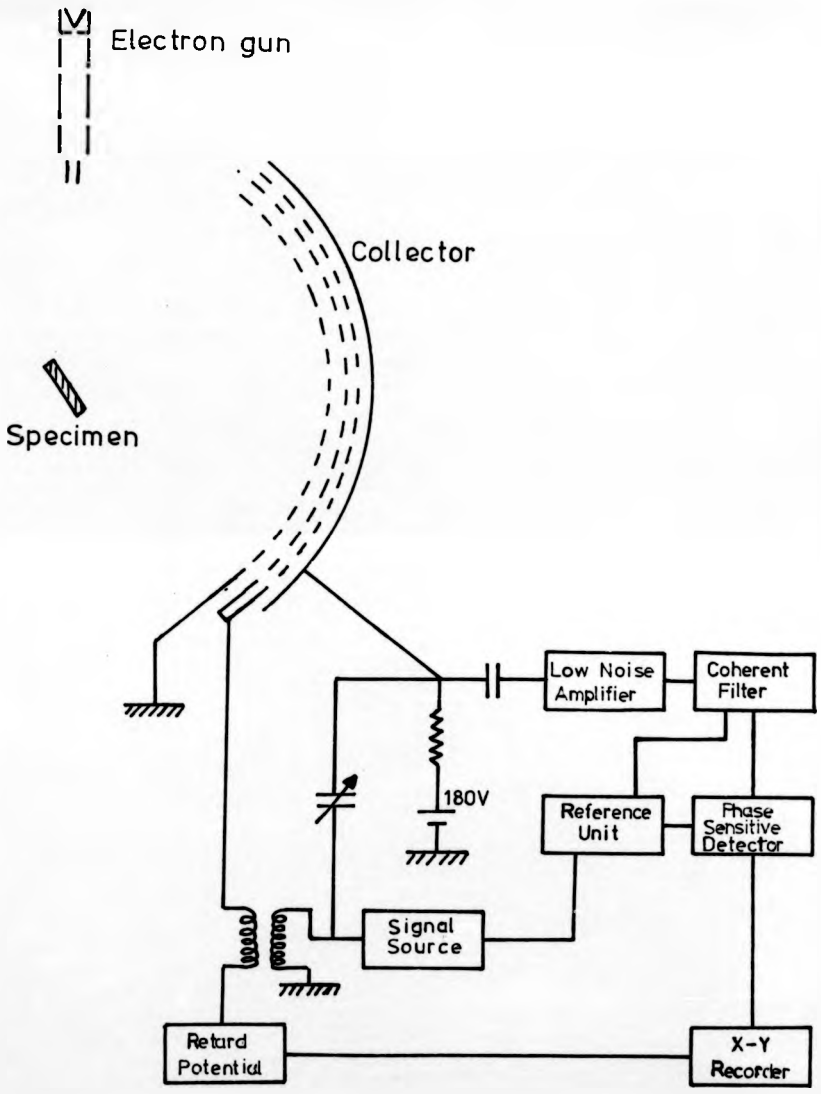

FIG. 2.4

The electronic configuration used for Auger electron spectroscopy.

The geometric arrangement of the target, retarding field analyser, and the electron gun, type V.G. LEG 3, is shown in fig. 2.4. In the early stages of this work, the electron gun was driven by the power supplies provided with the standard V.G. Fast Scan Auger system. In the later work, the potentials were supplied to the various elements of the gun from a simple circuit centred on a V.G. 180G E.H.T. supply. This circuit is shown in fig. 2.5. Electrodes A_1, A_2 and A_3 served as an einzel lens, the potential on A_2 being adjusted to focus the electron beam. The potential on G_1, the Wehnelt cylinder, was adjusted to vary the effective source aperture.

By applying d.c. voltages to the deflection plates at the end of the electron gun it was possible to deflect the electron beam to different areas of the specimen. Sawtooth modulations superimposed on the d.c. voltages caused the electron beam to scan a region of the target chamber. Using the electron current measured at the specimen to modulate the intensity of an oscilloscope whose beam was scanned in the X and Y directions synchronously with the gun, a picture of the specimen holder was displayed. It was then a simple matter of reducing the sawtooth modulation to direct the beam on to the specimen.

2.8 The Electronic Configuration used for the Metastable Atom Experiments.

Since the metastable atom beam caused the ejection of fewer secondary electrons from the specimen than did the electron beam used for AES, the resulting current of approx-

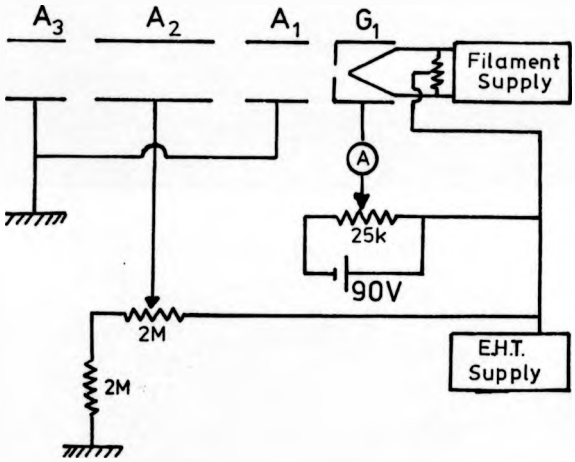

FIG. 2.5

The electron gun circuit.

imately 10^{-11} amps at the collector required a much more sensitive detection system. Both d.c. and a.c. techniques were used for the measurement of the secondary currents at the collector. For d.c. measurements the circuit shown in fig. 2.6 was employed. Currents were measured using a Keithley 402 electrometer floated up to the potential of the collector. A voltage proportional to the collector current was then fed from the electrometer to the Y-axis of the X - Y recorder (Bryans Southern Instruments Series 26000). The X-axis of the recorder was driven synchronously with the ramp. The displacement current between the grids and collector was neutralized by feeding the ramp into an inverting amplifier and then passing the inverted ramp from this across a neutralizing capacitor connected to the input of the electrometer. The I-V curves obtained on the recorder were then differentiated graphically to give N(E).

The a.c. method employed an electronic configuration for the measurement of secondary electron energy distributions N(E) similar to that used by R.C. Eden[3] for UPS experiments. The arrangement is shown in fig. 2.7. Neutralization of the displacement current between the grids and collector was achieved by the use of a centre-tapped transformer. In this case the transformer was made by winding 36 s.w.g. enamel covered copper wire on a pot core, type Mullard FX 2240. The ramp was applied to the centre tap of this transformer with one end of the winding directed to the retard grids and the other end to an air spaced neutralizing capacitor. With the application of a sinusoidal modulation to the other winding of the

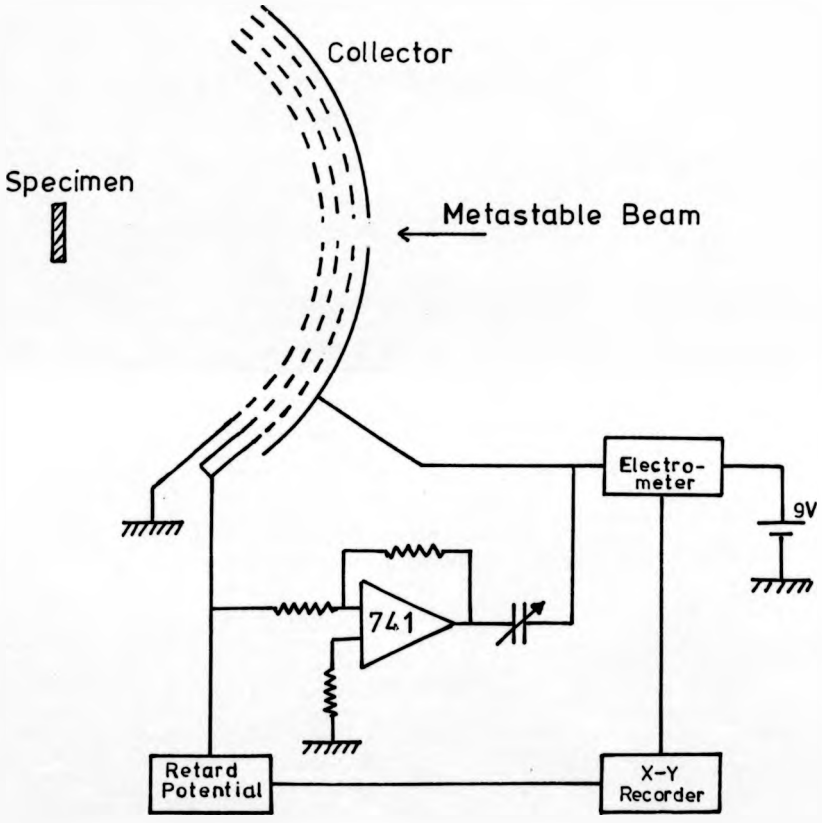

FIG. 2.6

The electrical circuit used for d.c. measurements of the secondary currents at the collector.

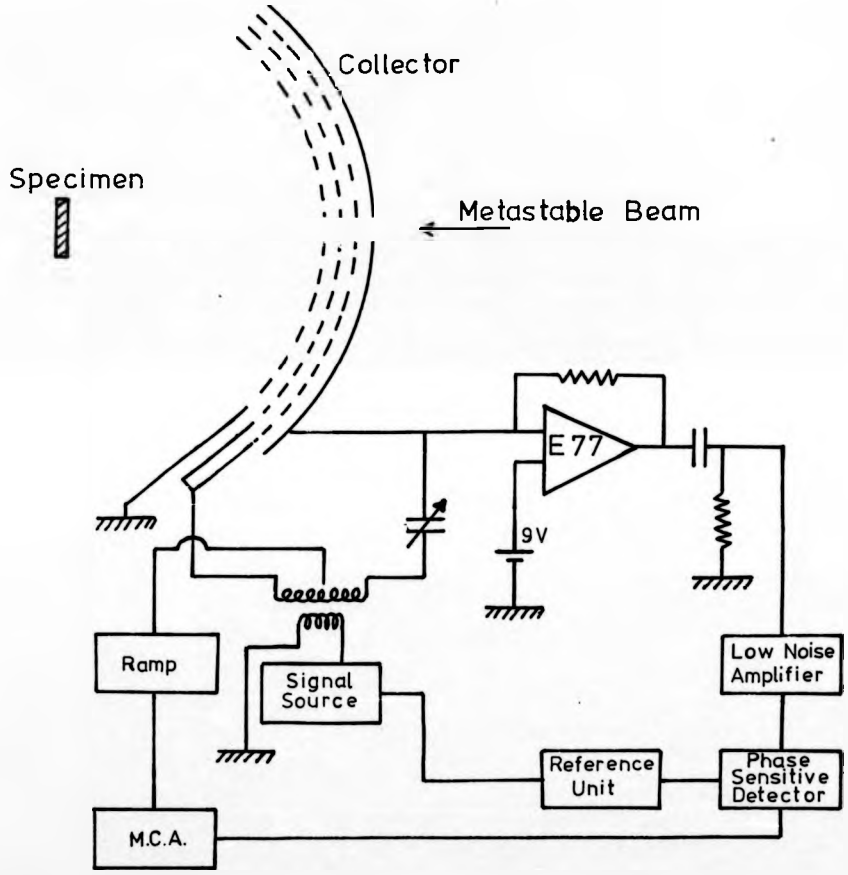

FIG. 2.7

The electronic configuration used for a.c. measurements of secondary electron energy distributions resulting from metastable atom impact.

transformer, modulations 180° out of phase were applied to the retard grids and neutralizing capacitor. Neutralization was more effective in this circuit than that used for AES because phase shifts in the two sinusoidal modulations caused by stray capacitances to earth were equal.

The collector was floated to +9V to suppress the emission of secondary electrons from its surfaces. The signal from the collector, along with the neutralizing signal, was fed directly into the input of a F.E.T. input operational amplifier wired in the current amplifier mode. This mode had a very low input impedance and low input capacitance. The operational amplifier used in this case was a Computing Techniques E77 which was ideal because of its low input bias current, less than a picoamp. The signal from this current amplifier was then a.c. coupled via a high pass filter to the low noise amplifier and finally the phase sensitive detector. Because the signal to noise ratio was still low at this stage, a digital memory oscilloscope, the Northern Scientific NS544, was used to average the energy distribution curves N(E) from a repeated number of scans. This unit also supplied a ramp which was fed via a buffer amplifier to the retard grids. It should be added that to relieve overload problems a small delay was introduced between each scan. At the end of an experiment the result of the averaging was plotted on the X-Y recorder.

The centre-tapped transformer, neutralizing capacitor and operational amplifier were all mounted in a metal box which was directly attached to the electrical

feedthrough into the target chamber. Because of earth loop problems, all instruments were earthed through one point, in this case the oscillator.

Unfortunately the system developed for the metastable atom experiments was not suitable for AES, as the comparatively large currents involved in the latter case caused severe overloading problems.

2.9 Summary

An ultra-high vacuum system, in which it is possible to examine the interaction of metastable atoms with metal surfaces, has been designed and constructed. Furthermore, it is possible to perform experiments on surfaces which have been cleaned in situ and whose cleanliness may be monitored by the techniques of AES. There also exists a facility for adsorbing different gases on the surfaces in a controlled fashion.

References

1. R. H. Jones, D. R. Olander and V. R. Kruger, J. Appl. Phys. 40, 4641 (1969).

2. N. J. Taylor, Rev. Sci. Instrum. 40, 792 (1969).

3. R. C. Eden, Rev. Sci. Instrum. 41, 252 (1970).

CHAPTER THREE

THE HELIUM METASTABLE ATOM SOURCE

3.1 The Metastable States of the Helium Atom

Given sufficient energy, any atom may be excited to states which have more potential energy than the ground state. These excited states have lifetimes typically of the order of 10^{-7} secs and an excited atom will de-excite to its ground state via transitions which obey the selection rules for LS coupling, namely

$$\begin{aligned} \Delta L &= 0, \pm 1 \\ \Delta J &= 0, \pm 1 \\ \Delta S &= 0 \end{aligned} \qquad (1)$$

Here ΔL, ΔJ, and ΔS refer to the changes in the total orbital angular momentum, total atomic angular momentum, and total spin angular momentum respectively as the atom makes the transition from one state to another. When only a single electron is involved a transition whereby $\Delta L = 0$ is prohibited and $\Delta L = \pm 1$ is the only possibility.

The helium energy-level diagram with allowed transitions is shown in fig. 3.1. Examination of this diagram reveals that two states, namely the singlet 2^1S and triplet 2^3S have no allowed transitions to lower levels. These two states are known as the metastable states of the helium atom; they may suffer de-excitation either via collisions or via radiative decay. However the radiative lifetime of the two states is relatively long compared with the other excited states: 0.1 sec for the singlet state and even longer for the triplet state.

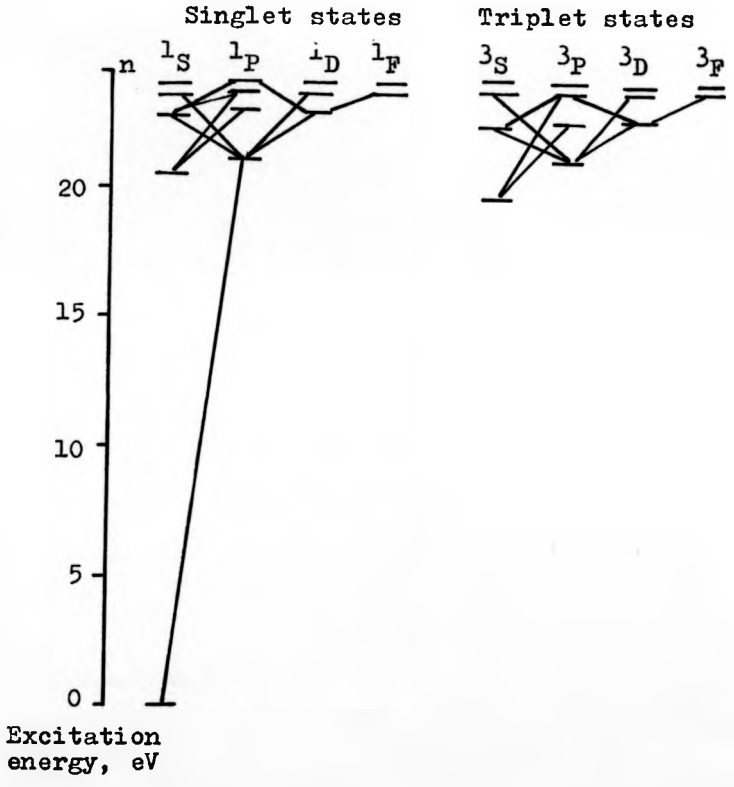

FIG. 3.1

Energy-level diagram for helium showing the division into singlet and triplet states.

3.2 Sources of Metastable Atoms

Atoms may be excited to their metastable states by a variety of techniques. These include the use of thermal sources, discharge sources, and sources involving collisions of the atoms with electrons or photons which have sufficient energy to cause excitation to the metastable state. Oven or thermal sources have been employed for certain atoms but this type of source has the disadvantage that the flux of metastable atoms produced tends to be small. Arc discharge sources have been used for producing helium metastable atoms[1, 2] but such sources have the disadvantage of requiring high gas purities and pre-discharge baking to avoid flux attenuation by Penning ionization and quenching collisions. A further disadvantage of the arc source is that resonance photons are produced in comparable quantities to the metastable atoms. The excitation of atoms by collisions with electrons is probably the most widely used method.

The sources employing this technique may be divided into two types; either a beam of excited atoms is formed by effusion from a source in which the collisions take place, or the beam is formed before entering an area where the collisions take place. The first type of source may provide any of the disadvantages described for the previously mentioned sources; the problem of contamination of the beam by resonance photons may be alleviated to some extent with the choice of operating conditions less favourable to their production[3]. The second type of electron collision source has none of these inherent

disadvantages, or at least they are greatly reduced. A distinct advantage of these sources is that a beam of excited atoms produced by the interaction of a helium beam and an electron beam travelling in a parallel or anti-parallel direction has a fairly narrow velocity distribution[4]. In the case where the helium beam and the electron beam travel in perpendicular directions there may well be a velocity spread of the order of 25%.

3.3 Tests on Different Metastable Atom Sources

In this work, the requirement for an intense flux of metastable atoms led to three different types of source being tested. Common to all three sources was the attempt to excite a well defined beam of atoms after it had been formed. As has been described in the previous chapter, the beam of atoms was formed by allowing the helium atoms to flow from the source chamber into the buffer chamber via an array of stainless steel tubes. The use of a multichannel array is necessitated by the requirement for a greater centre line intensity than would be obtained by simply allowing the gas to effuse from an orifice.

The pressure in the source chamber was such that the mean free path of the helium atoms was less than the length and radius of the capillary tubes. Jones et al[5] have examined the characteristics of a single capillary source operated under similar conditions in some detail. They measured the angular distribution and peaking factor from a capillary source having approximately the same

dimensions as the tubes used to construct the multi-channel array for the present experiment. The peaking factor of a source is defined as the ratio of the centre-line intensity from the source to the centre-line intensity from an ideal thin-walled source emitting at the same total leak rate. Jones et al found that the peaking factor for their capillary tube with the source operating at a pressure of 1 torr was approximately 4.0. The angular distribution they obtained is shown in fig. 3.2 together with the distribution from an equivalent cosine emitter. Examination of this figure immediately reveals the advantage of using capillary tubes. Both sources in the figure have the same total leak rate, a factor determined by the pumping speed on the buffer chamber, and yet the centre line intensity, the usable part of the beam, is higher from the capillary tube than from the orifice.

Having formed a beam, the problem became one of exciting sufficient numbers of the atoms to give a reasonable secondary electron current from the target. It was decided that rather than using the actual target as a monitor of the metastable flux, some measure of the efficiency of different sources could be obtained by placing a primitive collector/target system in the buffer chamber itself. By doing this, the problem of repeatedly aligning the array with the final collimating orifice and target was avoided. A diagram of the detection system used is shown in fig. 3.3. The "pot" had an entrance orifice which subtended a solid angle of 10^{-3} steradians at the array of tubes, and contained a target plate and

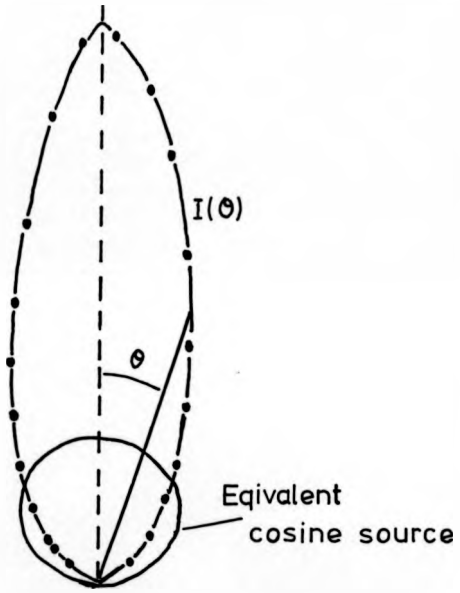

FIG. 3.2

The angular distribution $I(\theta)$ from a single capillary source together with that from an equivalent cosine source.

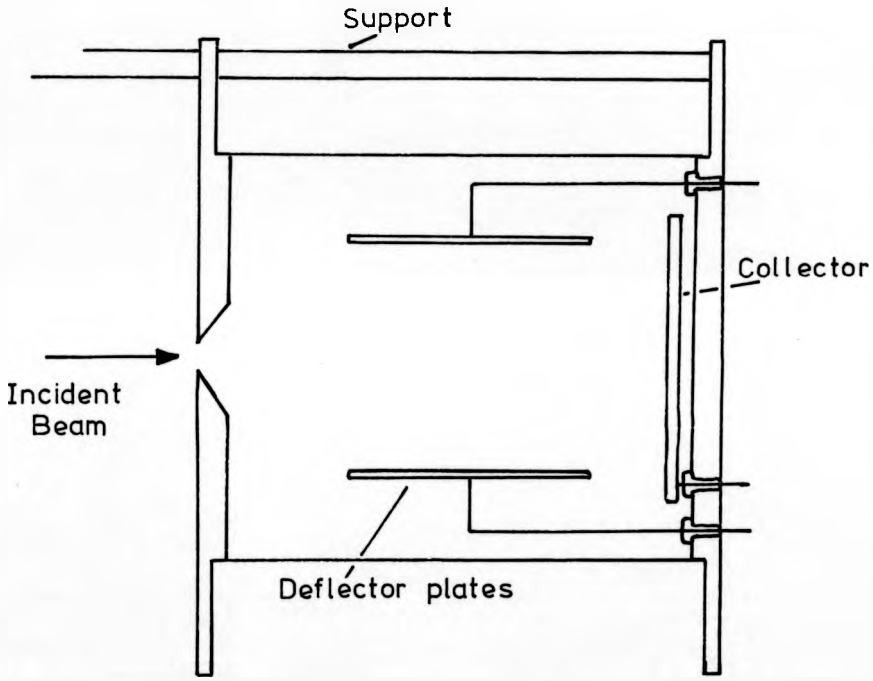

FIG. 3.3

The collector/target arrangement used for testing different metastable atom sources.

two deflector plates. These plates were manufactured from stainless steel and were electrically isolated from the outer can by ceramic insulators. The outer can consisted of a cylinder and two large end plates through which holes were drilled to enable the system to be supported by three rods extending from the flange on which the metastable gun was mounted.

Electrical connections were made such that with both deflector plates at earth potential and the target plate at -25V, any current measured leaving the target plate was due to both incident ions and metastable atoms. With one deflector plate at earth and the other at -120V the current leaving the target plate was due to metastable atoms alone. Thus it was a simple matter to get a measure of the efficiency of the source. For reasons given in section 3.2 it was hoped that any photoelectron component of the measured currents would be small. In the experiments described below, the pressure of helium in the buffer chamber was allowed to rise to the value it would be at in an actual experiment.

Three different sources were tested with this arrangement. The simplest and first source tried was based on the standard ion gauge, with the helium beam passing between a filament and an electron collector plate so that the electron path was perpendicular to that of the helium beam. A hemispherical guard was placed behind the filament to direct a larger percentage of the electrons to the collector plate. In an attempt to enhance the production of metastable atoms, a magnetic

field produced by a pair of Helmholz coils was directed perpendicular to these two paths. This would effectively direct the electrons into the helium beam. This source produced approximately 5 x 10^{11} metastable atoms sec^{-1} $steradian^{-1}$, the magnetic field having increased the production by a factor of 3.

The second source tested was similar in design to that used by Dunning et al[6]. Electrons from a circular filament, co-axial with and surrounding the helium beam, were accelerated by the application of a potential to a high transparency grid and then allowed to drift in a field free region defined by the grid and a cylinder approximately 2½" long. The electrons were constrained to move along the beam axis by the application of a magnetic field from a solenoid coaxial with the gun. Approximately 10^{12} metastable atoms sec^{-1} $steradian^{-1}$ were obtained from this source. Although the source was only marginally more efficient than the previous source, it had the advantage of causing a smaller spread in the resulting metastable atom velocities. However, neither of these sources produced metastable atoms in sufficient quantities to allow suitable experiments to be performed in the main chamber. It was felt that if the electrons could be focused on to the helium beam, the production of metastable atoms might be enhanced. With this in mind, a third source was designed by the author and this source was used for the experiments described in the following chapters.

The details of the gun are shown in the diagram

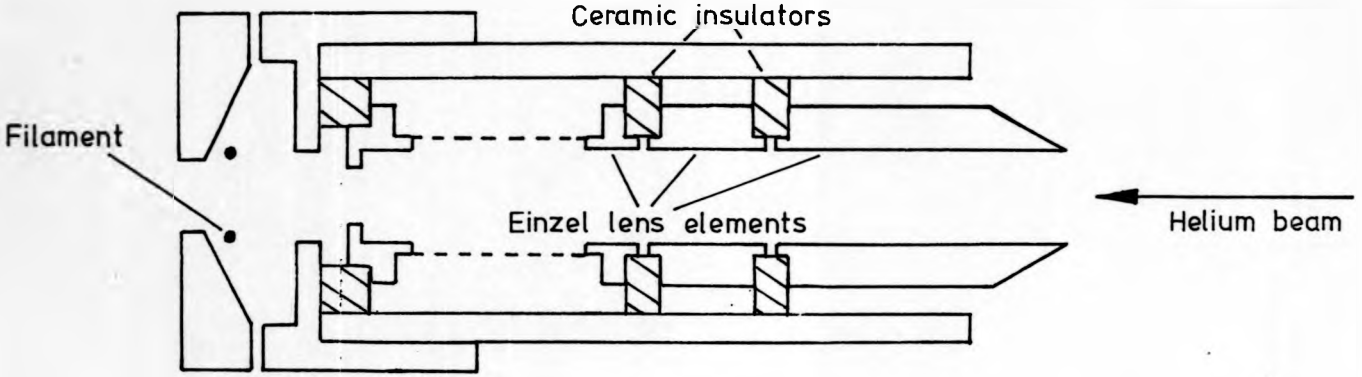

FIG. 3.4

The Metastable Atom Gun

PLATE 4

The Metastable Gun.

of fig. 3.4 and the photograph of Plate 4. The electron source was a single turn filament 6 mm in diameter made from .4 mm diameter thoriated tungsten wire and situated at the centre of a primitive Pierce electrode. As in the second source, this filament was set symmetrically around the axis of the beam. Electrons emitted from the filament passed into an einzel lens which crudely focused them onto the axis of the neutral helium beam. It should be noted that whilst the gun was designed using the principles of an electron gun, the size of the apertures in the lens elements will cause focal lengths to be rather ill-defined. All the gun elements were constructed from non-magnetic stainless steel with the first element of the einzel lens being largely composed of stainless steel mesh to facilitate the vacuum pumping of the region. The various elements were supported by ceramic spacers mounted inside a stainless steel tube which was then clamped to the Pierce electrode by screws. An additional increase in the intensity of metastable atoms was obtained by placing a solenoid around the gun assembly. The solenoid, made by winding copper wire onto a tufnol cylinder, was supported on two aluminium blocks which rested on the outside tube, and provided a field of between 100 and 200 gauss at the centre of the gun. The whole assembly was normally air cooled.

Typical operating conditions were to have the filament biassed at -40V, the first and third elements at 250V and the central element at -1.5kV. With 10.5

amps passing through the filament, approximately 15mA emission was obtained. All potentials were supplied by Farnell stabilised power supplies. The solenoid was driven with 2 amps taken from a Farnell power supply converted to give a constant current output. With this arrangement, a flux of 4×10^{14} metastable atoms $ster^{-1} sec^{-1}$ was typically obtained. It should be noted that this figure is an estimate based on the ejected electron current from a contaminated target. As has been described in Chapter 1 it was assumed that the results and hence the total electron yield would be in complete agreement with those obtained in Hagstrum's work on INS, and therefore no provision was made in the design for the measurement of absolute yields.

Typical characteristics of the gun are plotted in fig. 3.5. These curves represent the measured electron current from a tungsten single crystal for different operating conditions in the gun. It will be seen, fig. 3.5(a), that the current increases fairly linearly with applied magnetic field and that after a sharp increase, the current begins to level off as the voltage ratio V_2/V_1 on the electron lens is increased, fig. 3.5 (b). There is an approximately linear increase in secondary electron current with accelerating voltage for constant V_2/V_1 ratio, fig. 3.5 (c). In general the final operating conditions were decided by consideration of such problems as insulation breakdown and temperature rise in the gun region.

With helium flowing through this gun, the products included the metastable states of helium

FIG. 3.5

Overleaf is shown the variation in the total yield of secondary electrons from a contaminated tungsten surface as the conditions in the metastable gun are altered.

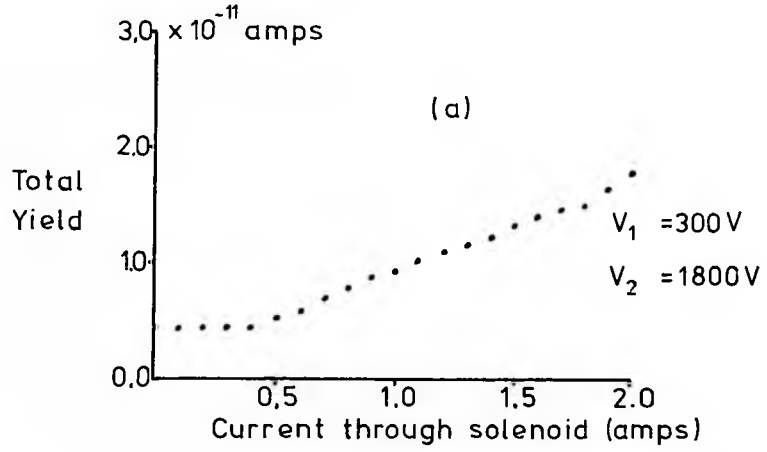
3.0 x 10^-11 amps
(a)
Total Yield
2.0
1.0
0.0
V1 =300V
V2 =1800V
0.5
1.0
1.5
2.0
Current through solenoid (amps)

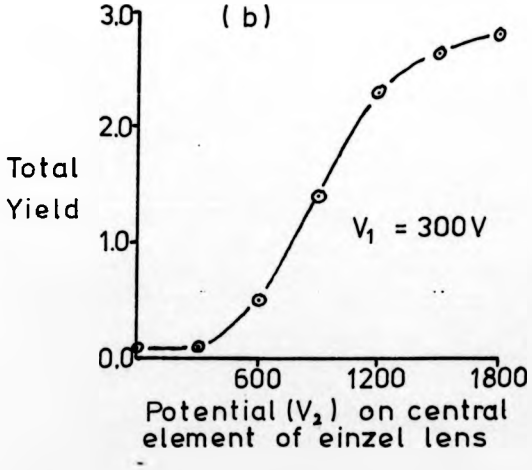
(b)
Total Yield
3.0
2.0
1.0
0.0
V1 = 300V
600
1200
1800
Potential (V2) on central element of einzel lens

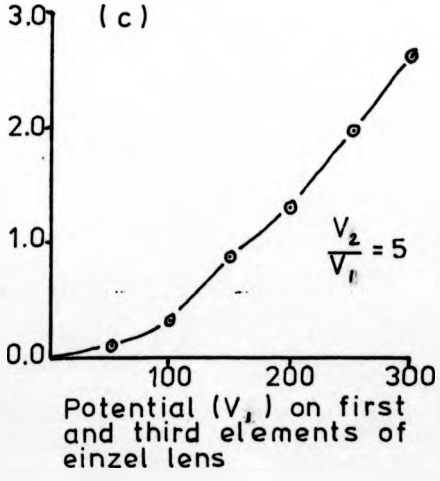
(c)
3.0
2.0
1.0
0.0
V2/V1 = 5
100
200
300
Potential (V1) on first and third elements of einzel lens

(2^3S and 2^1S), helium ions, stray electrons, helium atoms in the ground state, photons resulting from the relaxation of excited states and possibly helium atoms in the longer lived highly excited states.

The charged particles, that is the helium ions and electrons, were removed from the beam by the application of suitable potentials to deflector plates placed in the buffer chamber. It was found that by increasing the potential on the deflector plates, no further reduction in the current leaving the target occurred above a potential difference of approximately 60V, fig. 3.6. Therefore, by using 180V between the plates, there could be no charged particles in the beam. In fact the potential difference was raised to 1kV but no further reduction was noted.

To distinguish between the metastable atoms and resonant photons a technique based on that of R.F. Stebbings[1] was used. Ideally, an extra chamber for the beam to pass through should have been included in the original design. Increasing the pressure of some background gas such as argon in this chamber would gradually quench the metastable content of the beam and leave one with a measure of the photon content. However, as this chamber was not available, it was decided to increase the pressure of argon in the target chamber itself and monitor the target current as a function of pressure. As the target was at earth potential, this method was potentially fraught with problems, there being a number of ions and electrons drifting around the chamber as a result of Penning ionization. The results of this experiment are shown

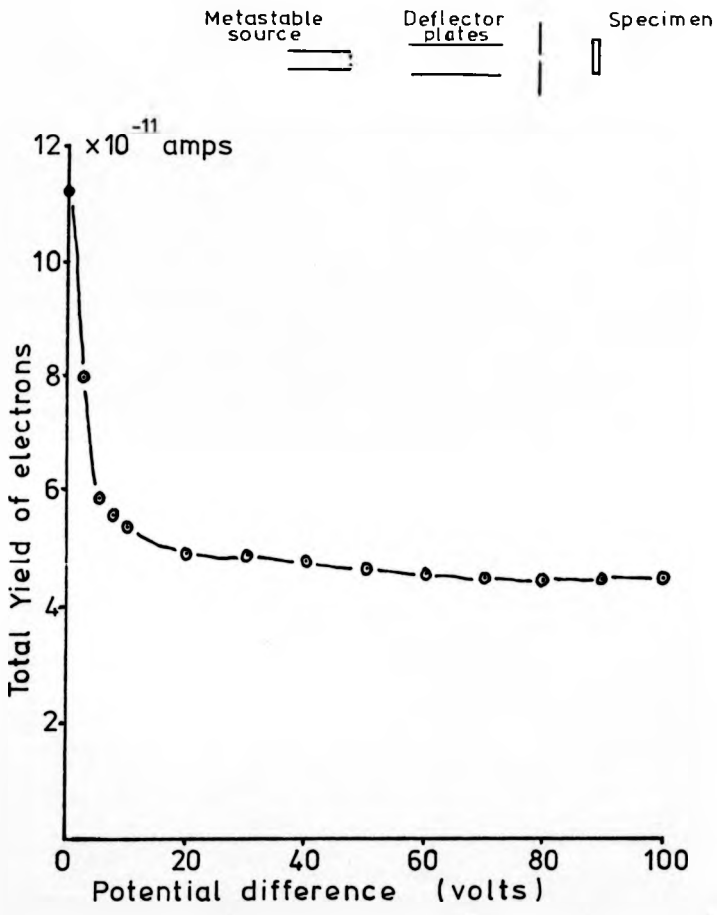

FIG. 3.6

The variation in the total yield of secondary electrons as a function of the potential difference applied to the deflector plates, positioned parallel to the beam as shown in the schematic diagram above.

in fig. 3.7.

The current at the target may be expected to follow the form

$$I = I_o \exp(-n\sigma x) \qquad (2)$$

where I_o is the initial flux, n is the density of argon atoms in the chamber, σ the cross-section for Penning ionization and x the distance travelled by the metastable atoms in the chamber. Using the relationship

$$n = 3.55 \times 10^{16} P \qquad (3)$$

where P is the pressure of argon, it will be seen that a graph plotting ln I against the pressure should be a straight line with gradient proportional to the cross-section for ionization. Such a graph has been plotted for the results of the present experiment in fig. 3.8. From this figure it will be seen that the gradient of the first half of the graph corresponds to an ionization cross-section of 6.45×10^{-16} cm^2 if it is assumed that the excited atoms travel a distance of 12 cm inside the target chamber. This value is in reasonable agreement with the cross-section for Penning ionization of argon by helium metastable atoms obtained by Benton et al[7] and Shollette et al[8], namely 6.6×10^{-16} cm^2 and 7.6×10^{-16} cm^2 respectively. The second half of the graph has a gradient which corresponds to an ionization cross-section of 5.575×10^{-17} cm^2. This value is slightly higher than that obtained by Stebbings[1] for the photo-ionization cross-section of argon by the helium resonance photon but this probably reflects the fact that there may still exist a few metastable atoms in this pressure range.

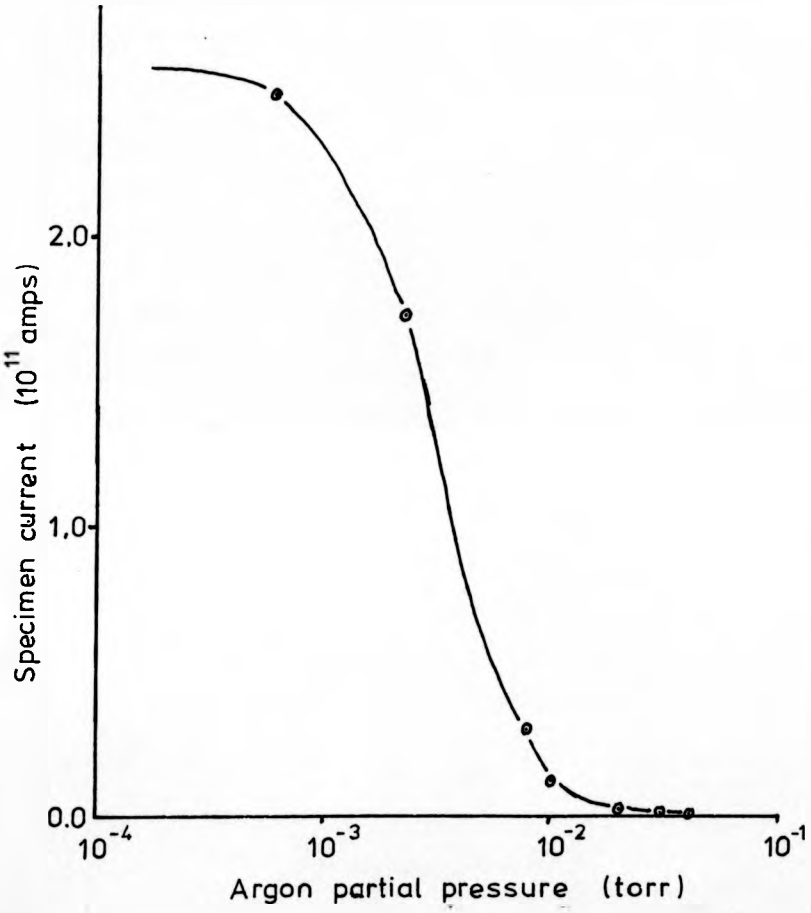

FIG. 3.7

The variation in the specimen current as a function of the partial pressure of argon in the target chamber.

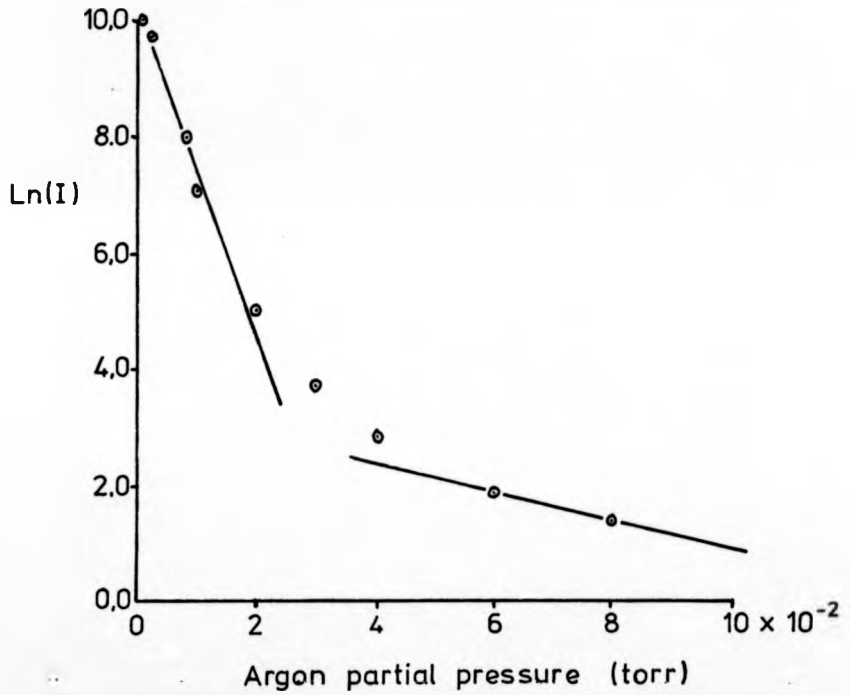
10,0
8,0
Ln(I)
6,0
4,0
2,0
0,0
0
2
4
6
8
10 x 10-2
Argon partial pressure (torr)

FIG. 3.8

By extrapolating the straight line due to the photon contribution back to the axis it is possible to obtain a measure of the percentage of secondary electrons excited by resonance photons. This procedure produces a figure of less than 0.1%, a negligible contribution.

Sibulkin and Gallaher[9] have shown that with helium in the source, the axial density n far downstream from a nozzle exhausting into a vacuum can be approximated by

$$\frac{n}{n_s} = 0.636 \left\{ \frac{a^2}{x^2} \right\} \qquad (4)$$

where n_s is the source density, a the radius of the nozzle and x the distance from the end of the nozzle. For a fully expanded nozzle beam (i.e., one in which the random thermal energy of the atoms in the source has been completely converted to directed translational energy along the beam axis), the mean velocity ratio becomes[5]:

$$\frac{v}{v_s} = \frac{\sqrt{\pi}}{2} \left[\frac{\gamma}{\gamma - 1} \right]^{1/2} \qquad (5)$$

where v_s is the mean velocity in the source and γ is the specific heat ratio of the helium. Using these equations and assuming that the secondary electron coefficient for a heavily contaminated tungsten surface is approximately 0.5, it is found that the metastable source excites approximately 1 in 10^6 of the atoms passing through it.

3.4 Neutral Helium Atoms Incident on a Metal Surface

As the majority of the incident atoms are in the neutral ground state it is necessary to consider the

interaction of such atoms with a metal surface. R. C. Amme[10] has shown that the secondary electron coefficient for neutral helium atoms only becomes comparable with that for incident helium ions when their incident kinetic energy is of the order of 200 eV. At normal room temperatures the secondary electron coefficient is so low that the neutral atoms may be expected to play no part in the electron emission from the metal surface. Further evidence supporting this conclusion may be drawn from the fact that the electron emission from the target was totally dependent on the excitation conditions in the source. The reduction in the secondary electron current as the pressure of argon in the target chamber was raised also leads to the conclusion that the metastable states of the helium atom were the source of secondary emission.

Finally it should be noted that the incident helium atoms will not be absorbed on the surfaces at room temperature. R. A. Fisher[11] has shown that the adsorption energy of a helium atom on a tungsten surface is only 300 cal./mole.

1. R. F. Stebbings, Proc. Roy. Soc. (London) A241, 270 (1957).

2. J. B. Hasted and P. Mahadevan, Proc. Roy. Soc. (London) A249, 42 (1958).

3. D. A. Maclennan and T. A. Delchar, J. Chem. Phys. 50, 1772 (1969).

4. B. Brutschy and H. Haberland, J. Phys. E 10, 90 (1977).

5. R. H. Jones, D. R. Olander and V. R. Kruger, J. Appl. Phys. 40, 4641 (1969).

6. F. B. Dunning, A. C. H. Smith and R. F. Stebbings, J. Phys. B: Atom Molec. Phys. 4, 1683 (1971).

7. E. E. Benton, E. E. Ferguson, F. A. Matsen and W. W. Robertson, Phys. Rev. 128, 206 (1962).

8. W. P. Sholette and E. E. Muschlitz, J. Chem. Phys. 36, 3368 (1962).

9. M. Sibulkin and W. H. Gallaher, AIAA J.1, 1452 (1963).

10. R. C. Amme, J. Chem. Phys. 50, 1891 (1969).

11. R. A. Fisher, Ph.D Thesis, The Pennsylvania State University, (1961).

CHAPTER FOUR

EXPERIMENTS PERFORMED ON THE NICKEL (100) SURFACE

4.1 Introduction

Experiments performed on the low index planes of pure metals can yield basic information about the nature of interactions in the surface region of metals. Because of the importance of nickel as a catalyst, its low index planes have been studied extensively in the past, using a variety of techniques. The experimental programme to be described was intended to investigate the potential and scope of the helium metastable interaction as a surface technique and nickel was chosen for the target metal thus allowing considerable scope for comparisons with other spectroscopies.

The original intention of this investigation was to study two or three of the low index planes, but time and circumstances did not allow the completion of this programme. A nickel specimen, cut to expose the (100) face, was prepared in the manner described in section 2.3. Following polishing, the specimen was mounted on the specimen holder which was vapour degreased before being installed in the target chamber.

4.2 Preparation of a Clean Nickel Surface

Following bakeout of the entire system, examination of the specimen using A.E.S. revealed contamination of the surface by phosphorus, sulphur, chlorine, and carbon. The "as loaded" Auger electron spectrum is shown in fig. 4.1. Following an anneal of the specimen at 800^{o}C for five minutes, it was found that sulphur had segregated

FIG. 4.1

Overleaf is shown an AES spectrum from the nickel surface before any cleaning procedure.

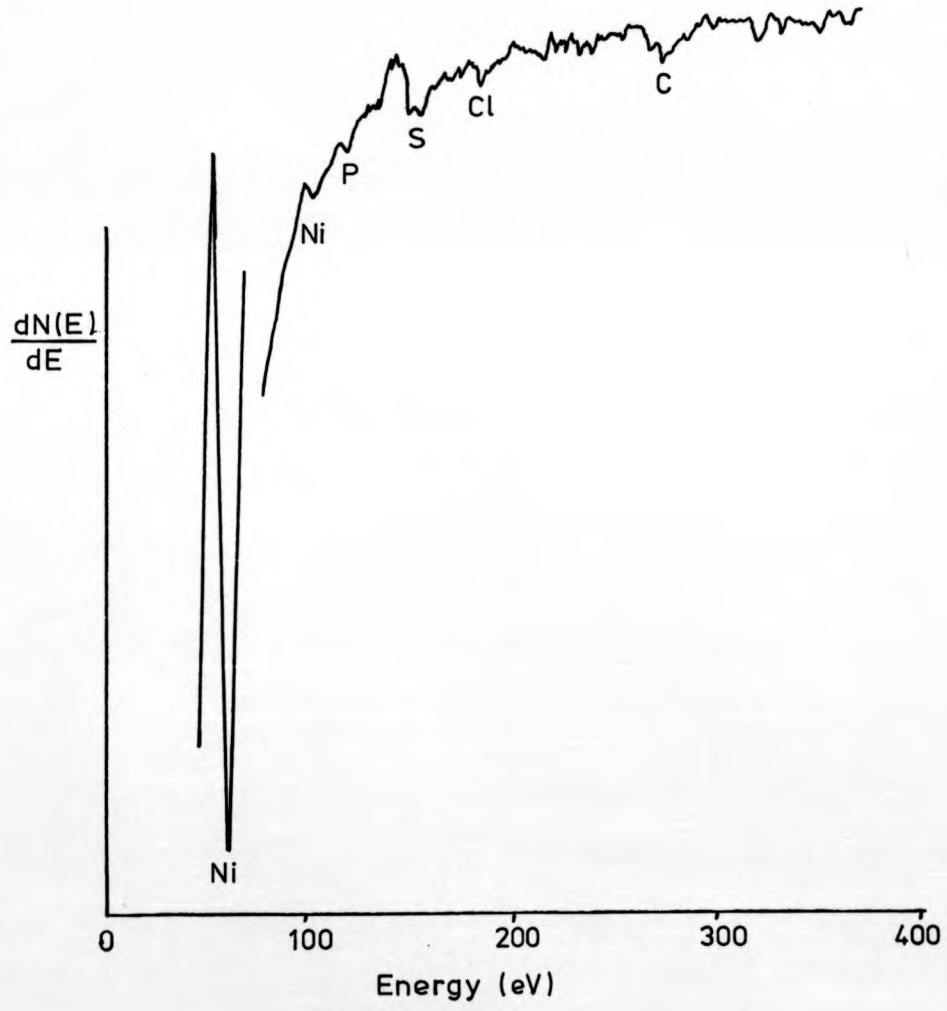
dN(E)
dE
Ni
Ni
P
S
Cl
C
0
100
200
300
400
Energy (eV)

to the surface and become the dominant contaminant as shown by the Auger electron spectrum; a typical spectrum is shown in fig. 4.2. This segregated sulphur was easily removed by bombarding the specimen for approximately 40 mins. with 2 μA of argon ions, of energy 500 eV. Although a LEED facility was not available in this particular system it is well known from both diffraction patterns and spot intensity measurements that argon ion bombardment damages the surface structure and therefore a short anneal is required to restore order to the crystal lattice. However, annealing causes more sulphur to segregate from the bulk and so it was found that cycles of bombardment followed by annealing had to be repeated until no further sulphur segregation occurred. At the end of this period, approximately 15 hrs. of bombardment, the main contaminant was found to be carbon, which was reduced by further cycles of bombarding and annealing. The Auger electron spectrum obtained from a surface having undergone this treatment is shown in fig. 4.3. At this stage it was thought that the specimen was clean and experiments were continued accordingly. However, examination of spectra obtained for the secondary electron energy distributions as a result of metastable atom impact would seem to indicate the presence of some residual contaminant, most probably carbon. In fact, a really clean surface was not obtained until the specimen had been annealed in an oxygen atmosphere at a later stage.

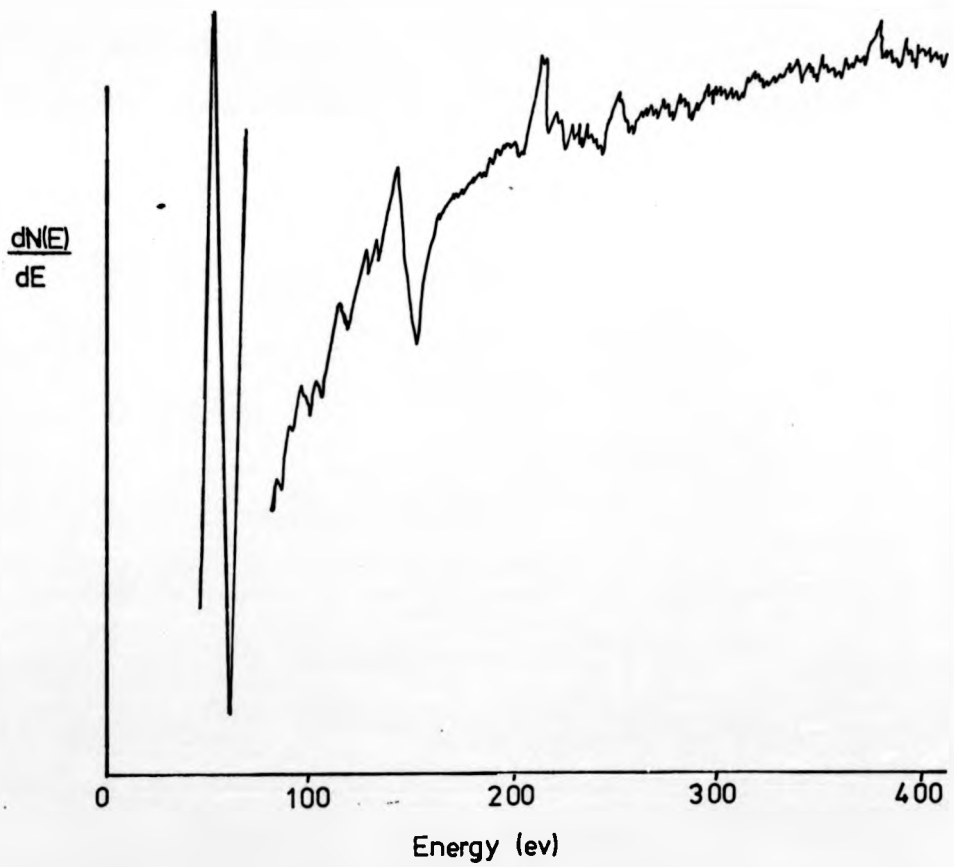

FIG.4.2

An AES spectrum showing that sulphur segregates to the surface during the annealing procedure.

FIG. 4.3

AES spectrum from the clean nickel surface.

When taking the Auger electron spectra shown here no attempt was made to look for the higher energy nickel peaks in the region of 850 eV. These peaks are more difficult to observe and do not give any further information on the degree of surface cleanliness.

4.3 Sulphur Adsorption on the Nickel (100) Surface

In an effort to understand the phenomenon of chemically irreversible poisoning of nickel catalysts by sulphur surface impurities, the interaction of sulphur with single crystal nickel surfaces, especially (100), has been intensely studied by numerous experimental techniques. These studies have shown that sulphur adsorption caused by thermal treatment following exposure to hydrogen sulphide in the gas phase, or segregation of sulphur from the bulk produces the same results in most experiments.

Marcus et al[1], from calculations based on LEED results, concluded that sulphur occupies a four fold site with the centre of the sulphur atom lying approximately 1.28 Å above the centre of the first layer of nickel atoms. Some quantitative measure of the degree of sulphur adsorption has been obtained by Perdereau[2] by means of AES. Using a radioactive form of hydrogen sulphide, she was able to calibrate the amount of sulphur adsorbed against the nickel as a standard. The system has been studied by Hagstrum[3] using INS and also in a number of experiments using low energy ion scattering[4, 5].

Early on in the course of this work, an experiment was performed to examine the effect of a slight

cleaning of the specimen surface on the total yield of secondary electrons arising from the de-excitation of the metastable atoms. It was found that the secondary electron current leaving the target continued to rise for about twenty minutes following a five minute anneal at 800°C. This experiment was performed five times in all and the average of the five sets of results is shown in fig. 4.4. At first it was thought that this may well have been a temperature effect due to cooling of the specimen but on repeating the experiment from a surface that was known to be clean it was found that the secondary electron current was constant over the same time period. The results of such an experiment are also included for comparison in the figure. The fact that the "dirty" surface curve lies under the clean surface curve in the early part of this graph is merely a reflection of the conditions in the metastable gun not being equivalent on the two occasions.

Concurrent with these observations, a series of Auger electron spectra was taken. Obviously with spectra which typically took times of three to four minutes to record it was not possible to take Auger electron data as frequently as the metastable secondary electron measurements. However it was noted that on these Auger electron spectra, the ratio of the sulphur 150 eV peak to peak height to the nickel 62 eV peak to peak height increased as the specimen cooled, fig. 4.5(a). Such an increase in the segregant coverage as the specimen cools is predicted by the segregation equation first derived by Maclean[6] to describe solute segregation to

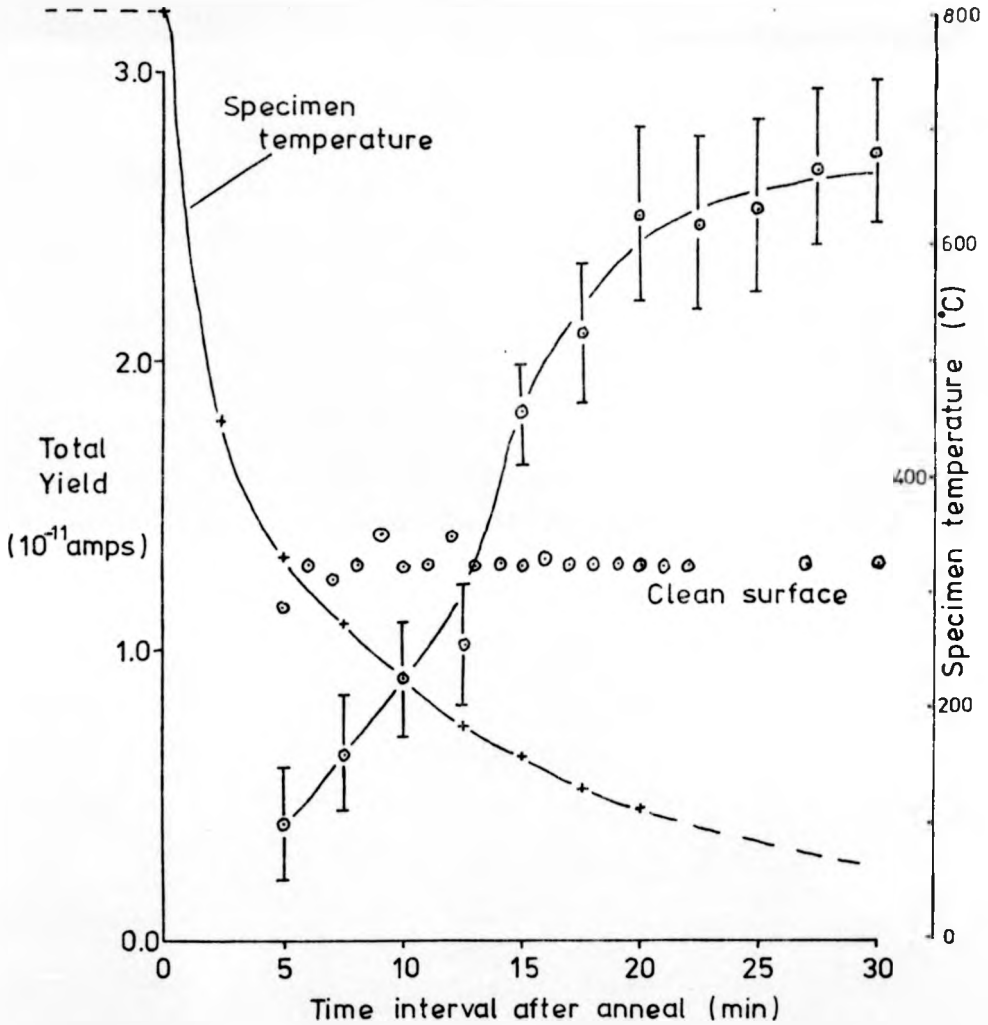

FIG. 4.4

The variation in the total yield of secondary electrons as the specimen cooled from 800 °C, both for the situation where sulphur segregated to the surface and for the clean surface. The specimen temperature is also shown.

FIG. 4.5

Overleaf are shown;

a) the variation in the ratio of the Auger peaks for sulphur and nickel as the specimen cooled from 800 ^{o}C, and

b) the total yield of secondary electrons plotted as a function of this ratio. Perdereau's calibration is also given in this latter figure.

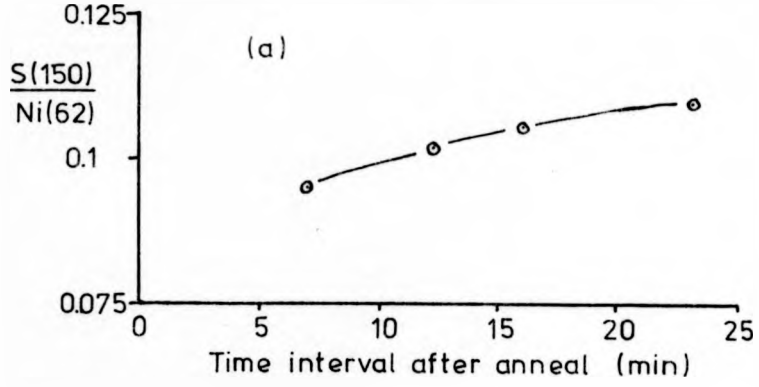
0.125
S(150)
Ni(62)
0.1
0.075
(a)
0
5
10
15
20
25
Time interval after anneal (min)

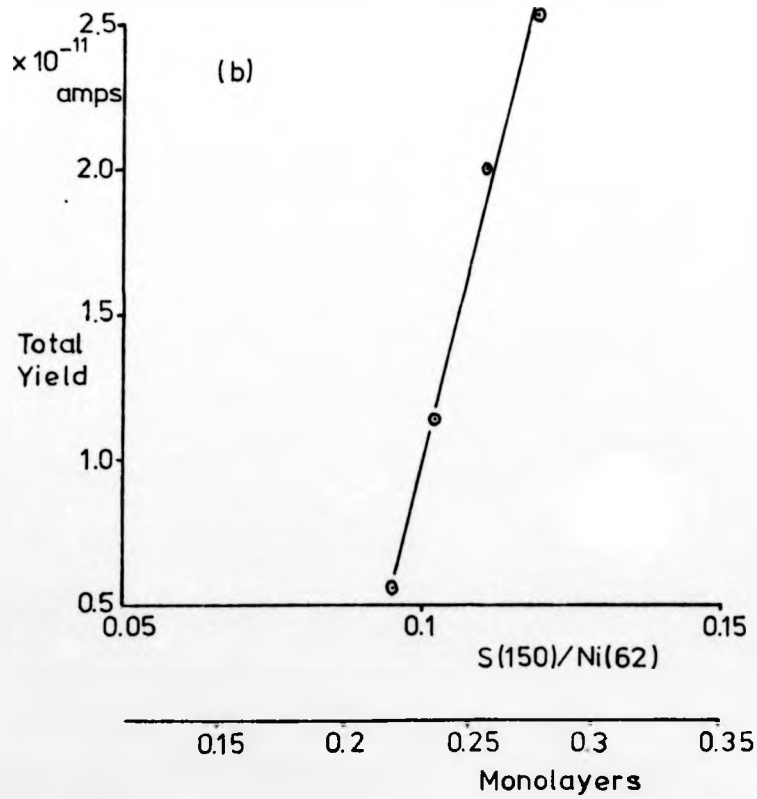
2.5
x 10^-11
amps
(b)
2.0
1.5
Total
Yield
1.0
0.5
0.05
0.1
0.15
S(150)/Ni(62)
0.15
0.2
0.25
0.3
0.35
Monolayers

grain boundaries. If X_s is the segregant coverage expressed as a molar fraction of a monolayer, Maclean's equation gives

$$\frac{X_s}{1 - X_s} = \frac{X_b}{1 - X_b} \exp(E/RT) \qquad (1)$$

where X_b is the solute molar fraction and E is the molar heat of adsorption of the segregant at the grain boundary. With $X_b \ll 1$, equation (1) may be rearranged to give

$$X_s = \frac{X_b \exp(E/RT)}{1 + X_b \exp(E/RT)} \qquad (2)$$

From this equation it will be seen that X_s will decrease as the temperature T of the specimen is raised.

Perdereau[2] demonstrated that the peak-to-peak intensity ratio of the sulphur 150 eV peak to the nickel 62 eV peak increased linearly with the sulphur coverage. It is therefore of interest to plot the total current yield against the Auger electron intensity ratio S/Ni as is shown in fig. 4.5(b). It will be seen in this figure that there exists a linear relationship between the increase in the total yield and the sulphur coverage. The rate of increase of the total yield with coverage is given by the gradient of this line and in this case it is 3.6×10^{-10} amps monolayer^{-1}.

What is thought to be a fairly representative metastable electron energy distribution taken whilst sulphur was the main contaminant is shown in fig. 4.6(a). For comparison, the electron energy distributions obtained by Hagstrum[3] using INS on sulphur contaminated surfaces

FIG. 4.6

a) The secondary electron energy distribution resulting from metastable atom impact on a sulphur contaminated surface.

b) The secondary electron energy distributions resulting from 5 eV helium ions incident on sulphur contaminated surfaces.

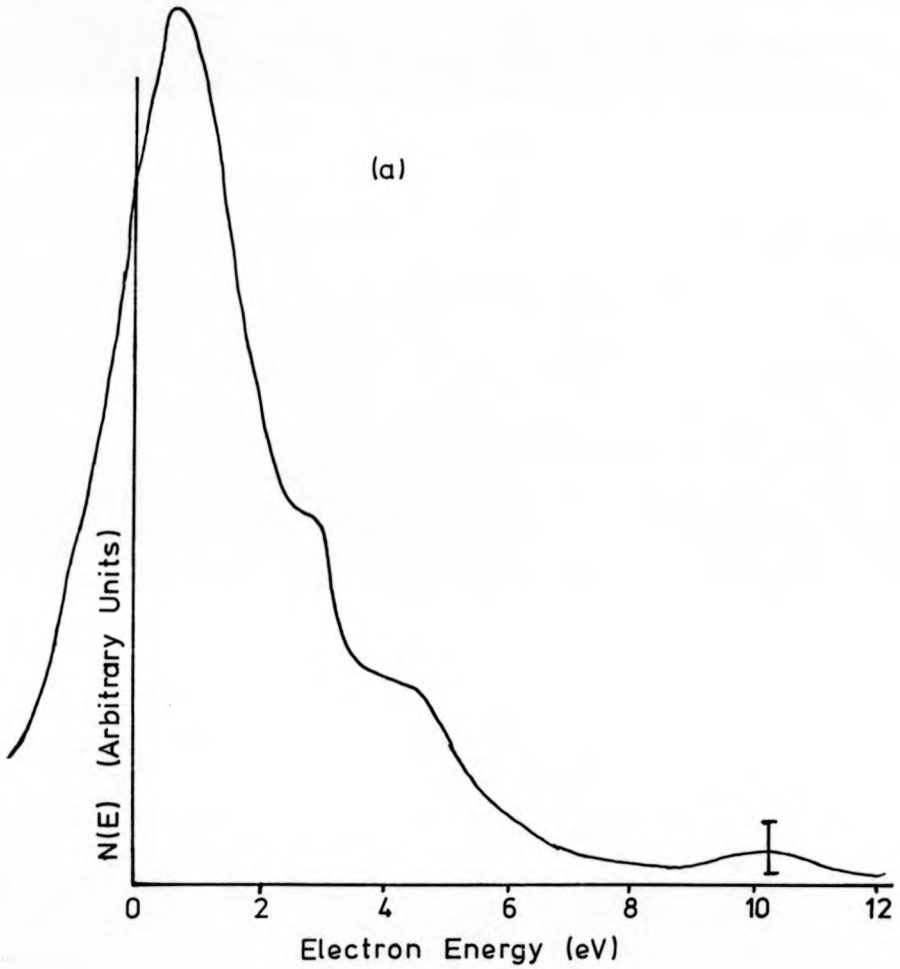
(a)
N(E) (Arbitrary Units)
0
2
4
6
8
10
12
Electron Energy (eV)

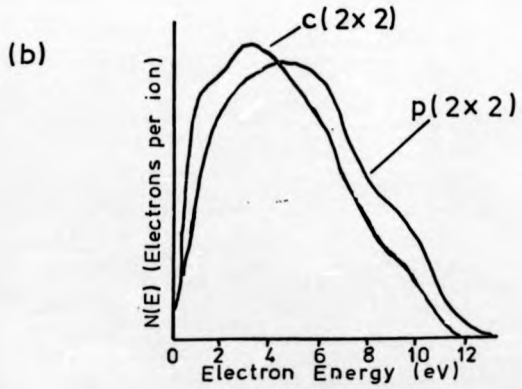
(b)
c(2x2)
p(2x2)
N(E) (Electrons per ion)
0
2
4
6
8
10
12
Electron Energy (eV)

are shown in fig. 4.6(b). He does not publish any figure for the total yields in his papers, but approximate integrations of his electron energy distributions show a decrease in the secondary current by a factor of 14.8% for the p (2 x 2) structure and 20% for the c (2 x 2) structure. These two structures correspond to ¼ and ½ monolayer coverage respectively.

4.4 Metastable Atom Impact on a Clean Nickel Surface

The metastable electron energy distributions displayed in the previous section and in this section were obtained using the a.c. techniques descibed in section 2.8. Spectra were taken using different time constants and ramp speeds. Following Sevier[7], ramp speeds were chosen so that the desired resolution ΔE was scanned in a time interval given by 5τ, where τ was the time constant of the detection system. The resolution was defined approximately by the modulation superimposed on the retard voltage applied to the grids. Thus, if the modulation was typically 300 mV peak to peak, then a time constant of 30 ms would mean that 300 mV was to be scanned in 150 ms or as an entire scan usually covered 22V, each scan would take approximately 12.5 secs. It was found that following the annealing procedure after argon ion bombardment of the specimen, the pressure in the target chamber would return to better than 5×10^{-10} torr in 2½ mins. Referring back to fig. 4.4 will show that, following this cleaning procedure, there is no change in the total yield of electrons resulting from metastable impact for at least 30 mins. This would indicate that the

state of cleanliness of the surface did not change during that period and it was therefore felt that electron energy distributions could be averaged for 30 mins without contamination problems.

A typical spectrum from a "dirty surface", that is a surface that had been standing in a vacuum of the order of 10^{-10} torr for 24 hrs., is shown in fig. 4.7. An Auger electron spectrum from this surface showed carbon contamination. Also shown in the figure is the metastable atom secondary electron energy distribution taken from a clean surface. The side structure, arrowed at 2.2 eV, was always clearly seen on the spectra taken from dirty surfaces. Upon cleaning the surface, the most obvious difference to be noted is the 75% drop in total yield of electrons. This reduction in yield lowered the signal to noise ratio making it difficult to label any possible features in the "clean surface" spectrum. As has been stated earlier in section 4.2, it now seems likely that the surface which was thought to be clean at this stage possibly had small traces of carbon left on it. Following a few trial experiments with oxygen, the "clean surface" spectrum changed slightly as will be shown later.

In view of the signal to noise problems associated with the low yields from the clean surface, it was decided to attempt to take data from the clean surface using a d.c. method. This method, which will be described more fully in the next chapter, consisted basically of measuring the collector current as a function of the

FIG. 4.7

The secondary electron energy distributions from a contaminated nickel surface and from the same surface following cleaning.

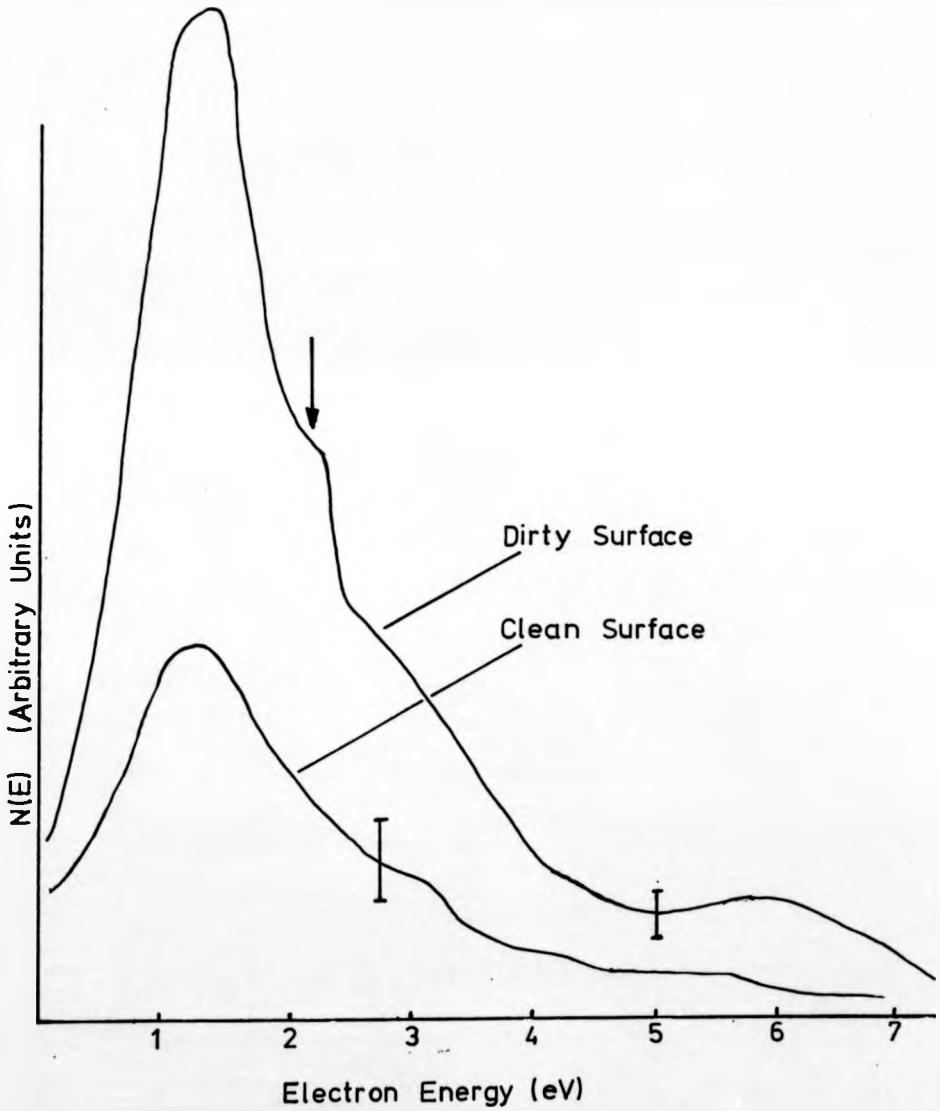
N(E) (Arbitrary Units)
Dirty Surface
Clean Surface
1
2
3
4
5
6
7
Electron Energy (eV)

retard voltage applied to the analyser grids, digitising the resulting curve, and then differentiating the digital function to give a measure of N(E). Using this method, the time taken to obtain a spectrum was reduced to two minutes as opposed to twenty, and a scan could be commenced more quickly after annealing the surface as the distortion of the grids, described earlier in section 2.4, had less of an effect on the resulting spectrum. Against these advantages it should be noted that this method obviously has poorer resolution.

The result of such an experiment conducted on a clean surface is shown in fig. 4.8. Clearly the energy distribution has now been resolved into two distinct peaks, a feature that was consistently reproducible. Rather fortuitously, an understanding of this structure is obtained by examination of a series of electron energy distribution spectra from a dirty surface, taken with the target biased at different potentials, fig. 4.9. At each stage, the target potential was made more negative, thus giving the electrons leaving it a higher energy. As will be seen in the figure, this process causes the distribution to separate into two components: one component moving along the axis with increasing target potential and one fixed and centred approximately on the zero of the energy scale. Obviously the component which moves with target potential is representative of the energy distribution of the electrons leaving the target. The other component is mainly composed of secondary electrons leaving the grids as a result of electron impact. Hagstrum[8] published a similar spectrum

FIG. 4.8

The secondary electron energy distribution from the clean nickel surface, measured using the d.c. technique.

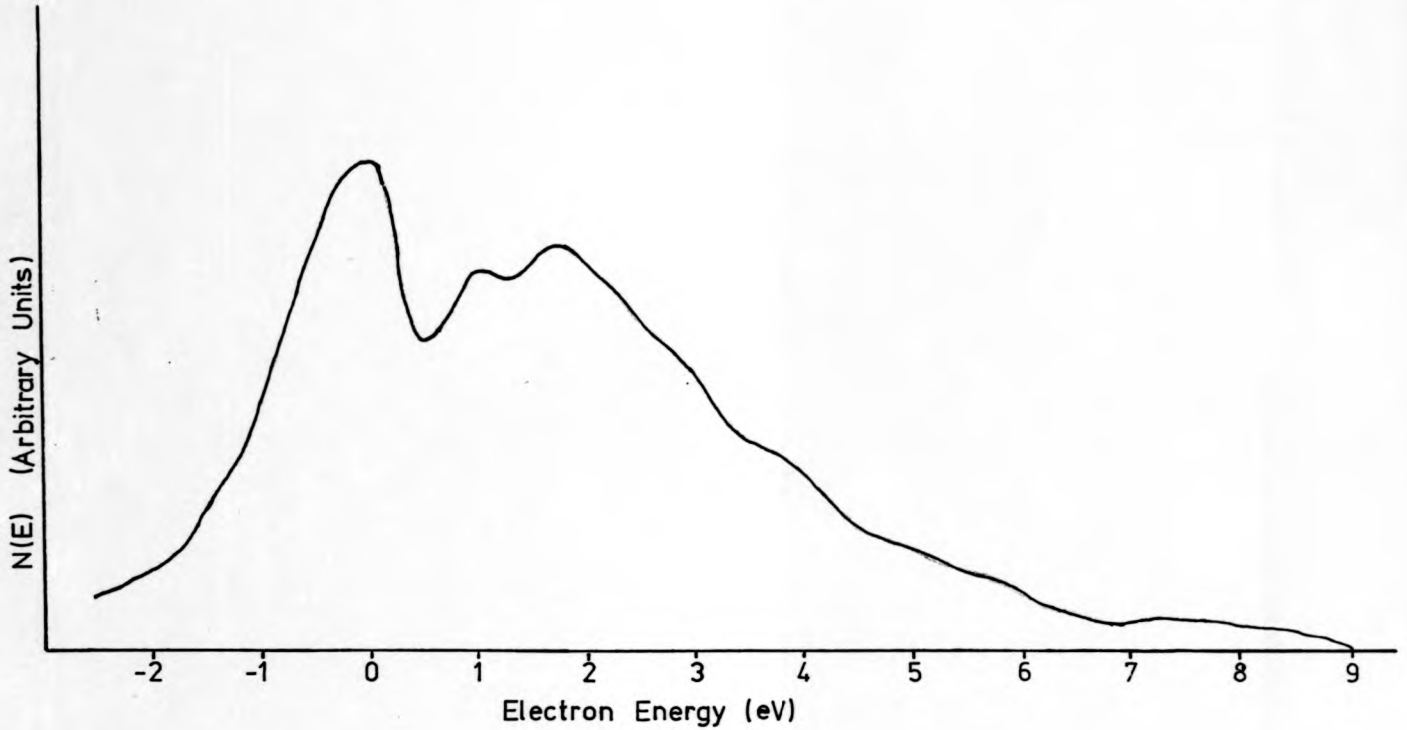
N(E) (Arbitrary Units)
-2
-1
0
1
2
3
4
5
6
7
8
9
Electron Energy (eV)

FIG. 4.9

Overleaf are shown the secondary electron energy distributions recorded from a contaminated nickel surface with the specimen biassed at different potentials.

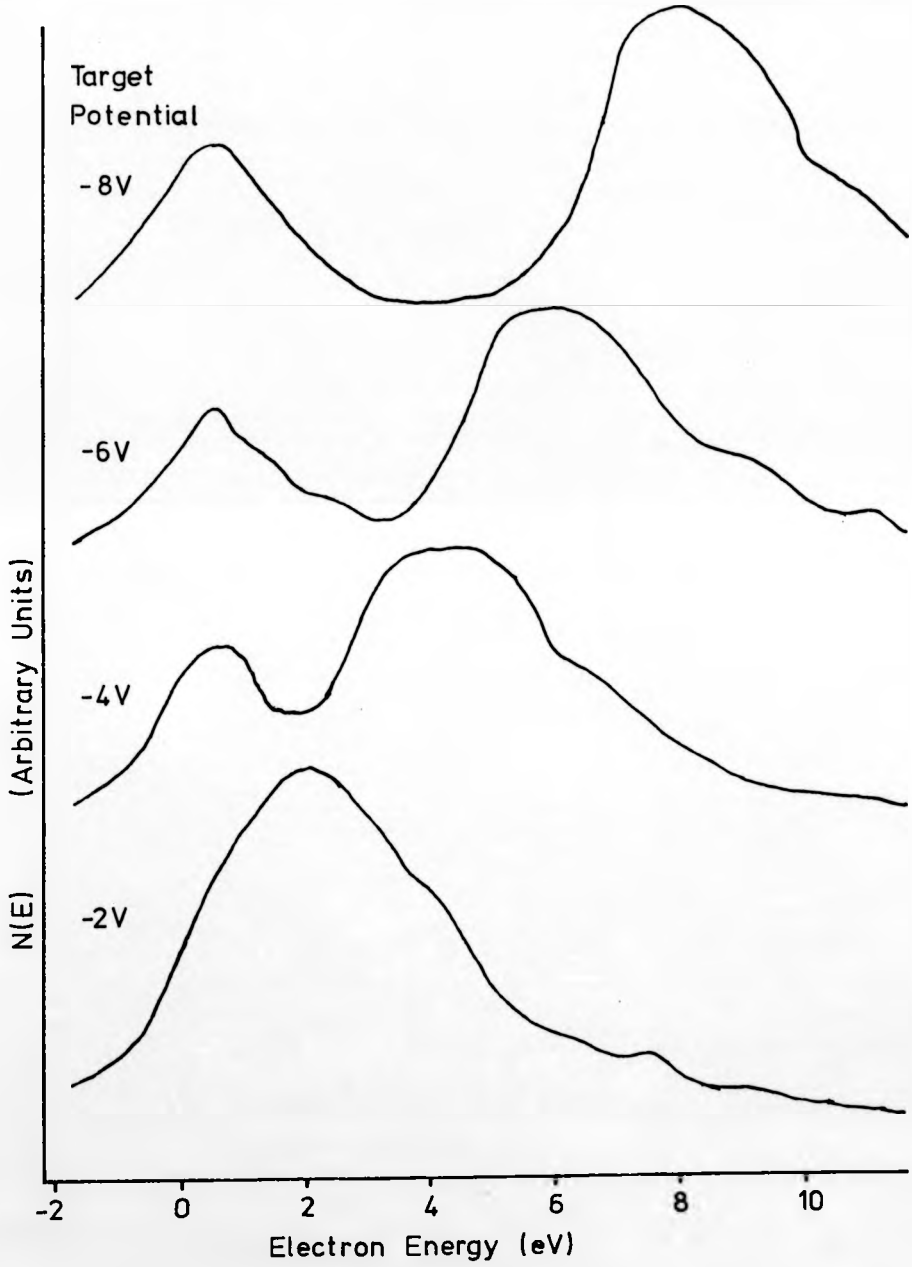
Target
Potential
-8V
-6V
-4V
-2V
N(E) (Arbitrary Units)
-2
0
2
4
6
8
10
Electron Energy (eV)

and attributed the low energy component as secondary electrons arising from the grid in his system.

We are now in a position to interpret the spectra of figures 4.7 and 4.8. The clean surface spectrum of figure 4.8 contains two components. The first, peaked at about zero eV, is an artifact due to the presence of the grids. The second component, peaked at 2.0 eV, is at approximately the same energy as the side structure on the dirty surface spectrum. Thus we might suspect the dirty surface spectrum of consisting of three components: two as seen on the clean surface spectrum and a third sited between these two and resulting from contamination of the surface.

Returning to a.c. techniques at a later stage, an unfortunate incident left the specimen holder with no filament for electron bombardment. This meant that it was not possible to anneal the surface following argon bombardment. However the electron energy distributions obtained before and after bombardment are shown in fig. 4.10. It will be seen that the "clean" surface spectrum reproduces that obtained using the d.c. method. It should be noted that for these spectra the time constant used was 1 sec as opposed to 30 ms for the other spectra and this reduced the effective bandwidth of the detection system. Auger electron spectra following argon bombardment revealed no trace of argon on the surface.

4.5 Oxygen on Nickel (100)

In recent years there have been many studies of the system of oxygen adsorption on nickel. It has been

FIG. 4.10

The secondary electron energy distributions obtained from the nickel surface before and after argon ion bombardment.

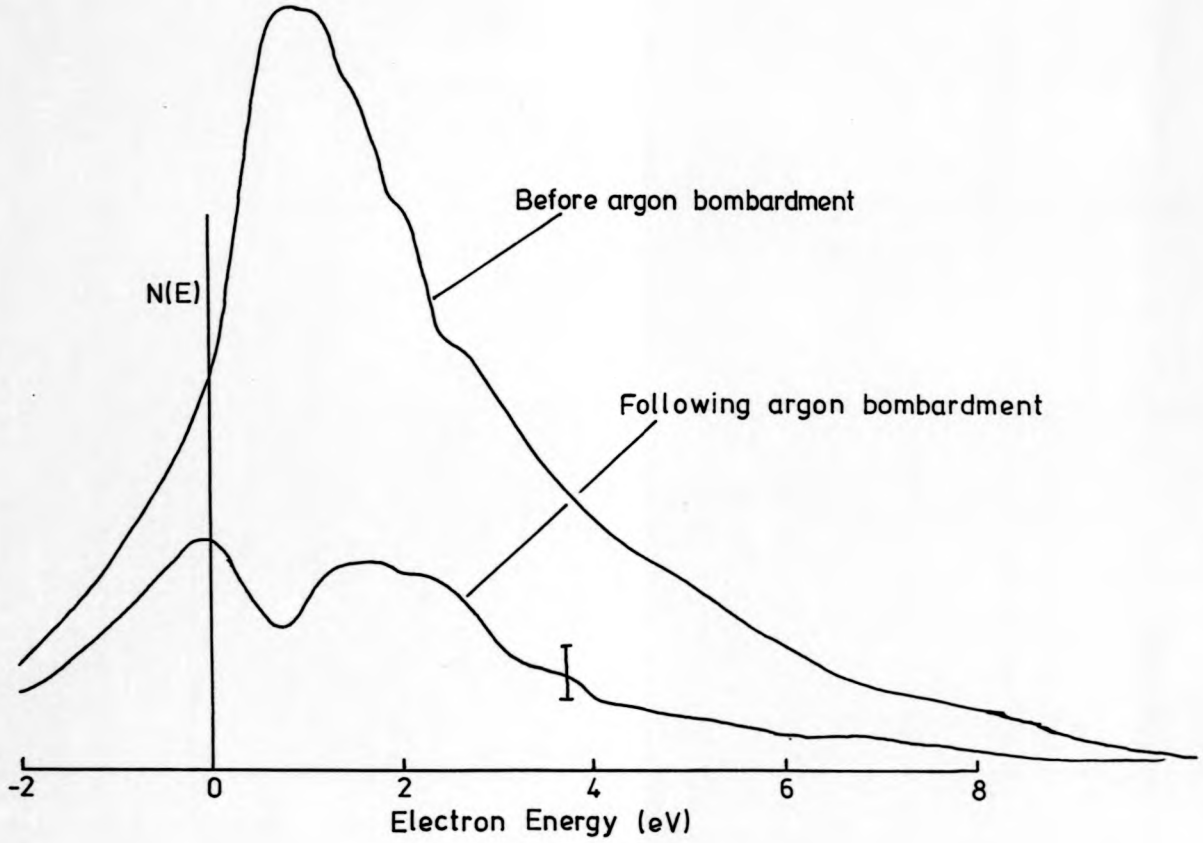
Before argon bombardment
N(E)
Following argon bombardment
-2
0
2
4
6
8
Electron Energy (eV)

known for many years from LEED studies that two ordered surface structures can be obtained during the adsorption of oxygen on a Ni (100) surface. A p (2 x 2) pattern is obtained at a coverage of $\frac{1}{4}$ monolayer and this becomes a c(2 x 2) pattern at $\frac{1}{2}$ monolayer. Various models have been put forward to explain these structures, but there now seems to be general agreement that the oxygen comprises a non-reconstructed layer, each oxygen atom forming a pyramid bonding with four nickel atoms as shown in fig. 4.11. Elaborate calculations based on the intensities of the LEED spots have produced a value of 0.9 Å for the distance between the oxygen layer and the first nickel plane[1].

Using INS, Hagstrum[3] examined the electronic density of states for both the clean and oxygen covered Ni (100) surface. Upon adsorption of oxygen, he observed a decrease in emission from the nickel d band and the emergence of a resonance approximately 5.5eV below the Fermi level. A similar feature has been observed in UPS experiments[9].

There has also been a considerable amount of work carried out on the kinetics of the oxygen uptake[10,11]. In general, a two step process is observed: chemisorption followed by oxidation. Horgan and King[12] interpreted their data as indicative of non-dissociative chemisorption. However photoelectron spectroscopic studies have shown that the process is dissociative chemisorption, followed by oxide nucleation and lateral oxide growth to a limiting coverage of 3 NiO layers.

FIG. 4.11

Overleaf are shown the different ordered structures of oxygen adsorbed on the Ni(100) surface. On the clean surface the two-dimensional surface net (a) is compared with the projection of the three-dimensional (or X-ray) unit cell (b). On the c(2 x 2) oxygen structure the two commonly accepted notations are indicated, namely c(2 x 2) (d) and $(\sqrt{2} \times \sqrt{2})R45^{\circ}$ at (e).

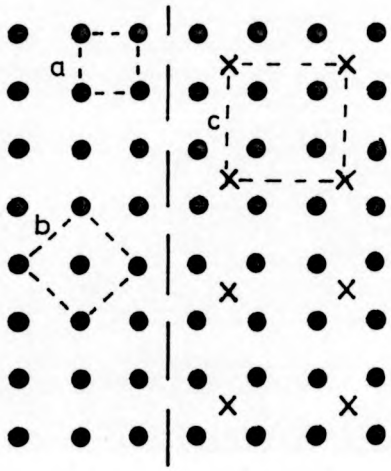
a
b
c
CLEAN
P(2x2)

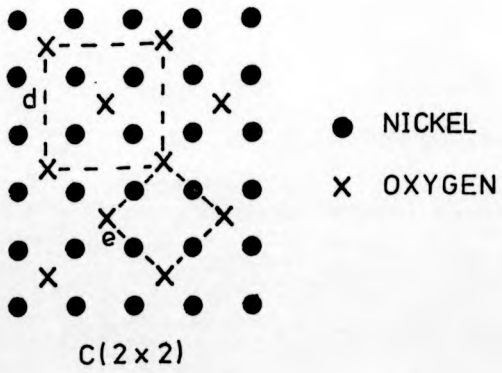
d
e
NICKEL
OXYGEN
C(2x2)

For the purposes of the present investigation, it was felt that it would be of interest to examine the possibility of linearity between the increased total yield of secondary electrons and surface coverage of oxygen atoms. The metastable atom beam was directed at the target and the secondary electron current measured. Oxygen was introduced to the target chamber via a silver thimble to a pressure of 10^{-8} torr. With the high purity of gas to be expected from such a system, no attempt was made to analyse the actual gas content of the chamber. The total yield of secondary electrons was then measured as a function of the length of exposure of the target surface to the oxygen with the heat shield being used to prevent the helium beam hitting the target in between measurements. The results of this experiment are shown in fig. 4.12 where the measured yields have been plotted against exposure (1 Langmuir = 10^{-6} torr sec). These exposures have been corrected to the relative nitrogen pressures allowing for the sensitivity of the ion gauge to oxygen. Also included in the figure is the calibrated coverage as a function of exposure from the work of Norton et al[11].

It will be seen that there is quite remarkable agreement in the general shape of the curves although there is a slight discrepancy in the total exposures required. This disagreement could easily be explained by incorrect pressure measurement in one or both experiments. It is interesting to note that for $\frac{1}{4}$ monolayer of adsorbed oxygen the total yield had increased by an extra 1.18×10^{-11} amps over the value of 1.5×10^{-11} amps

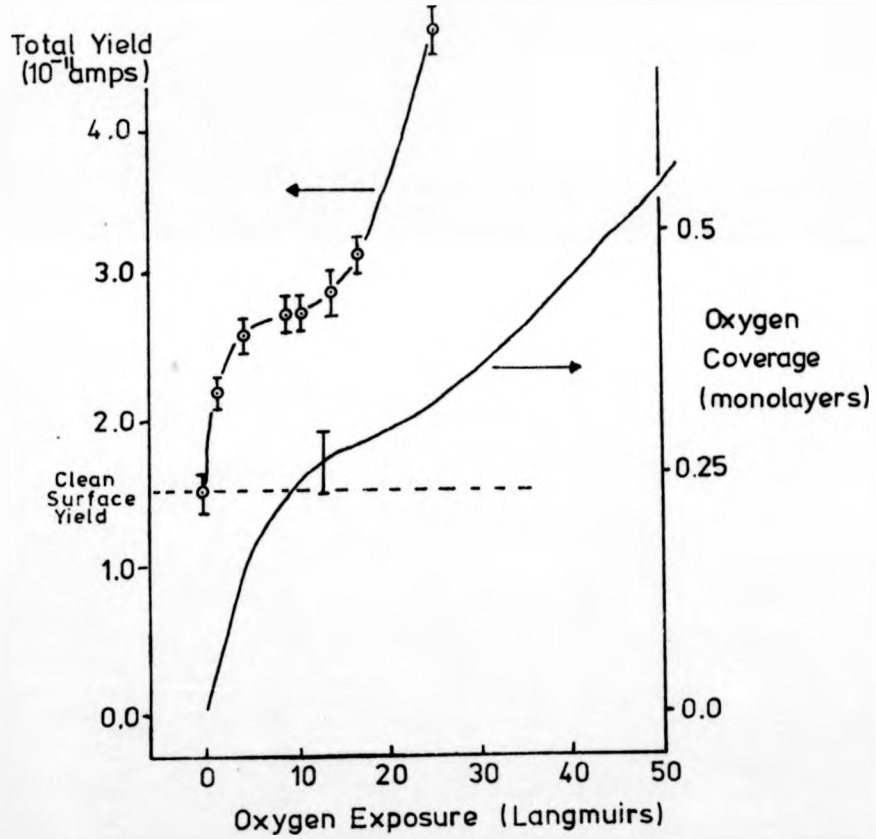

FIG. 4.12

Comparison of the increase in the total yield of secondary electrons as a function of oxygen exposure with the growth of the O 1s peak area as measured in XPS experiments[11].

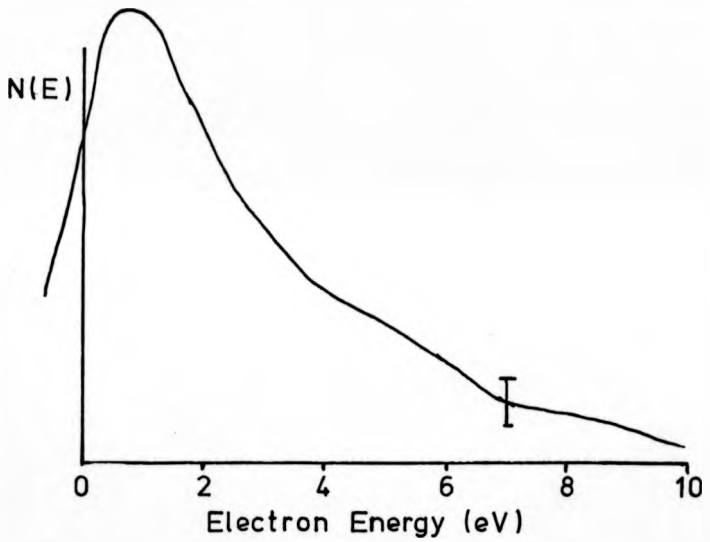

FIG. 4.13

The secondary electron energy distribution recorded from a surface with adsorbed oxygen.

from a clean surface. For ½ monolayer the total yield had increased by an extra 2.34 x 10^{-11} amps or twice the value for a ¼ monolayer. From this experiment it would therefore seem that the increase in yield is linear with coverage, as was the case with sulphur. The rate of increase in the total yield with oxygen coverage is 4.72 x 10^{-11} amps monolayer^{-1}. If this is to be compared with the rate of increase for sulphur adsorption the latter rate must be multiplied by a factor of approximately five to account for different operating conditions in the metastable source. This results in the rate of increase of the total yield being approximately four times higher for sulphur than for oxygen. Examination of the actual electron energy distribution following oxygen exposure revealed no new structure. In fact the distribution gave every indication of returning to that from a "dirty" surface. The distribution obtained after an exposure of 12 Langmuirs is shown in fig. 4.13.

4.6 Reflection of Metastable Atoms and Emission of Ions

Hagstrum[13] has demonstrated that for the simple collector- target system, secondary and tertiary emission plays an important and often misleading part in the measurement of any currents. His analysis is applied to the interaction of ions with the target, but it is quite instructive to apply a similar argument to the case of incident metastable atoms.

The possible secondary and tertiary emission currents in a conventional target and collector assembly are shown in fig. 4.14. The addition of grids will further complicate the matter but will be neglected for the present. Referring

FIG. 4.14

Overleaf are shown the secondary and tertiary currents to be expected in the conventional collector/target system. The effect of the inclusion of retard grids biassed at -175V is shown in the second half of the figure.

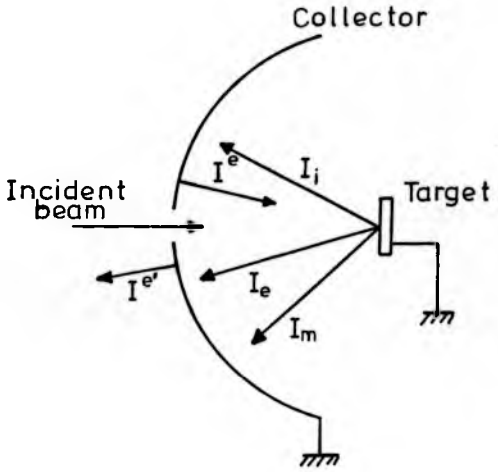
Collector
Incident beam
Target
I^e
I_i
$I^{e'}$
I_e
I_m

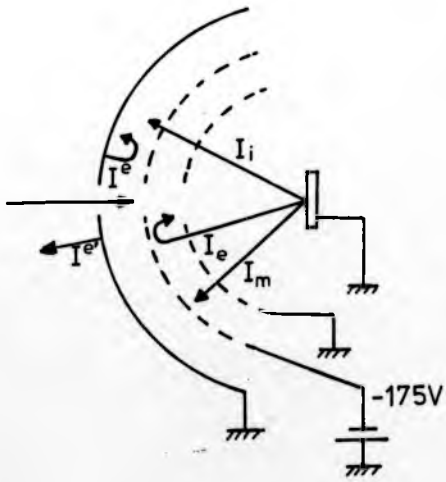
I^e
I_i
$I^{e'}$
I_e
I_m
-175V

to the figure, it will be seen that the incident metastable atom beam can give rise to secondary electrons, ions and also reflected metastable atoms. These currents leaving the target will all give rise to secondary and tertiary emission from the collector and therefore the resulting current I measured at the collector should be

$$I_c = I_e - I_i - I^e - I^{e'} \qquad (3)$$

The subscripts refer to species arriving at the collector, e for electrons and i for ions, and the superscripts to electrons leaving the collector: I^e includes secondary electrons resulting from incident electrons, ions and metastable atoms. $I^{e'}$ refers to electrons leaving as a result of metastable atoms hitting the back of the collector. In order to look for possible ion emission it is necessary to suppress the electron currents that are arriving at and leaving the collector. This is simply achieved if retarding grids biased at - 175V are included in the picture. With a retarding voltage of this order electrons will be prevented from travelling to the collector and also from leaving the front of the collector. The resulting collector current is thus

$$I_c = - I_i - I^{e'} \qquad (4)$$

However the current leaving the back of the collector $I^{e'}$ was of the same order of magnitude as the ion current I_i and therefore it was necessary to bias the target at -24V to suppress ion emission from its surface. Thus the measured collector current became

$$I_c = - I^{e'} \qquad (5)$$

The difference in measured collector currents, (4) and (5), will then be a measure of the positive ion flux from the target.

This measurement was performed for a dirty surface and a clean surface. For the dirty surface, the positive ion current was 1.5×10^{-13} amps when the electron current ejected from the target was 5.5×10^{-11} amps. For the clean surface, the ion current was immeasurable within the noise limits. This result suggested that the ions leaving the target were desorbed contaminant species rather than incident metastable helium atoms reflected as ions. In order to check this hypothesis, an attempt was made to monitor the positive ion emission as oxygen was gradually adsorbed onto the nickel surface. The target was exposed to six Langmuirs of oxygen, by which time the electron emission had increased by 80% but no ion emission was observed.

Oliphant[14] examined the problem of reflection of the metastable atoms and reported a change in the reflection coefficient both with the incident energy of the metastable atoms and with the state of cleanliness of the surface. Allison et al[15] also considered the possibility of reflection but found no change in the reflection probabilities upon heating their targets from 20°C to 250°C. The latter authors suggested that the results which Oliphant had interpreted as evidence of reflection may well have been caused by spurious scattering and excitation transfer effects due to a high residual pressure of helium.

For an examination of the reflection of

metastable atoms in this system, it was decided that it would be convenient if the reflected atoms struck another surface that was well away from the incident beam axis. Any attempt to measure reflected metastable atom currents at the collector would be complicated by tertiary electron currents. Accordingly an attempt was made to measure the reflected metastable intensity on the deflection plates at the end of the electron gun. As has already been described (section 2.7) the axis of this gun was perpendicular to the axis joining the target and collector.

With the target held at + 50V, to prevent secondary electrons leaving it, and the gun deflection plates at -9V, the current leaving these plates was measured as a function of the angle between the target normal and the incident beam direction. It should be noted that with this experimental arrangement ions are capable of arriving at the deflection plates. The results of this experiment conducted on a dirty surface are shown in fig. 4.15. It can be seen that the maximum current was obtained when the target had been turned through 50°. Considering the orientation of the deflector plates, this result is indicative of specular reflection for a small percentage of the incident metastable atoms. With the target turned through 50° it was found that for a "dirty" surface the ratio of the current leaving the deflector plates to the current leaving the target was 0.012. On cleaning the surface it was found that whilst the measured current from the target fell by 80% the current leaving the deflector plates had fallen by only

FIG 4.15

The variation in the measured current leaving the deflector plates of the electron gun as a function of the angle between the surface normal of the specimen and the incident beam direction.

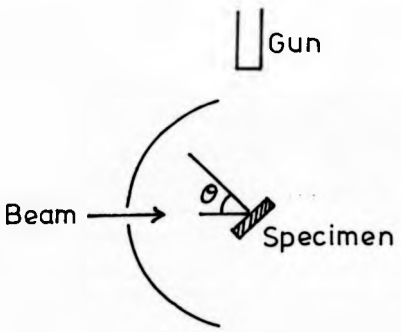
Gun
Beam
θ
Specimen

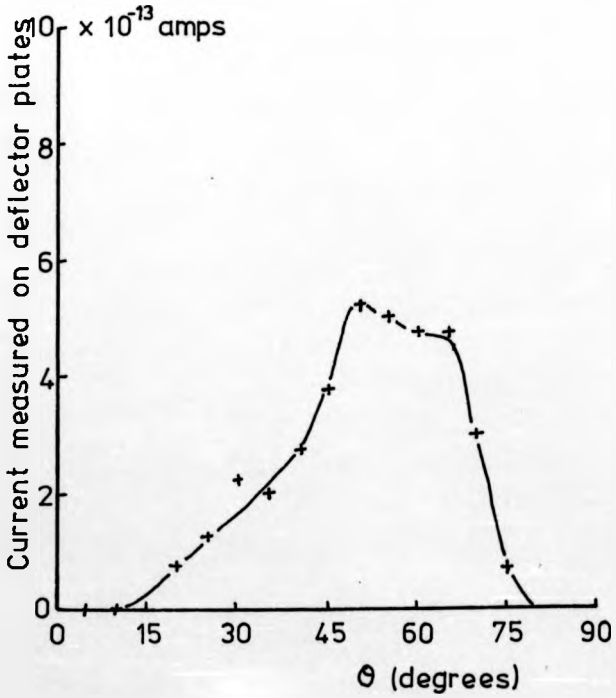
Current measured on deflector plates
x 10⁻¹³ amps
10
8
6
4
2
0
0
15
30
45
60
75
90
θ (degrees)

9.4%. A small part of the reduction in current leaving the deflector plates may be accounted for by the fall in ion current leaving the specimen as its surface is cleaned. Although it is not a significant change, these results would seem to indicate a slight variation in the reflection coefficient for the metastable atoms dependent on the surface conditions. However the crudeness of the reflected metastable atom detector does not allow any firm conclusions to be drawn from this experiment.

4.7 Conclusions

An examination of the de-excitation of helium metastable atoms at the nickel (100) surface has revealed that the yield of secondary electrons is strongly dependent on the condition of the surface, increasing as the surface contaminates. Further, studies of oxygen adsorption on nickel and the surface segregation of sulphur indicate that for a given species the total yield of electrons increases linearly with the degree of surface coverage. However it was found that the rate of increase of the total yield was not necessarily the same for different species, it being higher for sulphur than oxygen. Experiments on the reflection of metastable atoms from a surface do not show a significant change in the reflection coefficient as the surface is cleaned. It has also been shown that positive ion emission is possible from a very dirty surface.

References

1. P. M. Marcus, J. E. Demuth and D. W. Jensen, Surf. Sci. 53, 501 (1975).

2. M. Perdereau, Surf. Sci. 24, 239 (1971)

3. H. D. Hagstrum and G. E. Becker, J. Chem. Phys. 54, 1015 (1971).

4. H. H. Brongersma, J. Vac. Sci. Tech. 11, 231 (1974).

5. E. Taglauer and W. Heiland, Appl. Phys. Lett. 24, 437 (1974).

6. D. Maclean, Grain Boundaries in Metals (Oxford Univ. Press, London, 1957).

7. K. D. Sevier, Low Energy Electron Spectrometry (Wiley-Interscience, New York, 1972).

8. H. D. Hagstrum and G. E. Becker, Phys. Rev. B8, 107 (1973).

9. D. E. Eastman and J. K. Cashion, Phys. Rev. Lett. 27, 1520 (1971).

10. S. Evans, J. Peilaszeck and J. M. Thomas, Surf. Sci. 56,644 (1976).

11. P. R. Norton, R. L. Tapping and J. W. Goodale, Surf. Sci. 65, 13 (1977).

12. A. M. Horgan and D. A. King, Surf. Sci. 23, 259 (1970).

13. H. D. Hagstrum, Phys. Rev. 123, 758 (1961).

14. M. L. E. Oliphant, Proc. Roy. Soc. (London) A124, 228 (1929).

15. W. Allison, F. B. Dunning and A.C.H. Smith, J. Phys. B: Atom Molec. Phys. 5, 1175 (1972).

CHAPTER FIVE

EXPERIMENTS ON TUNGSTEN SURFACES

5.1 Introduction

With the results described in the previous chapter for experiments on the interaction of helium metastable atoms with a nickel single crystal differing so markedly from the tungsten single crystal work of Delchar et al[1, 2], it was felt that a re-examination of some of this earlier work was necessary. Accordingly, a tungsten single crystal, cut to expose the (100) plane, was prepared in the manner described earlier. Following mounting on the specimen holder and degreasing in the trichloroethylene vapour bath, this specimen was introduced to the target chamber.

A standard cleaning treatment for tungsten involves heating the sample to 2300°K, which, with this specimen holder, is achieved by electron bombardment. However, following a few preliminary observations, continuous problems with insulation breakdown prompted the author to resort to using a polycrystalline sample which could be heated more easily. This polycrystalline sample was approximately 3 mm. by 10 mm. and cut from tungsten sheet 0.15 mm. thick. After electropolishing in a caustic soda bath, the sample was spot welded to tantalum supports and vapour degreased before being installed in the chamber. It was then possible to flash the specimen to high temperatures by passing 40 amps a.c. through it directly.

5.2 Preliminary Observations

As stated in the previous section, a few prelim-

inary observations were made on the tungsten single crystal. An ejected electron energy distribution was taken from the specimen before the vacuum system was baked and this spectrum is shown in fig. 5.1. The sharply peaked distribution was reproducible and an ejected electron energy spectrum from the polycrystalline molybdenum heat shield was similar. This latter spectrum is also shown in fig. 5.1. for comparison. On heating the specimen to approximately 1000°C for two minutes the distribution had lost its sharp peak and now took the form shown in fig. 5.2. The distribution from the molybdenum heat shield had not changed following this process. As both the molybdenum heat shield and the specimen had undergone the same vapour degreasing procedure it may be that the sharply peaked distribution was a characteristic of a particular type of contamination left on the surface by this procedure.

5.3 Cleaning Treatment for Tungsten

Following the system bakeout and outgassing procedure of section 2.2, the Auger electron spectrum was dominated by the presence of carbon. After flashing the specimen to temperatures of the order of 2300°K, as measured by optical pyrometry (see Appendix III), the Auger electron spectrum shown in fig. 5.3. was obtained. The specimen was then cleaned by flashing to 2300°K for periods of approximately two seconds with intermittent flashings in an oxygen atmosphere (1×10^{-8} torr) over a period of three or four days. At the end of this period, following an initial flash, repeated flashings disturbed the background pressure by no more than 2 or 3×10^{-10} torr.

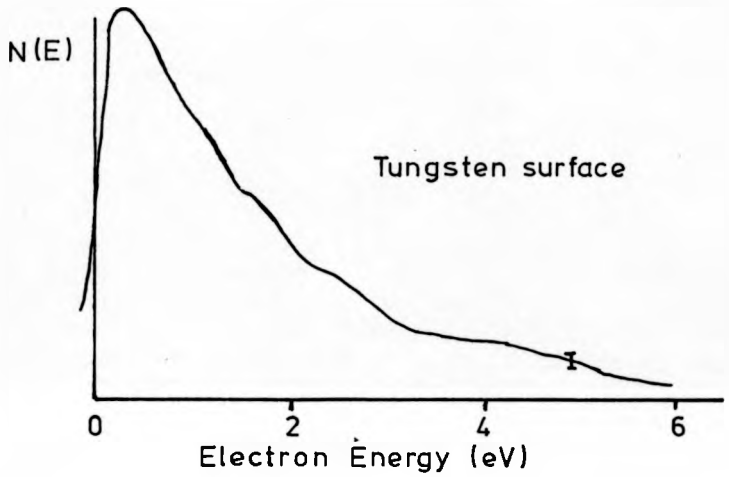

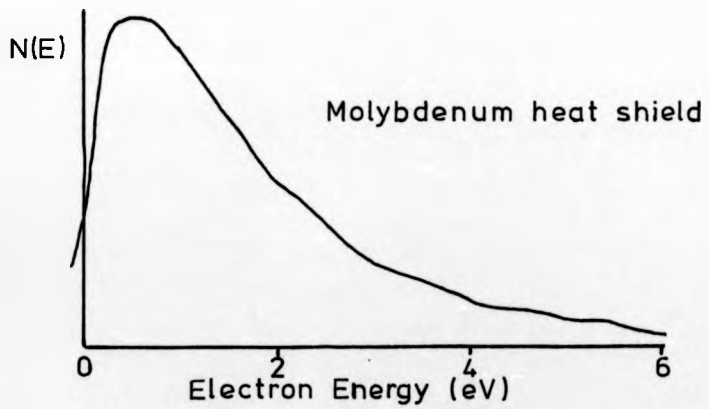

FIG. 5.1

The secondary electron energy distributions recorded from the tungsten surface and from the molybdenum heat shield before bakeout.

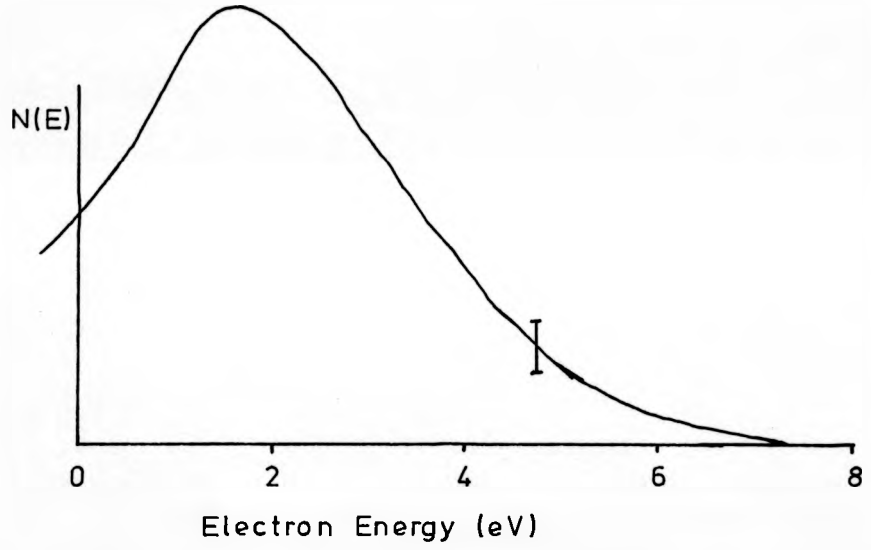

FIG. 5.2

The secondary electron energy distribution recorded from the tungsten surface before the system was baked but after annealing the specimen to 1000 °C.

FIG. 5.3

An AES spectrum from the contaminated tungsten surface.

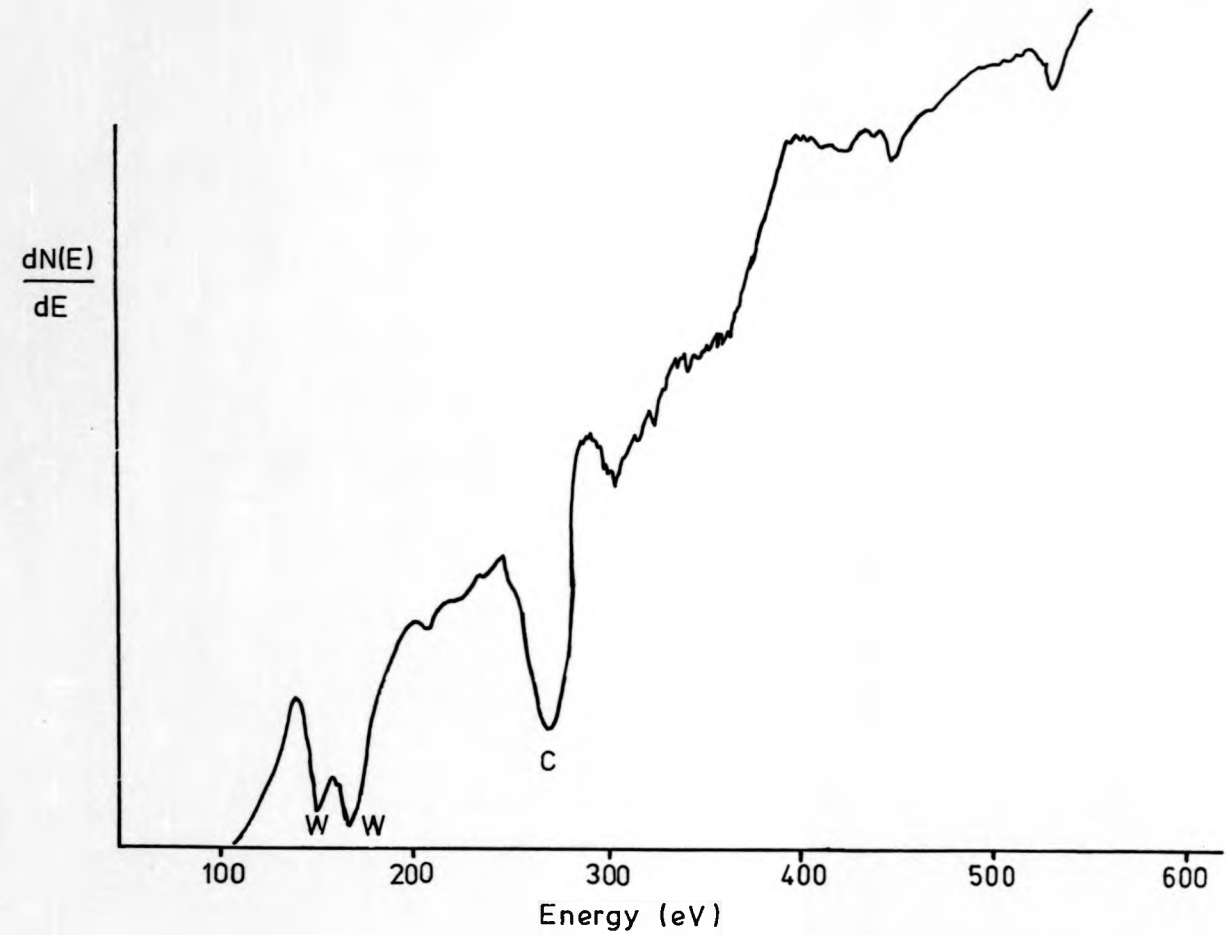
dN(E)
dE
W
W
C
100
200
300
400
500
600
Energy (eV)

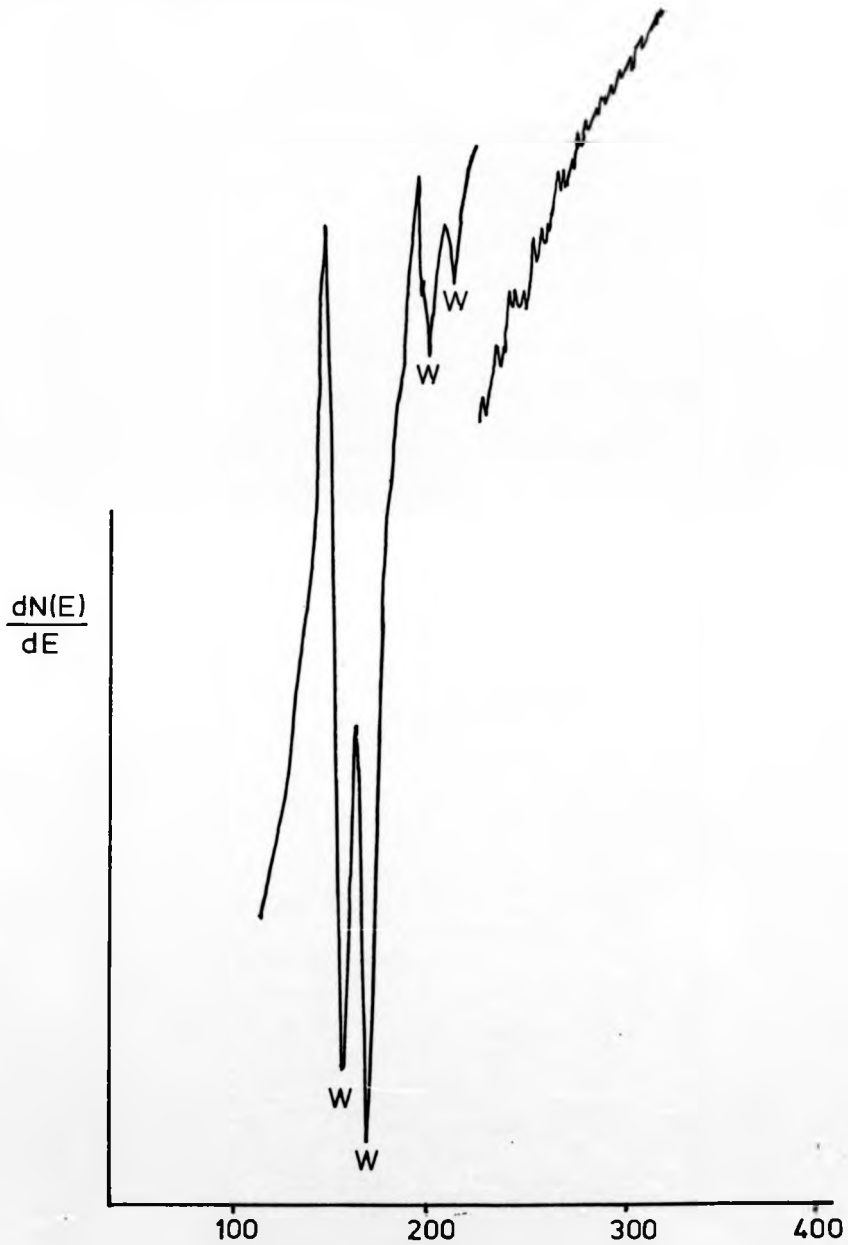

FIG. 5.4

An AES spectrum from the clean tungsten surface.

The Auger electron spectrum shown in fig. 5.4. was then obtained.

5.4 The Measurement of the Ejected Electron Energy Distributions from the Tungsten Surface

As has been described elsewhere, considerable problems were caused by movement of the retarding field analyser's grids during heating cycles of the specimen. This movement meant that the neutralizing capacitor (section 2.8) had to be readjusted quite frequently when using the a.c. method for measuring the electron energy distributions. It was consequently felt that with the higher temperatures used for the tungsten work, this might prove to be even more of a problem and that the use of a d.c. method might be more convenient. This view was probably not justified in view of the short times subsequently used for flashing the specimen.

The basic system used for the d.c. measurements has been described previously in section 2.8. A voltage proportional to the current arriving at the collector as measured by the electrometer was fed into the Y axis of an X-Y recorder whilst the X-axis was driven directly in synchronisation with the retard voltage on the grids. These I-V plots were then digitised by hand at increments of 100 mV along the X-axis. This is obviously not the most accurate method but no facility was available for directly digitising the output from the electrometer. As a check, two or three people were asked to digitise the same curve and comparisons were made between the results of their efforts. There was little difference other than obvious mistakes.

Following digitisation, a computer was used to calculate values of dI/dV giving a measure of N(E), the number of electrons ejected with a given energy E, at points midway between consecutive points on the X-axis of these curves. For this simple procedure

$$\left(\frac{dI}{dV}\right)^2_{n+\frac{1}{2}} = \frac{Y_{n+1} - Y_n}{\Delta X} \qquad (1)$$

and here $\Delta X = X_{n+1} - X_n$ is a constant. Examination of the curve obtained for a dirty surface and plotted in fig. 5.5. shows that it was necessary to use a smoothing routine as a guide to the best line to draw through the resulting points. Hagstrum[3] considered this problem in some detail and it was decided that in this work the same procedure would be followed as was suggested to Hagstrum by Kaplan. Whereas the formula of equation (1) puts all the weight on points adjacent to the point $(n+\frac{1}{2})$ it is not difficult to show that the slope of the straight line fitted to the data by the least squares method

$$\left(\frac{\Delta I}{\Delta V}\right)_{n+\frac{1}{2}} = \frac{8\sum_{i=n-3}^{i=n+4} X_i Y_i - \sum_i X_i \sum_i Y_i}{8\sum_i X_i^2 - (\sum_i X_i)^2} \qquad (2)$$

weights most heavily points which are more distant from the point $(n+\frac{1}{2})$. As a compromise, Kaplan suggested the formula

$$\left(\frac{\Delta I}{\Delta V}\right)_{n+\frac{1}{2}} = \frac{Y_{n-3}+Y_{n-2}+Y_{n-1}+Y_n+Y_{n+1}+Y_{n+2}+Y_{n+3}+Y_{n+4}}{16\Delta X} \qquad (3)$$

which weights all points equally. Included in fig. 5.5 is the result of applying such a programme to the I-V curve for the electrons ejected from a dirty surface. The resolution of this method of data reduction is not

FIG. 5.5

Overleaf is shown the computer output of the differentiation of an I-V curve taken from a contaminated tungsten surface. Also plotted are the results obtained from the smoothing routine.

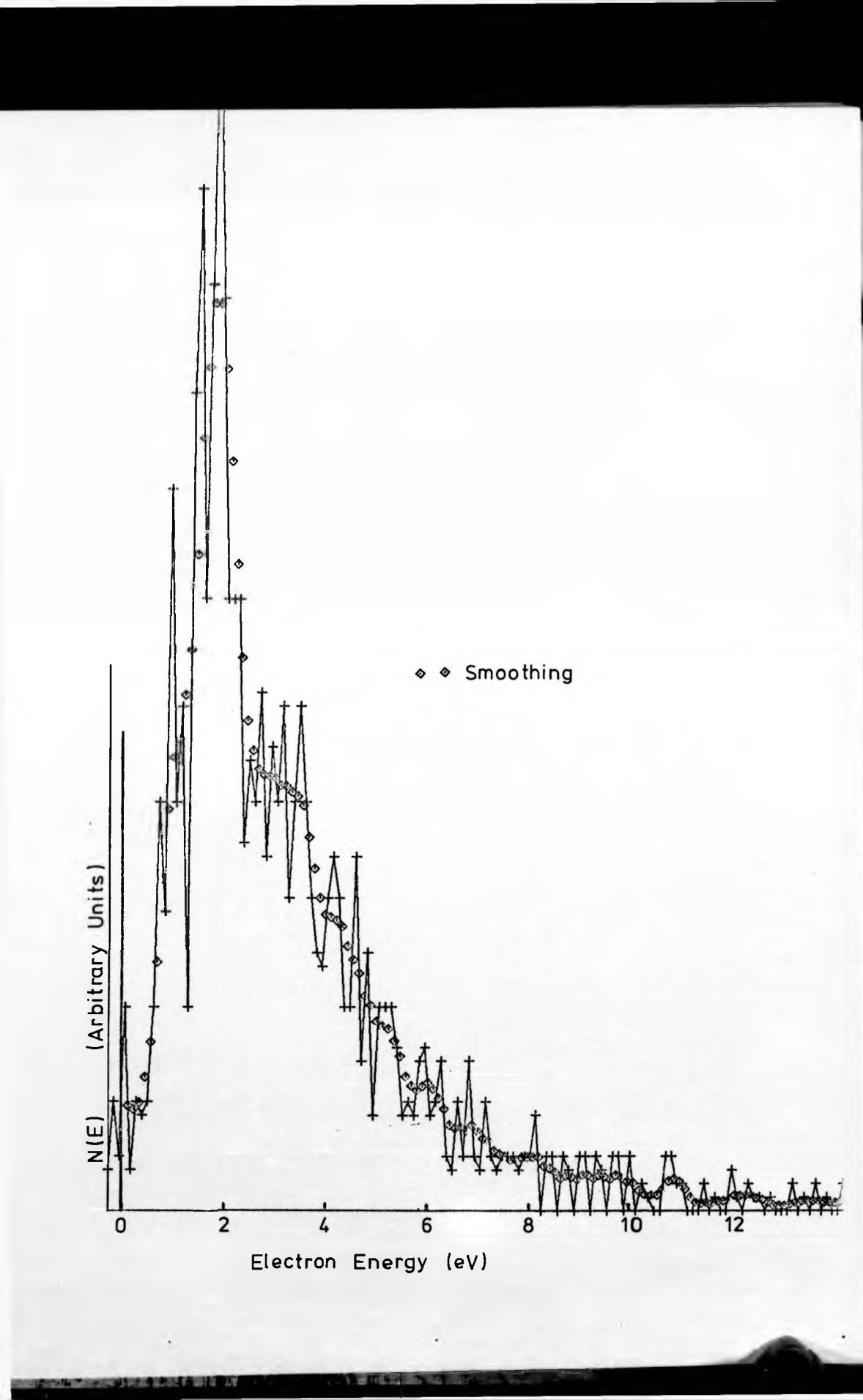
Smoothing
N(E) (Arbitrary Units)
0
2
4
6
8
10
12
Electron Energy (eV)

very good as has been pointed out by Hagstrum. In fact with a 9-point smoothing routine and a 100 mV point separation on the X digitisation the resolution of the resulting spectrum will be of the order of .9V.

5.5 Interaction of Metastable Helium Atoms with a Clean Tungsten Surface

With the problem of secondary emission from the grids (Section44) it was decided to follow the example of Hagstrum and bias the sample at -4V. This allowed the component from the grids to be distinguished from the target electrons in the secondary electron distribution. As has been described in the previous section the method of data reduction did not give good resolution. However even with the limited resolution available the spectrum for the ejected electron energy distribution shows some divergence from that obtained by Delchar et al[1] using metastable atoms and by Hagstrum[3] using incident ions.

Figure 5.6 shows the result of averaging five individual smoothed curves for the ejected electron energy distributions from a clean surface. It is felt that in view of the resolution limitations detailed above, little meaning can be attached to any of the "structure" in this curve. Also included in the figure is the electron energy distribution for the electrons leaving the dirty surface. The curves used in the average for the clean surface were obtained at odd times over a period of seven days. The "dirty surface" distribution was obtained midway during this period after allowing the system up to a pressure of the order of 10^{-3} torr of "atmospheric" gases. When the chamber had been re-evacuated to a

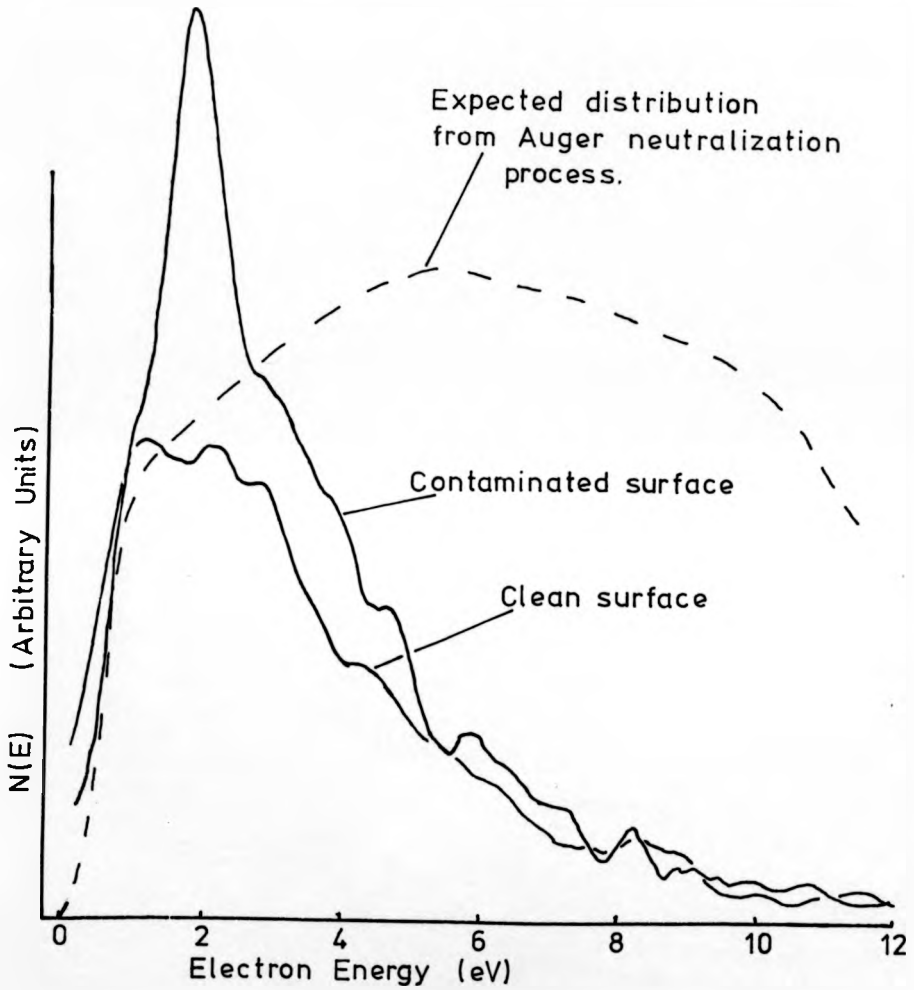

FIG. 5.6

The secondary electron energy distributions recorded both from the contaminated tungsten surface and the same surface after cleaning. The expected distribution should Auger neutralization of incident ions occur is also shown.

pressure in the range 10^{-10} torr there had been an increase by a factor of three in the total yield of electrons as a result of metastable atom impact and the electron energy distribution took the form shown in the figure. Once again, the contrast between this result and the results of Hagstrum for slow incident ions should be noted. He observed an increase in the yield as the surfaces under investigation were cleaned rather than the reverse process described here for metastable atoms. However there is agreement between the present work and the findings of Allison et al[4] and the earlier work of Hasted[5]. Allison observed a decrease in the total yield of ejected electrons per incident metastable helium atom upon heating both tungsten and stainless steel surfaces to 800°C. Hasted found that the yield γ_m of electrons per incident metastable atom decreased from .17 to .14 upon flashing a tungsten target. The earlier work of Sonkin[6], whilst performed in vacuum conditions rather poor by today's standards, produced similar results. Examining the interaction of metastable mercury atoms with a tungsten surface, he found that the yield of secondary electrons decreased upon flashing his target to high temperatures and remained at a low level if the target was kept at a high temperature.

Also included in fig. 5.6 is the distribution that might have been expected from a clean surface if the process was of the type postulated by Hagstrum. This curve, estimated from Hagstrum's results for 40 eV helium ions incident on a tungsten surface, shows the

characteristic "broad" distribution to be expected from the process of Auger neutralization. The difference between the two curves, one resulting from ion impact and one from metastable impact suggests that there are different processes occurring at the surface for the two cases.

5.6 Carbon Monoxide on Tungsten

Following the work on oxygen adsorption on nickel, it was felt that it would be worthwhile examining the process for another adsorption system. Carbon monoxide adsorption on tungsten was chosen as this system has also been extensively studied in the past and provides opportunities for comparisons with the results of other techniques.

Erlich[7] and Redhead[8], carrying out flash desorption experiments on carbon monoxide layers adsorbed at 300°K on polycrystalline tungsten filaments, demonstrated that the carbon monoxide adsorbs in two distinct states. They observed the initial desorption of an α-state at 400°K followed by the desorption of multiple β - CO states above 800°K. This general behaviour has been confirmed by a number of workers. More recently the α - CO state has been shown to consist of two types of species, designated α_1 - CO and α_2 - CO which respectively exhibit:

a) different binding energies[9] ($\sim$ 15 kcal mole^{-1} and $\sim$21 kcal mole^{-1})

b) different electron impact desorption products[9] (CO^+ and O^+), and

c) different C-O infrared stretching frequencies[10] ($\sim$2128 cm^{-1} and 2090 cm^{-1}).

On the basis of the infrared observations, the α - CO states have been assigned as linear CO species bound via sp hybridized carbon to tungsten. King and Goymour[11] have suggested that the multiple β - CO states observed in flash desorption may originate from lateral interactions between dissociated CO molecules. Adams,[12] on the other hand, has suggested that the multiple β - CO states observed in flash desorption from W (210) may originate from lateral interactions between undissociated CO molecules. Irrespective of whether β -CO is dissociated or not, both King and Adams postulate that the multiple β - CO states observed are a consequence of coverage changes (and associated interactional changes) during thermal desorption, rather than being indicative of multiple β states present in the adsorbed layer prior to adsorption. The commonly accepted structures for the two states are shown in fig. 5.7. β_2 - CO states form first on adsorption leading on to both α - CO and β_1 - CO formation as the CO coverage reaches higher values. Integrating CO pressure curves as a result of flash desorption Goymour and King[11] found that at full coverage the ratio of occupied β sites to α sites was 3 : 1. Finally it should be noted that several authors have reported the reversibility of α-coverage as a function of pressure.

For this particular experiment carbon monoxide was obtained from BOC in 1 litre research grade X flasks.

α - state

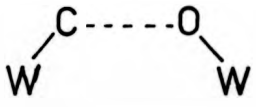

β - state

FIG. 5.7

The commonly accepted structures for the different adsorption states of carbon monoxide on tungsten.

The gas was introduced to the target chamber via a Granville-Phillips valve and glass pipeline, both of which were maintained at the same level of vacuum as the target chamber until the gas bottle itself was opened. Under these conditions it was felt that the partial pressures of any impurities would be the same as for the clean surface experiments.

For different partial pressures of carbon monoxide in the target chamber, the total yield of electrons was measured as a function of time of exposure. Ordinarily the easiest method of performing this experiment would be to measure the current leaving the target, but low resistance paths to earth prevented such measurements being carried out with ease and consequently changes in the yield were monitored by measuring the current arriving at the collector. As described earlier (section 5.5), both the target and the retard grids were held at -4V to discriminate between electrons from the target and secondary electrons produced at the grids. Before each change of partial pressure, the carbon monoxide was pumped away and the tungsten flashed to $\sim 2500^{\circ}K$ several times to restore a clean surface.

The results of such measurements are shown in fig. 5.8. Noting that the total yield increased to an equilibrium level which seemed to be a function of the partial pressure of CO, this experiment was repeated in a different way. Having produced a clean surface, the total yield was monitored as the partial pressure was increased in steps at approximately four minute intervals

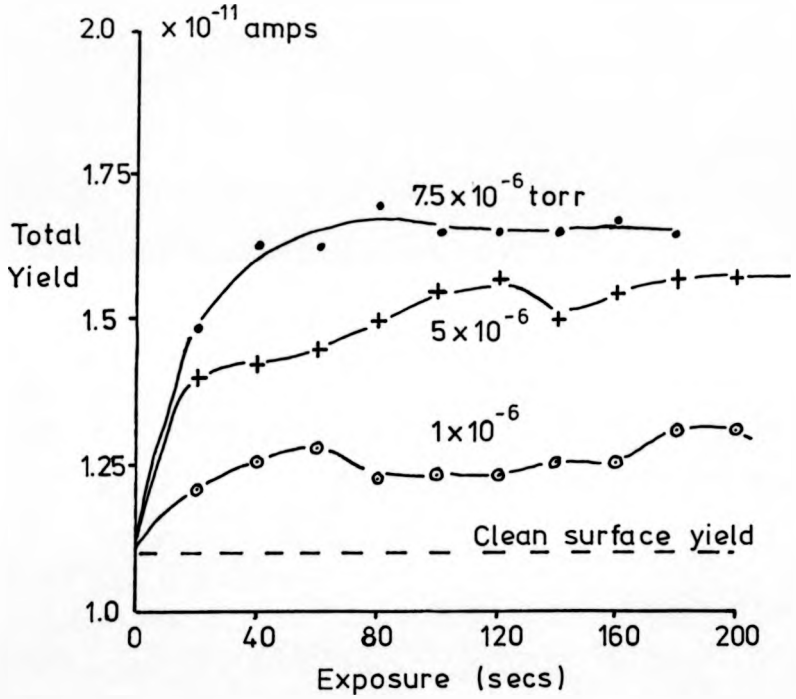

FIG. 5.8

The increase in the total yield of secondary electrons as a function of exposure to CO. The different partial pressures of CO are indicated.

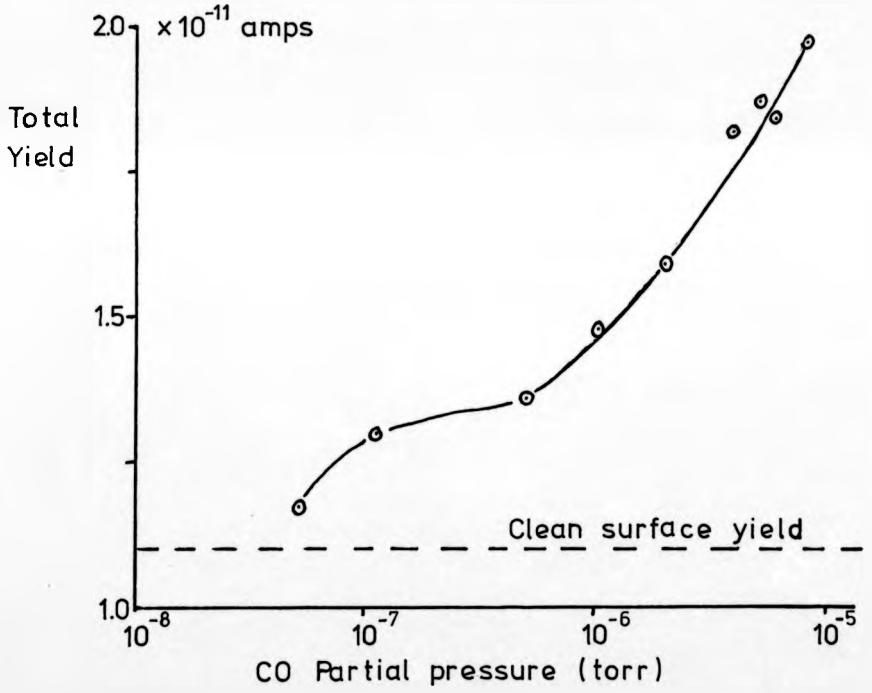

FIG. 5.9

The equilibrium total yield of secondary electrons as a function of the partial pressure of CO.

to allow an equilibrium to be achieved at the surface. The result of this experiment is shown in fig. 5.9. This experiment was not continued to higher partial pressures as the onset of gas phase quenching of the metastable atom beam should be about 10^{-4} torr (section 3.3). It was found that increase in yield was reversible as the carbon monoxide was pumped away but that it was never possible to return to the yield value found for a clean surface. In fact, the increase in yield from the clean surface to the final value after the carbon monoxide had been pumped away was approximately 12%.

The spectrum of the electron energy distribution from the tungsten with adsorbed carbon monoxide obtained after the above procedure is shown in fig. 5.10.

For comparison, the relative occupation of the different CO states as a function of the pressure or impingement rate Zp obtained by Erlich[7] for adsorption on a polycrystalline tungsten wire at $300^{\circ}K$ is shown in fig. 5.11. Replotting on the same graph the equilibrium total secondary yield as a function of impingement rate, it can be seen that the yield of electrons becomes more pronounced at exposures where adsorption into the α-state is taking place. Erlich demonstrated that adsorption into this state was dependent on the pressure and not just on the occupation of the β state, and that it followed a Langmuir isotherm. This isotherm is easily derived. If R_a and R_d are respectively the adsorption and desorption rates then

$$R_a = K_a P (1 - \theta) \qquad (4)$$

FIG. 5.10

The secondary electron energy distribution recorded from the tungsten surface with CO adsorbed in the β-state.

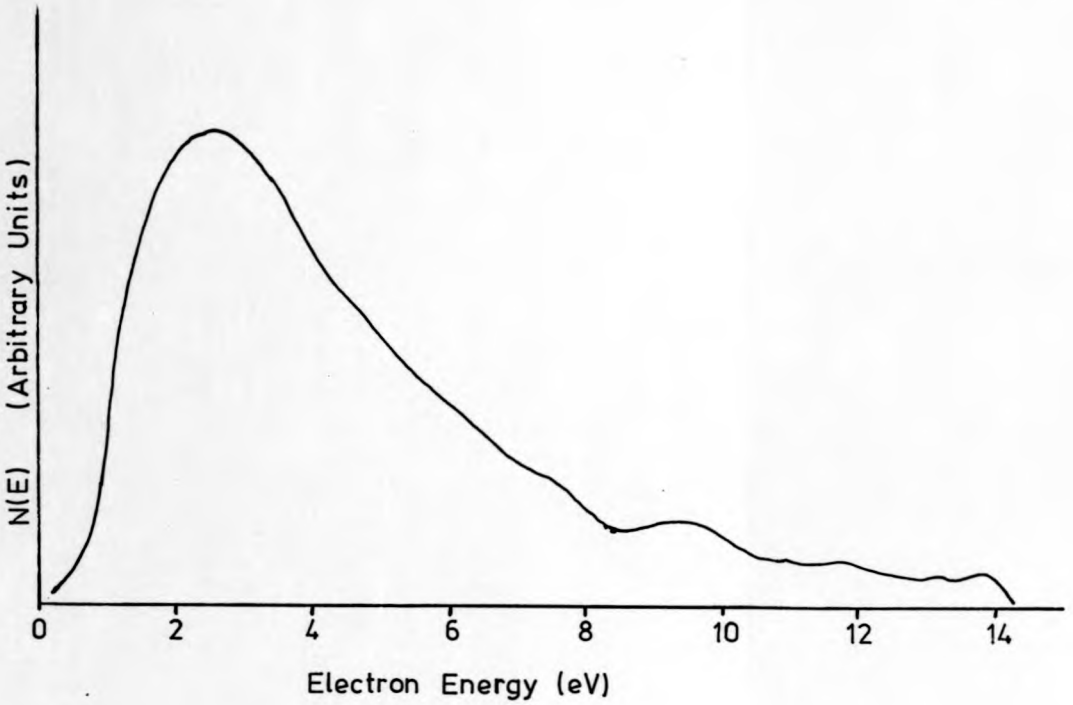
N(E) (Arbitrary Units)
0
2
4
6
8
10
12
14
Electron Energy (eV)

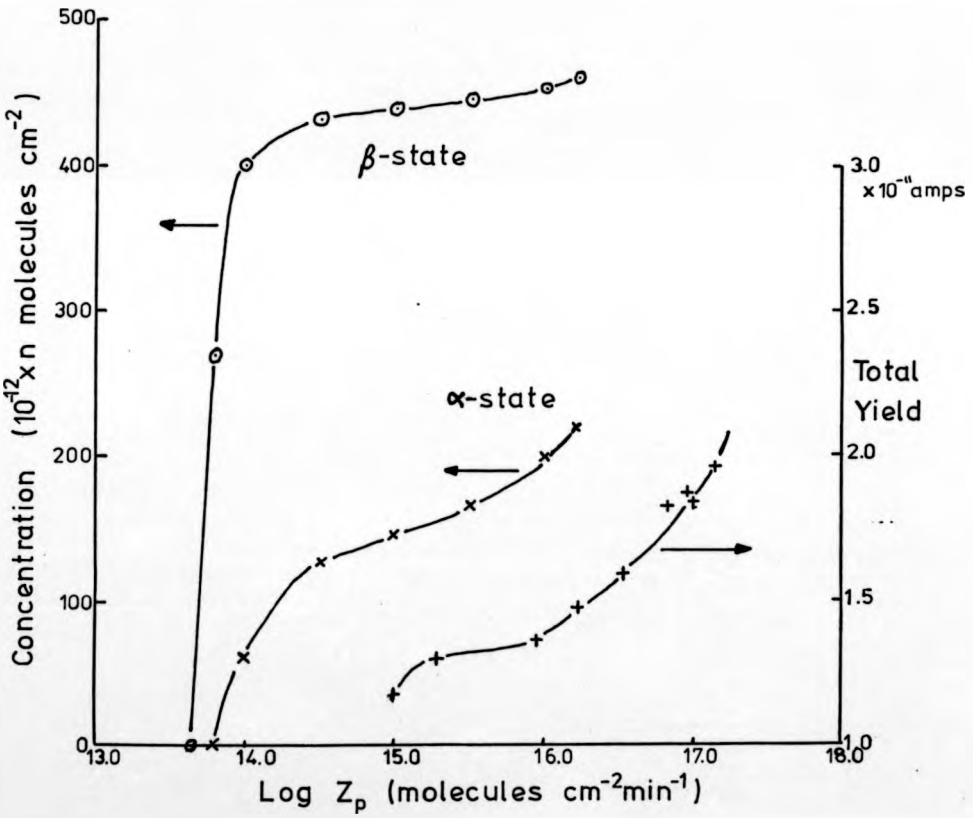

FIG. 5.11

The concentration, n, of the different adsorption states[7] and the equilibrium total yield of secondary electrons plotted as a function of the partial pressure of CO.

which indicates that the rate of adsorption is proportional to the number of collisions with the surface, i.e. to the pressure, and to the proportion of vacant sites. K_a is a constant and θ is the fractional coverage. The rate of desorption is proportional to the number of adsorbed atoms, thus

$$R_d = K_d\theta \qquad (5)$$

For equilibrium $R_a = R_d$ or

$$K_aP(1 - \theta) = K_d\theta \qquad (6)$$

so that $bP(1 - \theta) = \theta$ where $b = K_a/K_d$ the ratio of the two constants. The above equation is more generally presented in the form

$$\theta = \frac{bP}{1+bP} \qquad (7)$$

From the adsorption work on nickel it is to be expected that the increase in the total yield of electrons ΔI will depend linearly on the number of contaminant atoms. This will be given by $An_s\theta$ where A is the area of the incident metastable beam, n_s the number of adsorption sites cm^{-2}, and θ is defined as above.

Thus $\Delta I \propto An_s\theta$

or $\Delta I = kAn_s\theta$ where k is a constant.

From (7) above $$\Delta I = \frac{kAn_sbP}{1 + bP} \qquad (8)$$

or $$\frac{P}{\Delta I} = \frac{P}{kAn_s} + \frac{1}{kAn_sb} \qquad (9)$$

Thus a plot of $P/\Delta I$ against P should be a straight line of gradient $\frac{1}{kAn_s}$. In fig. 5.12 such a graph is plotted.

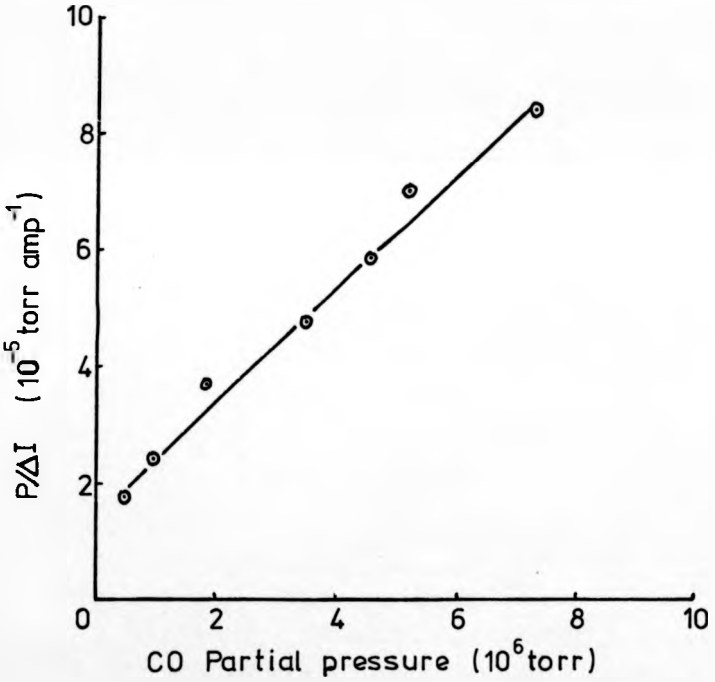

FIG. 5.12

The ratio of the partial pressure to increased total yield plotted against the partial pressure of CO.

From the linearity of this graph it would therefore seem likely that the metastable atom beam was monitoring the occupation of the α - CO states at higher partial pressures. Several authors [11, 13] report that in the electron stimulated desorption of ions from a carbon monoxide covered surface the growth of the total ion current correlates with the late appearance and growth of the α state in the desorption spectra.

Finally it should be noted that several authors have found that the weakly bound α - state is desorbed at room temperature by pumping alone [9, 13, 14]. This fact would then explain the reversibility of the adsorption studies here and support the assignment of the α state as the source of the secondary electrons. This would imply that the metastable atoms have a greater cross-section for interaction with the α - CO states than the β - CO states.

5.7 Conclusions

An examination of the interaction of helium metastable atoms with a tungsten surface has revealed an ejected electron energy distribution which disagrees with that found by Delchar et al for tungsten single crystals. Further the results would seem to indicate a different process from that predicted by Hagstrum, namely resonance ionization followed by Auger neutralization. Experiments on the carbon monoxide adsorption on tungsten show an increase in the yield with surface coverage. They also indicate a different cross-section for interaction with different adsorption states.

References

1. D. A. Maclennan and T. A. Delchar, J. Chem. Phys. 50, 1772 (1969).

2. T. A. Delchar, D. A. Maclennan and A. M. Landers, J. Chem. Phys. 50, 1779 (1969).

3. H. D. Hagstrum, Phys. Rev. 96, 325 (1954).

4. W. Allison, F. B. Dunning and A.C.H. Smith, J. Phys. B: Atom. Molec. Phys. 5, 1175 (1972).

5. J. B. Hasted, J. Appl. Phys. 30, 22 (1959).

6. S. Sonkin, Phys. Rev. 43, 788 (1933).

7. G. Ehrlich, J. Chem. Phys. 34, 39 (1961).

8. P. A. Redhead, Trans. Faraday Soc. 57, 641 (1961).

9. J. T. Yates, Jr. and D. A. King, Surf. Sci. 32, 479 (1972).

10. J. T. Yates, Jr., R. Greenler, I. Ratajczykowa and D. A. King, Surf. Sci. 36, 739 (1973).

11. C. G. Goymour and D. A. King, J. Chem. Soc. Farad. Trans. 169, 736 (1973).

12. D. L. Adams, Surf. Sci. 42, 12 (1974).

13. J. T. Yates, Jr., T. E. Madey and J. K. Payn, Nuovo Cimento Suppl. 5, 558 (1967).

14. E. W. Plummer, B. J. Waclawski, T.V. Vorburger and C. E. Kuyatt, Prog. Surf. Sci. 7, 149 (1976).

CHAPTER SIX

COMPARISONS BETWEEN THEORY AND EXPERIMENT

6.1 Introduction

In the previous chapters a description has been given of various experiments performed in an attempt to gain a better understanding of the interaction of helium metastable atoms with metal surfaces. The surfaces examined have included a clean nickel (100) single crystal plane, a clean polycrystalline tungsten sample and these surfaces with different adsorbed contaminants.

It was found that the electrons ejected from either the clean nickel surface or the clean tungsten surface had approximately the same distribution in energy. Furthermore it was found that contamination of either surface led to an increase in the total yield of electrons. However it was found that the rate of increase of the total yield with coverage was different for different contaminants, being higher for sulphur on nickel than oxygen on nickel. A crude experiment designed to measure the reflection coefficient of the metastable atoms found little variation between clean and contaminated surfaces.

Two mechanisms have been proposed for the de-excitation of an excited atom at a surface, namely resonance ionization and Auger de-excitation. When an atom undergoes resonance ionization, the electron in the excited level tunnels through the potential barrier between the metal and the atom into a vacant level of the metal, leaving an ion adjacent to the surface. With

Auger de-excitation, an electron from the metal falls to the hole in the ground state of the atom and the energy released from this transition is transferred to the electron in the excited level. In this chapter comparisons will be made between the results detailed above and the results to be expected from examination of the two different mechanisms.

6.2 The Possibility of Resonance Ionization

Cobas and Lamb[1] demonstrated that the resonant or electron-exchange processes, resulting from the tunnelling effect in the system, take place at large atom (ion) - solid surface distances and are characterised by high probabilities. At smaller atom - surface distances the most prominent process is the two-electron Auger type, resulting in electron emission. For both types of process the transition probability at a distance s from the surface has the form

$$R_t(s) = A \exp(-as) \qquad (1)$$

where the constants A and a take different values for the resonant and Auger processes. However, Hagstrum[2] observed a considerable discrepancy between theory and experiment in the pre-exponential factor for the Auger process. Rather than the values of $a = 7.3 \times 10^8 cm^{-1}$ and $A = 9.6 \times 10^{16} sec^{-1}$ predicted by Cobas and Lamb, he found that the values of $a = 5.0 \times 10^8 cm^{-1}$ and $A = 1.5 \times 10^{20} sec^{-1}$ gave a better fit to his experimental data.

This discrepancy led Janev[3] to reconsider the problem of resonance ionization. Rather than use a perturbation technique similar to Cobas and Lamb's, Janev considered the resonant process as an electron tunnelling into the

potential well of the metal through the barrier created between the metal and the Coulomb field of the atomic core during the collision. He derived the following expression for the probability of a transition at a distance R from the surface

$$P_t(R) = \frac{C}{V_0} R^{\alpha-1} \exp\left(-\beta R - \frac{C}{V_0} R^{\alpha-1} \exp(-\beta R)\right) \quad (2)$$

where α, β and C are constants calculated from the appropriate parameters of the asymptotic atomic wave-functions for the atom involved. Substituting the relevant values for the constants, it is found that for the helium metastable states resonance ionization most probably occurs at a distance of about 7.5Å from the surface as shown in fig. 6.1.

Examination of the effects of shifts in the energy levels as the excited atoms approached the surface led Hagstrum[2] to propose that the excited atom would first be resonance ionized and the ion thus formed subsequently neutralized. The ion formed in the initial process will be accelerated to the surface as a result of its image potential and at some distance s_m from the surface the probability for Auger neutralization will pass through a maximum dependent on the ion's velocity. For a process with a transition rate given by equation (1), Cobas and Lamb found that the distance s_m at which this maximum probability occurs is given by

$$s_m = \frac{1}{a} \ln\left\{\frac{A}{av_0}\right\} \quad (3)$$

where v_0 is the ion's velocity.

In the present case the ion's velocity will

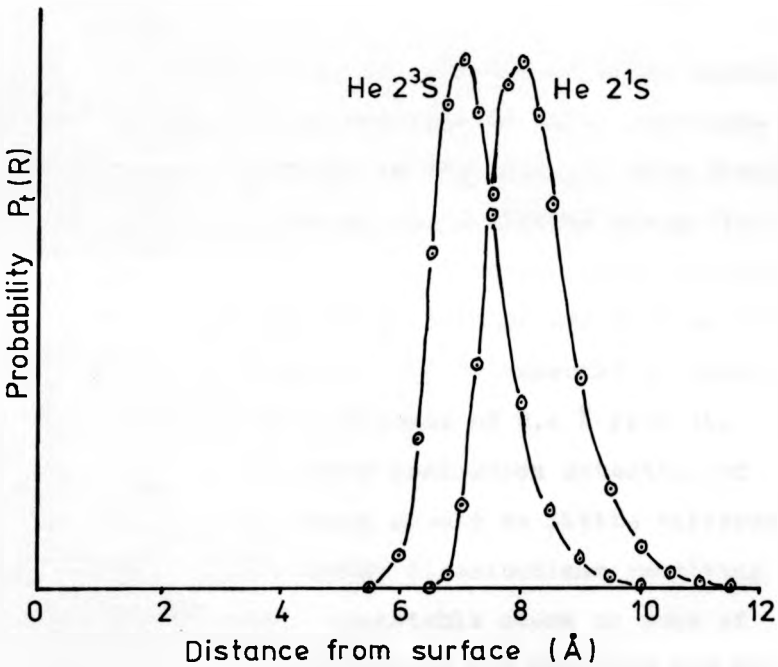

FIG. 6.1

The probability of resonance ionization as a function of distance from the surface for the metastable states of the helium atom.

be given by

$$\frac{mv_o^2}{2} = \frac{e^2}{4s_m} - \frac{e^2}{4S_R} \qquad (4)$$

where the image potential of an ion at a distance s from the surface is given by

$$V = \frac{e^2}{4s} \qquad (5)$$

and S_R is the distance from the surface at which resonance ionization occurs. It is possible to solve equations (3) and (4) graphically as shown in fig. 6.2 and this yields a value of about 2.6 Å for s_m and a kinetic energy for the ion of about 1 eV. At this distance from the surface the effective ionization energy for the ion will be 23.2 eV. An ion of incident energy 5eV may be expected to undergo Auger neutralization at a distance of 2.4 Å from the surface and have an effective ionization potential of 23.1 eV. Consequently there should be little difference in the ejected electron energy distributions resulting from the impact of either metastable atoms or ions of low kinetic energy. That this is not the case may be seen by referring back to fig. 4.8 for the metastable atom spectrum and to fig. 1.2 for the slow incident ion situation, both taken from a Ni (100) surface. The metastable atom spectrum consists mainly of low energy electrons in contrast to the INS spectrum which reveals the d-band of the nickel by the appearance of a peak at about 11 eV.

It has to be noted, however, that in numerous studies of adsorption systems using INS, Hagstrum[4, 5] has observed a decrease in the total yield of secondary

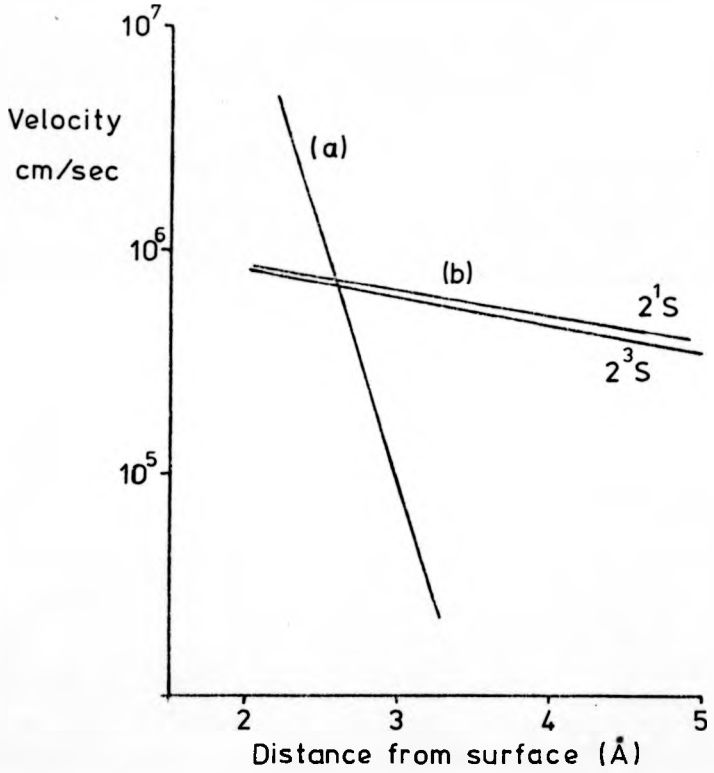

FIG. 6.2

a) The variation of the most probable distance s_m for Auger neutralization with the ion's incident velocity.

b) The velocity of the incoming ion under the influence of it's image potential.

electrons and a reduction in the number of electrons with higher energies. This obviously raises the question as to whether the surfaces in the present experiment were highly contaminated. Several experiments were performed in an attempt to answer this question. A mass spectral analysis of the gases present in the chamber, both with the helium beam on and with the beam off, showed the beam to consist of approximately 99.996% helium, 0.002% nitrogen and 0.002% chlorine. At this impurity level, and referring to Hagstrum's work on monolayer adsorption[4], it is unlikely that a monolayer of contaminant will form in under 10 hrs. An Auger electron spectrum taken from the surface of the specimen after the helium beam had been on the surface showed no contamination. Finally a flash desorption experiment was performed from the tungsten surface both before and after the helium beam had been on for 10 minutes. In both cases the pressure rise in the target chamber was of the order of two or three times 10^{-10} torr. All of these results suggest that the target was not contaminated and that for incident metastable atoms some process other than resonance ionization was occurring at the surface. However it was decided to model the INS process for very slow incident ions using a computer simulation.

6.3 Computer Simulation of Auger Neutralization

Appelbaum and Hamann[6] have calculated the effective density of states for silicon at different distances from the surface. They found that the electron energy distributions observed by Hagstrum in INS experiments

on silicon surfaces were actually a convolution of the effective density of states of silicon in the region of the ion with the density of states for the bulk. However they also found that the self-convolution of the effective density of states midway between the surface and the ion was a good approximation to the experimentally observed energy distribution. Accordingly it was felt that in any modelling it would be necessary to estimate the effective density of states midway between the surface and the ion at a distance s from the surface as given by equation (3).

Within the one-electron model an electron in the bulk of the metal of energy E given by

$$E = \frac{\hbar^2 k^2}{2m} \qquad (6)$$

is assumed to have a wavefunction $\psi_k(r)$ where

$$\psi_k(r) = e^{i\,\underline{k}.\underline{r}} \qquad (7)$$

It will be seen that this function obeys the Bloch theorem

$$\psi_k\,(\underline{r} + \underline{l}) = e^{\,i\,\underline{k}.\underline{l}}\,\psi_k\,(\underline{r}) \qquad (8)$$

However if the crystal is finite, then at the boundaries $\underline{k}$ is complex; thus

$$\underline{k} = \underline{k}_r + i\,\underline{k}_i \qquad (9)$$

where $\underline{k}_r$ and $\underline{k}_i$ refer to the real and imaginary parts respectively. From equation (6) above, the energy is

$$E = \frac{\hbar^2}{2m}\left\{k_r^{\,2} - k_i^{\,2} + 2i\,\underline{k}_r.\underline{k}_i\right\} \qquad (10)$$

As any measured energy value must be real, either $k_i = 0$, (the bulk situation) or k_r and k_i must be mutually perpendicular. If k_r is taken as parallel to the surface, then the wavefunction describing the electron outside the

surface is

$$\Psi(z) = e^{-k_i z} \qquad (11)$$

where z is taken as the axis perpendicular to the surface.

At any distance z from the surface, the charge density n(z) will be given by

$$n(z) = \sum_i n_i \Psi_i^2(z) \qquad (12)$$

where n_i refers to the occupancy of different orbitals i. $\Psi_i(z)$ given by (11) above will not be the same for electrons in different orbitals, even though they may have the same energy. This stems from the fact that electrons in a 4s orbital may be expected to be less localized than electrons in a 3d orbital. Consequently this means that k_r is smaller for a 4s orbital and thus from equation (10), for electrons of the same energy, k_i will be smaller for a 4s electron than a 3d electron. Having found an effective density of states for which the self-convolution produces the measured secondary electron energy distribution of Hagstrum's INS, it should then be possible, using equations (11) and (12), to produce an effective density of states for other distances from the surface. For the purpose of this modelling it is assumed that the s and d orbitals are unhybridized.

The Auger neutralization of the incident ion produces an internal electron energy distribution $N_i(\epsilon)$ which is the self-convolution of the density of states $N(\epsilon')$: thus

$$N_i(\epsilon) = \int N(\epsilon''') \, N(\epsilon - E_i'(s) + \epsilon''') \, d\epsilon''' \qquad (13)$$

In the above equation ϵ is given by

$$\epsilon = E_i'(s) - \epsilon' - \epsilon'' \qquad (14)$$

where $E_i'(s)$ is the effective ionization energy for the ion at the distance s from the surface and ϵ' and ϵ'' are the energies of the two valence band electrons involved in the transition, fig. 1.1. The effective ionization energy is simply the ionization potential at infinity minus the image potential of the ion.

The true internal distribution will be broader than that obtained by the convolution procedure of equation (13) by virtue of the facts that:

1) not all of the ions are neutralized at a distance s but at a finite spread in distance around s, and,

2) the initial and final states of the process have finite lifetimes. Hagstrum[2] has demonstrated that these two processes may be taken into account by the convolution of the distribution of equation (13) with a Gaussian distribution

$$\Phi(x) = \frac{1}{\sigma\sqrt{2\pi}} \exp\left(\frac{-x^2}{2\sigma^2}\right) \qquad (15)$$

giving the broadened internal distribution $N_i'(\epsilon)$,

$$N_i'(\epsilon) = \int_{-\infty}^{\infty} \Phi(x) N_i(\epsilon + x)\,dx \qquad (16)$$

In equation (15), σ is adjusted to fit the high energy tail of the observed electron energy distribution. Having obtained the internal distribution, it is then a simple matter to obtain an external electron energy distribution $N_o(\epsilon)$ through an electron escape function $P(\epsilon)$. Thus

$$N_o(\epsilon) = N_i'(\epsilon) P(\epsilon) \qquad (17)$$

Hagstrum has derived a suitable form for the electron escape function which takes account of angular

variations in the matrix element for the process. $P(\epsilon_k)$ has a value which rises rapidly for low energies and then levels off for higher energies. The various steps in the modelling procedure, detailed above, are probably best understood by reference to the schematic diagram of fig. 6.3. To summarise, the steps are:

1) estimate an effective density of states $N(\epsilon')$,

2) self-convolute this density of states to give an an internal distribution $N_i(\epsilon)$,

3) broaden this distribution by the use of equation (16), and

4) calculate an external distribution by the use of an escape function.

The effective density of states for the Ni (100) surface, which, when convoluted with itself, gave the best fit to Hagstrum's experimental data for 5eV helium ions[5], is shown in fig. 6.4. The shape of this curve was established by trial and error but the relative weighting of the d and s orbitals was adjusted by use of equation (12) with $\psi(z)$ being approximated by the radial wavefunction for the isolated nickel atom (Herman and Skillman[7]). The results of using this density of states in the computer model is shown in fig. 6.5. It will be seen that there is reasonably good agreement between this distribution and Hagstrum's distribution shown earlier in fig. 1.2, the major difference being the greater number of electrons observed with low energies in the experimental distribution.

Moving from the effective density of states

FIG. 6.3

Diagram illustrating the different stages in the computer simulation.

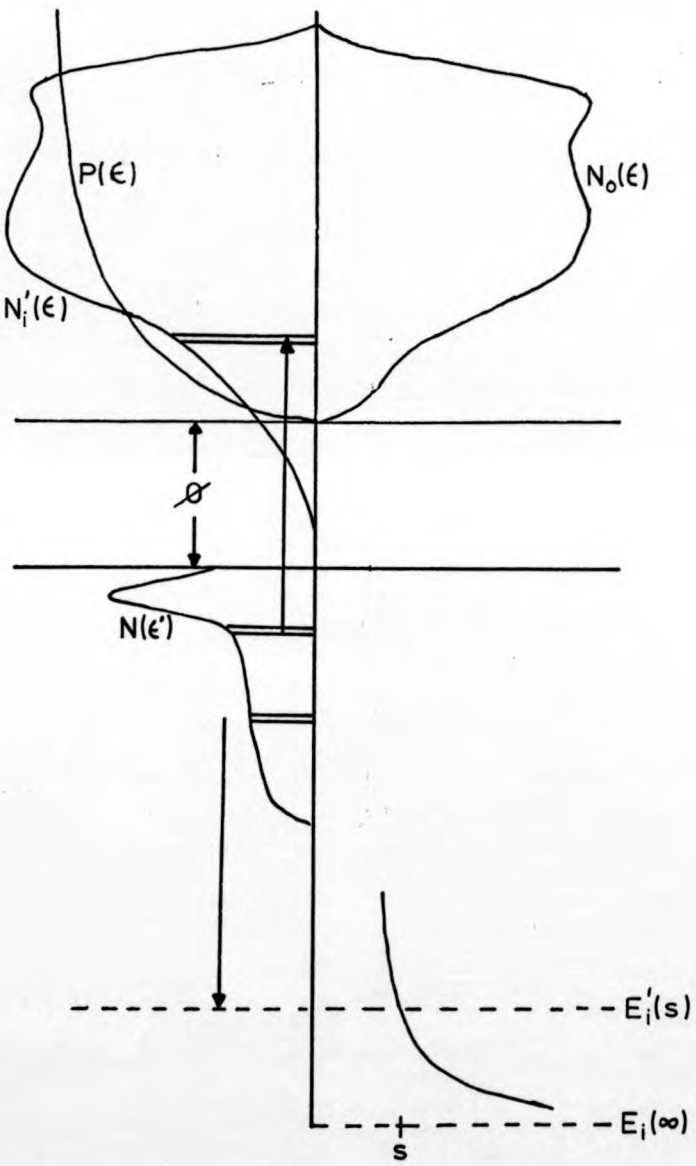
P(ϵ)
N₀(ϵ)
N'ᵢ(ϵ)
ϕ
N(ϵ')
E'ᵢ(s)
Eᵢ(∞)
s

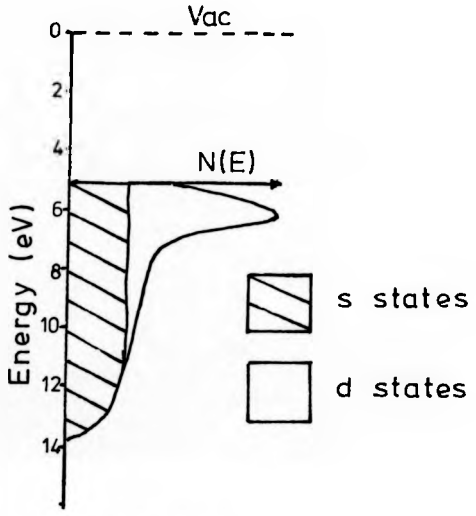

FIG. 6.4

The effective density of states used in the computer simulation for 5 eV helium ions incident on a Ni(100) surface.

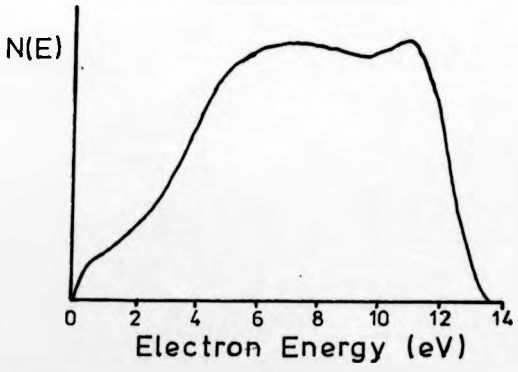

FIG.6.5

The external electron energy distribution produced by the computer using the density of states shown above.

appropriate to the situation for 5 eV ions it is then merely a matter of extrapolation to model the process for slower ions. This extrapolation was performed by the use of equation (12) by first employing the wavefunction of equation (11) and then the radial wavefunctions of the atomic orbitals. The results of both these methods applied to the case of an ion of incident energy 1eV are shown in fig. 6.6. It will be seen that both methods give approximately the same result but that the atomic orbital method has given a greater reduction in the d band. These results confirmed the expectations of the model. However it should be noted that no allowance has been made for

1) the different ionization energies of the electrons within the valence band which will cause k_i of equation (11) to vary, and

2) the variation in the width of the potential barrier between surface and ion as the ion is moved back from the surface.

Both of these effects will tend to favour the participation of electrons from higher in the valence band as the ion is neutralized further from the surface.

The main reason for producing this modelling procedure was to attempt to answer a question related to contamination of the surfaces. If in Hagstrum's experiments contamination leads to a reduction in the number of high energy electrons, could it be possible that contamination combined with an ion being neutralized further from the surface would result in a secondary electron distribution of the type observed in the metastable atom experiments?

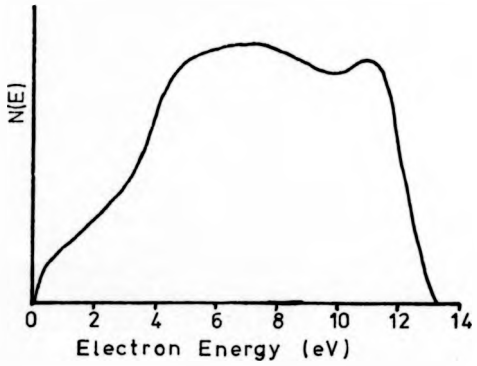

The exponentially decaying wavefunction approximation.

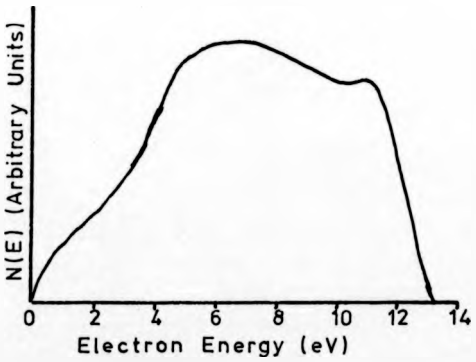

The atomic orbital approximation.

FIG. 6.6

The external electron energy distributions produced by the computer for 1 eV ions incident on a Ni(100) surface.

To answer this question, an effective density of states was produced, which, when used in the computer model, gave an external energy distribution similar to that observed by Hagstrum for 5eV ions incident on a Ni (100) surface with sulphur adsorbed in the c (2 x 2) structure[5]. For this calculation the atomic orbital approximation was used but to achieve a good match between theory and experiment, it was found to be necessary to adjust the values of n_i, the occupancy of each orbital. However, having achieved a reasonable match, changing the values of ψ_i (z) produced the expected distribution for slower ions. The density of states used (based on that obtained by Hagstrum) is shown in fig. 6.7. The resulting secondary electron distribution for 5eV He ions is compared with Hagstrum's experimental results in fig. 6.8 and the result for slower ions is shown in fig. 6.9. From the figures it will be seen that this rather simple model suggests that there will not be a significant difference between the secondary electron distribution for an ion of incident kinetic energy 5eV and that for a 1eV ion, even for a contaminated surface.

It must then be concluded that the results of the present experiment would seem to suggest that the interaction of an ion or metastable atom with a surface will not result in the same final process occurring at the surface as predicted by Hagstrum[2]. From the modelling it is easy to see that following adsorption the change in the work function and form of the effective density of states will result in a drop in the total yield of electrons.

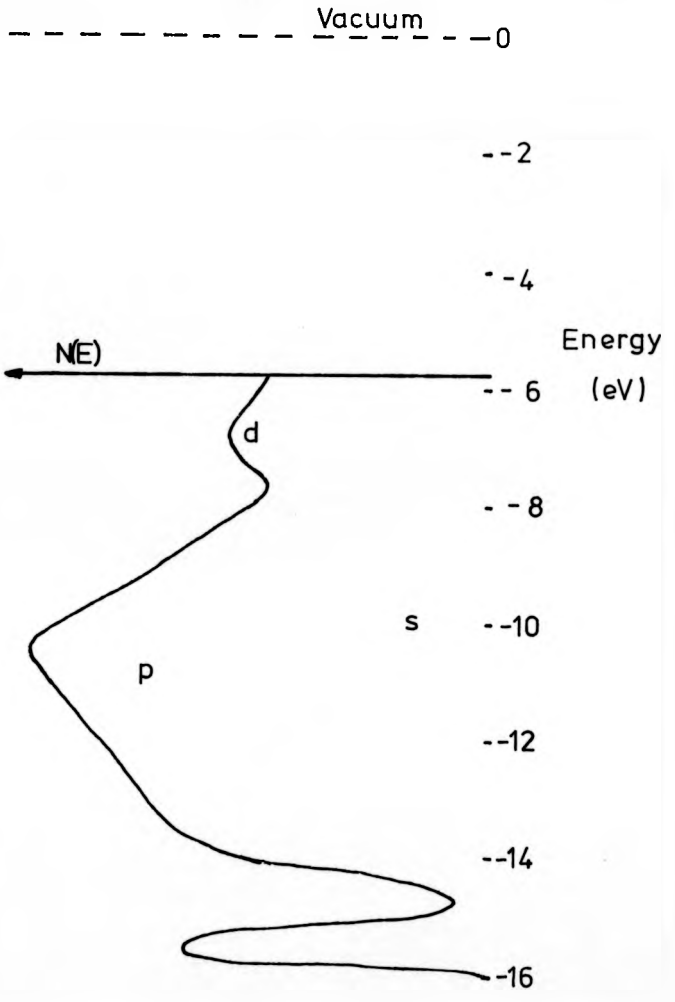

FIG. 6.7

The density of states used for sulphur adsorption on the Ni(100) surface.

FIG. 6.8

Overleaf is shown a comparison of the computer produced external electron energy distribution for 5 eV helium ions incident on a Ni(100)c(2 x 2)S surface and Hagstrum's experimental results for the same system.

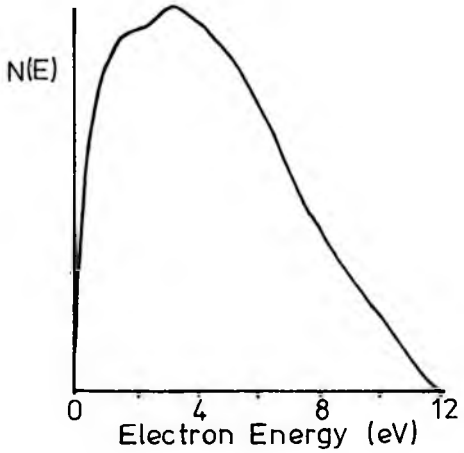

(a) Computer simulation

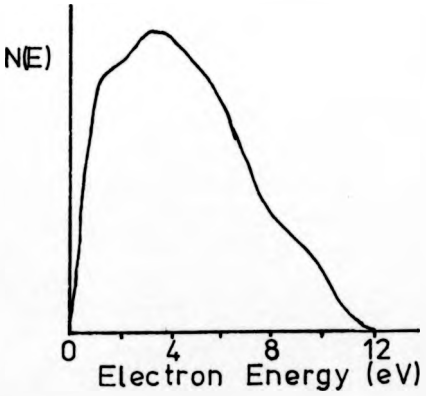

(b) Hagstrum's experimental results.

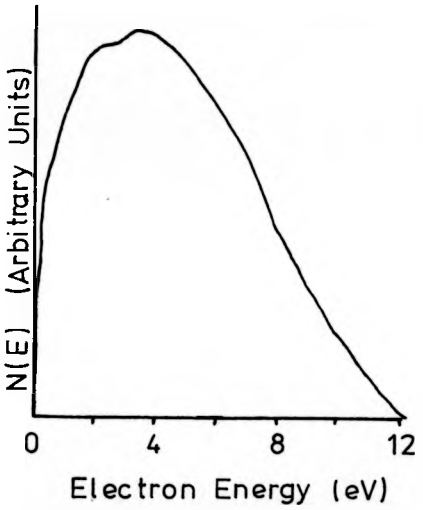

FIG. 6.9

The computer produced external electron energy distribution for 1 eV helium ions incident on a Ni(100)c(2 x 2)S surface.

Such a decrease was not observed in the present experiments with metastable atoms. On the contrary, any contamination was found to cause an increase in the secondary yield. The experiments of Hasted[8], Sonkin[9] and Allison et al[10] have all revealed a similar increase. However, the experiment of Maclennan and Delchar[11, 12] did seem to agree with the mechanism proposed by Hagstrum. These experiments will be discussed in the next section.

6.4 Other Experiments with Metastable Atoms incident on Metal Surfaces

Maclennan and Delchar examined the interaction of argon and helium metastable atoms with the (110) and (111) planes of tungsten. The work function of the (110) surface is 5.3 eV and that for the (111) surface is 4.35 eV. However, they observed no variation in the maximum energy of the electrons ejected from these two planes when using incident helium metastable atoms. If the maximum energy is to be given by

$$E_i'(s) - 2\emptyset \qquad (18)$$

as Hagstrum predicts, they should have found a difference of 1.9 eV. Using two different metastable atoms probes on the same crystal plane, namely argon and helium, they found that the two probes gave a value for the work function which disagreed by 2 eV. With INS, energy broadening is not thought to be an important factor at low energies. Maclennan and Delchar argue that their result of a 2 eV difference in the work function is possibly related to the fact that the two different ions, helium and argon, are neutralized at different distances from the surface and thus $E_i'(s)$ will be different from the respective values

at infinity. However if we consider the case of the argon metastable probe, their results produce a value for $E_i'(s)$ greater than the value at infinity for the (110) surface and suggest that the ion was neutralized at a distance of 60 Å from the (111) surface!

It is possible to apply the computer model to the case of tungsten surfaces. At all times it is assumed that, following repeated anneals at 2300°K, a polycrystalline tungsten surface may be approximated by a (100) plane. The effective densities of states used have been based on the band structure calculations of Christensen and Feuerbacher[13], reproduced in fig. 6.10. The result obtained for a 10 eV helium ion incident on a polycrystalline tungsten surface is shown in fig. 6.11, where it is compared with the experimental results of Hagstrum. The results for a 1 eV ion incident on all three planes are shown in fig. 6.12. As might be expected, the results reflect the change in work function of the different planes. However, more importantly, the effect of the band gap in the density of states of the (110) plane should be noted. This gap results from hybridization of the s and d bands and therefore it could be argued that the model is wrong to use an effect of hybridization in an approximation not including hybridization. In answer, it has to be remembered that Appelbaum and Hamann did show that this bulk density of states is directly involved in the convolution. To some extent, the effect of the band gap in the modelling has been reduced by narrowing its width as might be expected

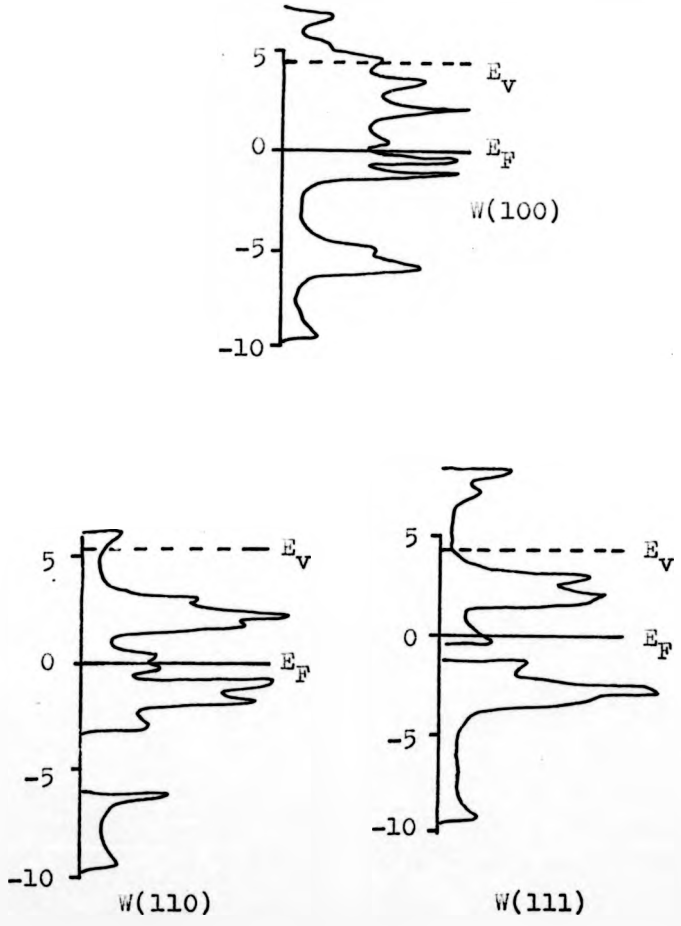

FIG. 6.10

Calculated densities of states for the low index planes of tungsten[13].

FIG. 6.11

Overleaf a comparison is made between (a) the computer simulation of the secondary electron energy distribution resulting from the neutralization of 10 eV ions on a polycrystalline tungsten surface and (b) the experimental results of Hagstrum.

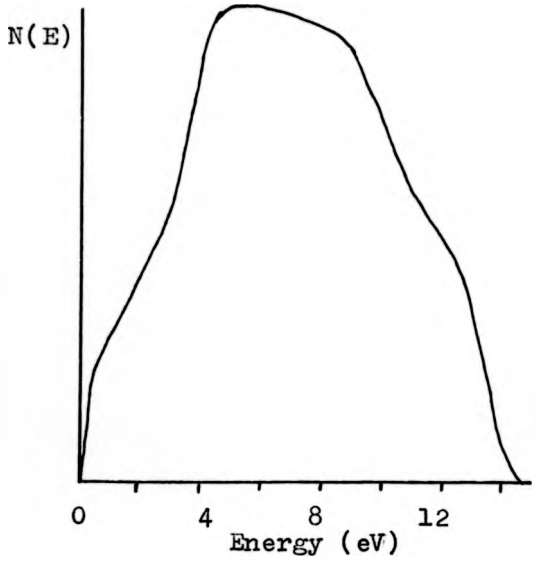

(a) Computer simulation

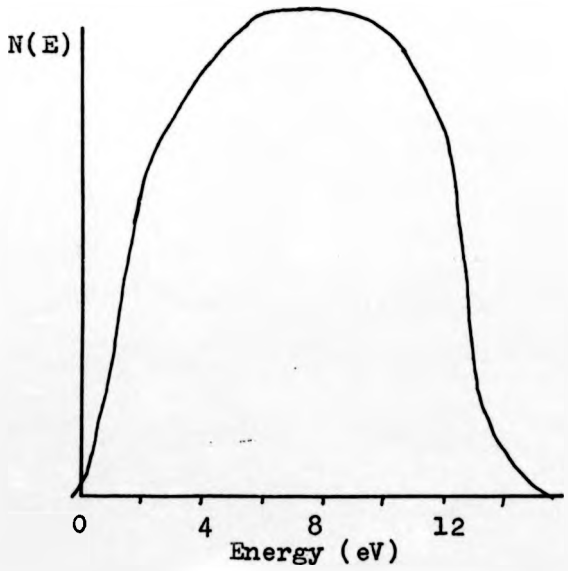

(b) Hagstrum's experimental results

FIG. 6.12

Overleaf are shown computer simulations of the secondary electron energy distributions to be expected from the neutralization of 1 eV helium ions on the low index planes of tungsten.

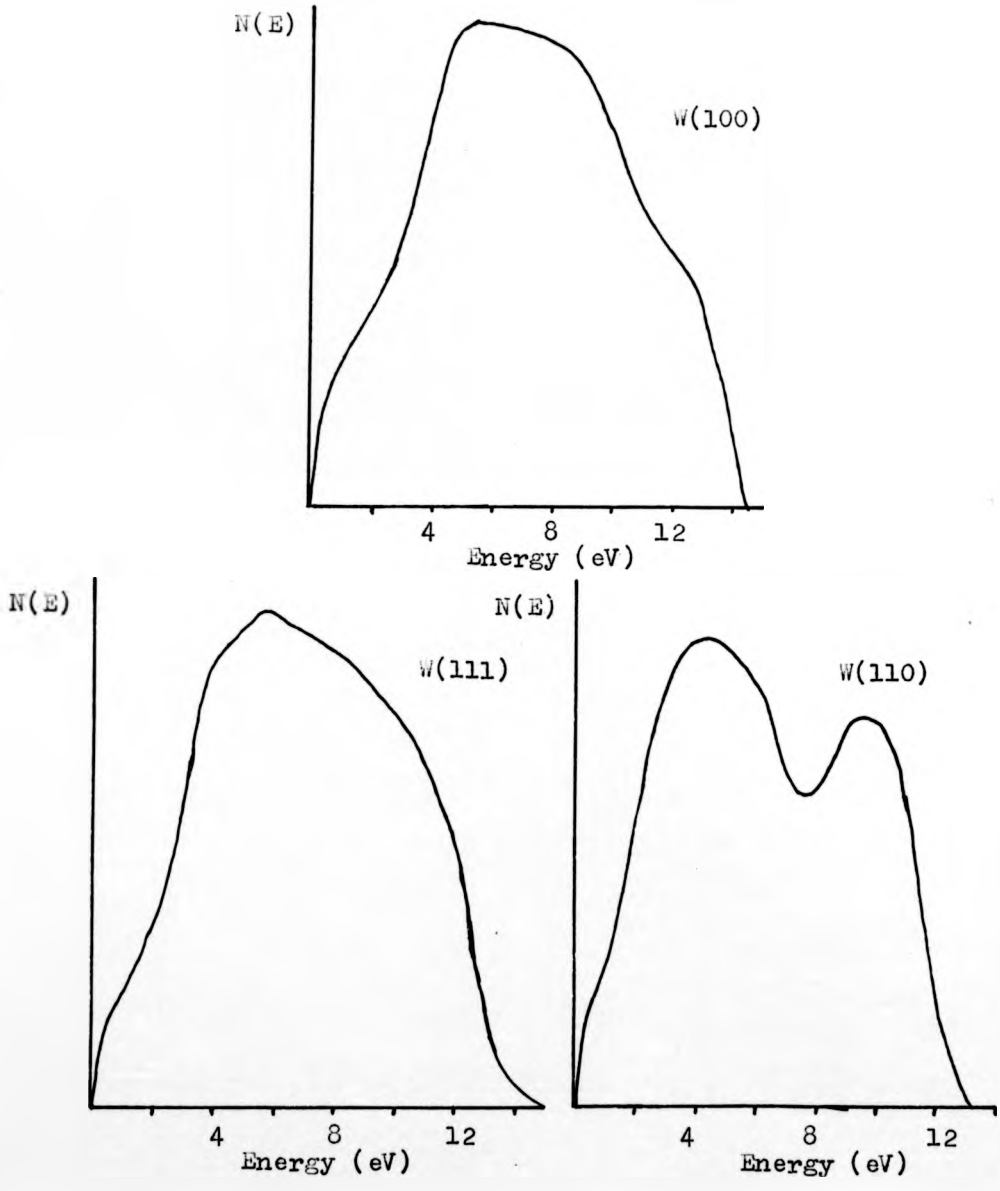
N(E)
W(100)
4
8
12
Energy (eV)
N(E)
W(111)
4
8
12
Energy (eV)
N(E)
W(110)
4
8
12
Energy (eV)

of the d band of a transition metal near the surface. Comparing the results of this model with the results of Maclennan and Delchar, reproduced in fig. 6.13, reveals that their work did not show any structure resulting from this band gap. The results obtained by them are consequently not easily explained by reference to Hagstrum's theory. However it is of interest to examine in more detail the experimental arrangement used to make the measurements. T. A. Delchar has been kind enough to supply the information which is shown in fig. 6.14.

It will be noticed that the metastable atom source is of the type where the atoms are first excited and then formed into a beam by effusion through an orifice. As has already been noted in section 3.2, this type of source produces a beam which may well contain a large percentage of photons. However the source shown in the figure also includes a plate biased at -15V positioned on the exit side of the chamber. Whilst this was undoubtedly included to repel electrons back into the excitation region, it will have the effect of attracting ions in the direction of the exit. In order to remove such ions from the beam the authors have included a series of circular plates which are mounted so as to be coaxial with the beam. It is doubtful whether such an arrangement would be capable of removing an ion that was moving directly on axis towards the target. There will also be the problem of secondary emission of electrons from these plates as a result of impact of either ions or metastable atoms; the resulting electrons may well begin to move

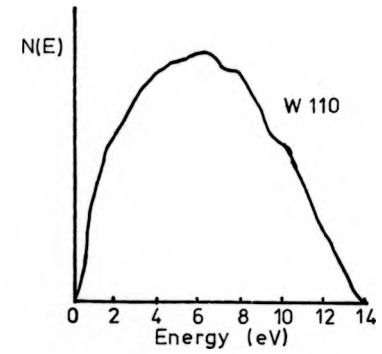

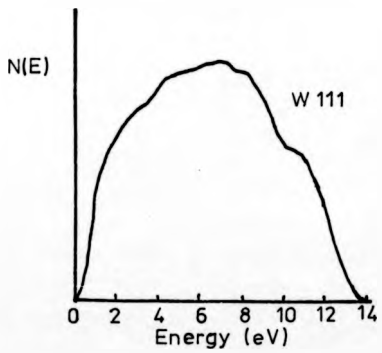

FIG. 6.13

The secondary electron energy distributions obtained by Maclennan and Delchar from different tungsten surfaces.

FIG. 6.14

The experimental arrangement used by Maclennan and Delchar.

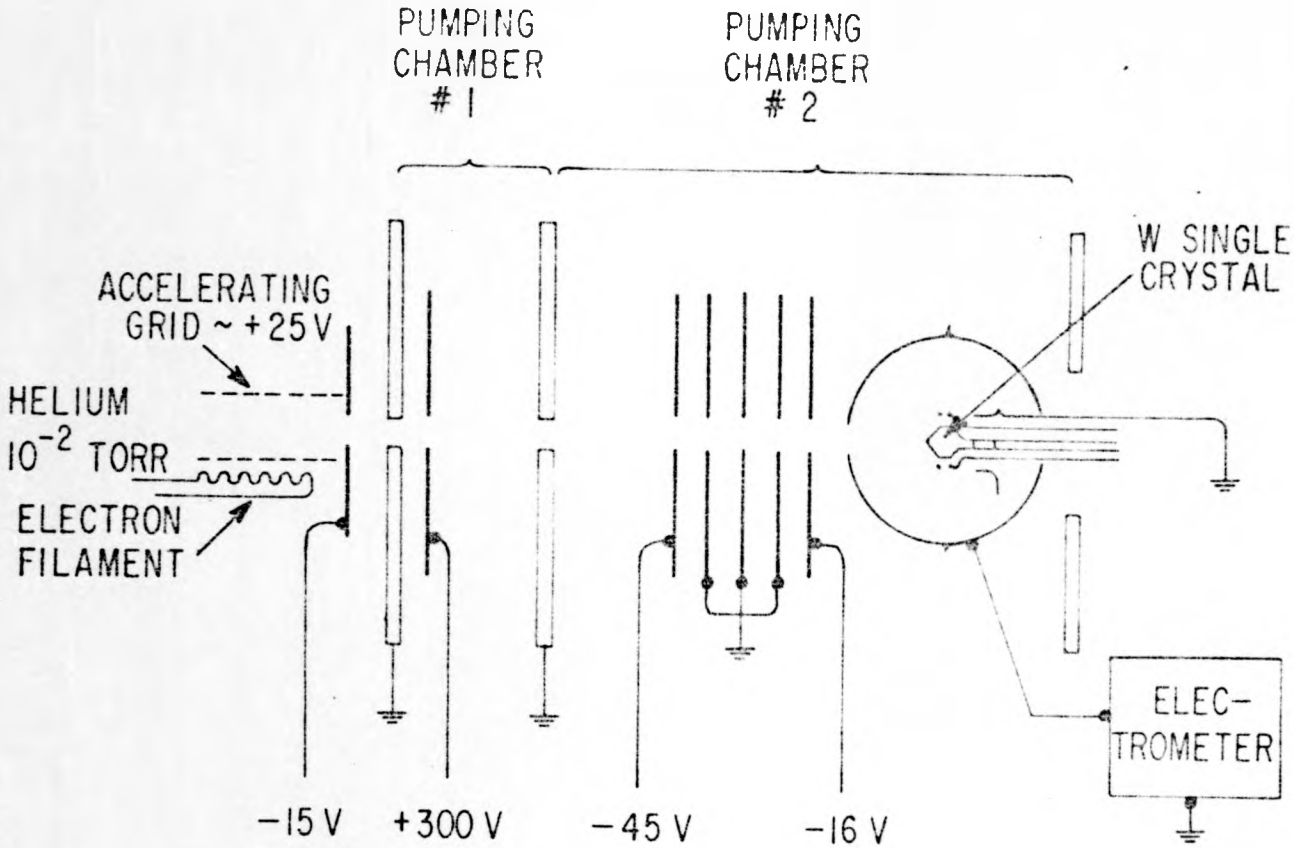
PUMPING CHAMBER #1
PUMPING CHAMBER #2
ACCELERATING GRID ~ +25 V
HELIUM
10^{-2} TORR
ELECTRON FILAMENT
W SINGLE CRYSTAL
ELEC-TROMETER
−15 V
+300 V
−45 V
−16 V

along the axis towards the target. One further possible source of error is the fact that the electron energy distributions were obtained by differentiating the current arriving at the collector. No account is taken of secondary electron emission from the collector and Hagstrum has shown that such emission may well produce a broadened distribution curve[14].

Boiziau et al[15] have recently examined the interaction of helium, argon and xenon metastable atoms with a clean and gas covered molybdenum surface. They used a source similar to Delchar's but it was operated at a higher accelerating voltage $\simeq$ 100V. Such a source should be capable of producing ions but no details are given of methods used for removal of ions from the beam; nor are any deflection plates included in schematic views of the experimental arrangement. Like Delchar, they found that the total yield decreased on exposure of their clean surface to an adsorbate gas but they also had difficulty in explaining the variation in total yield in terms of corresponding work function changes.

Varney[16] examined the interaction of various atoms and molecules in excited states with metal surfaces. In particular he used argon metastable atoms incident on a clean tungsten surface and the same surface in various states of contamination. From a tungsten surface coated with barium oxide, he measured a secondary electron current of 1×10^{-11} A. He concluded that, because of the low work function for this surface, 1.6 eV, the excited atoms were unable to resonance ionize and the electrons resulted

from Auger de-excitation of the atoms. Having cleaned the surface and thus increased the work function to 4.5 eV, he measured a secondary electron current of 3×10^{-13} amps and also a positive ion current of 3×10^{-13} amps. He concluded that the excited atoms were now able to undergo resonance ionization and this resulted in an ion current being reflected from the target. If it is assumed that Hagstrum's theory is correct, then for the clean tungsten surface all of the metastable atoms should undergo resonance ionization. Hagstrum[17] has measured the reflection coefficient for argon ions from a clean tungsten surface and found that it is independent of energy and has a value of 10^{-3}. This would mean that in Varney's experiment the ion current incident on the clean surface was 3×10^{-10} amps. A secondary electron current of 3×10^{-13} amps will then give him a value of 10^{-3} for the secondary electron coefficient from the surface. This value is much less than that measured by Hagstrum[2], who obtained a value of 0.1.

The above experiments may be grouped together and may or may not be considered as evidence supporting the theories of Hagstrum. On the other hand, attention may be drawn to the experiments of Allison et al[10] and Shibata et al[18]. These authors once again measured the energy distributions of electrons ejected from different surfaces as a result of metastable atom impact. Allison et al found that the total yield of electrons tended to increase as their surfaces contaminated and like Shibata

et al proposed a model for the electron ejection process based on Penning ionization.

The details of the Penning ionization process have been described earlier in section 1.7. Briefly, Allison et al proposed a model whereby the incident metastable atom ionized a contaminant surface atom via the Penning mechanism and then the resulting contaminant "ion" was Auger neutralized to produce another free electron. The latter authors went on to suggest that if they were able to produce a clean surface they might well obtain a distribution similar to that of Delchar et al.

In as much as the results of the present experiment were similar to those obtained by Allison et al, their hypothesis of Penning ionization is appealing. In the first approximation it explains the results quite well; as the surface contaminates there are more atoms capable of being ionized and thus more free electrons are produced. However, if the ionized atoms have lost their electrons from the valence band, the neutralization of the resulting ions will produce a relatively low yield of secondary electrons. This may be seen by comparison with experimentally observed total yields of Hagstrum's experiments where he used ions with lower ionization potentials than helium. The authors who proposed this mechanism were not working under U.H.V. conditions and consequently they noted that the degree of contamination might well allow certain atoms to maintain their atomic-like nature with discrete energy levels as opposed to the band like energy levels of the solid. They argued that under these conditions, resonance ioniz-

ation was unlikely as there probably was no suitable resonant energy level to accept the excited electron. However it is unlikely that a chemisorbed atom such as oxygen on nickel will maintain a quasi-atomic nature. In bonding to the surface, the valence electrons of the oxygen will almost certainly hybridize with the band structure of the solid. Both theory[19] and experiment[20] have shown that the chemisorption of oxygen on nickel may be expected to increase the number of empty states above the Fermi level and this may consequently increase the transition rate for resonance ionization. It is therefore not really possible to apply the same arguments to the surfaces in the present experiments.

6.5 A Re-examination of the Resonance Ionization Process

The discussion in the previous two sections leads to the conclusion that there has been no definite evidence, either in the present experiments or the experiments of other authors, that resonance ionization does occur when an excited atom is incident on a metal surface. Such a conclusion prompted the present author to re-examine the resonance ionization mechanism to see if there was any obvious reason why the process should not occur. It was felt that one possible reason might be that the process occurs closer to the surface than has previously been assumed. There have been two attempts to calculate the transition rate for the resonance processes, namely Cobas and Lamb's[1] and Janev's[3], which have been mentioned earlier. Gadzuk[21] has also examined the resonance process in

connection with the adsorption of alkali atoms on a metal surface. The latter author pointed out that the approach of Cobas and Lamb was not formally correct as it is not possible to naively apply a perturbation approach to initial and final states which are eigenfunctions of drastically different Hamiltonians. This is the situation where the initial state is an atomic electron and the final state a metallic electron. It was therefore decided to attempt a perturbation approach to the problem of the resonance ionization of an excited helium atom again, but this time to follow the guidelines from Gadzuk's work.

It will be shown later that in any calculation of the transition rate, it is necessary to know the shift of the 2s energy level of the excited atom as a function of distance from the surface. This shift has been considered by Hagstrum[2] who derived approximate values by considering the interaction of the atom with the surface to be compounded of the following possible components:

1) the Coulombic image force attraction for ions,

2) the Van der Waals attraction resulting from the particle's polarizability,

3) a possible exchange force of the type responsible for the covalent bond, and

4) the repulsion resulting from interpenetration of the electron clouds and the Pauli principle.

Whilst such approximations will give an indication of the shift, the more formal method used both by Gadzuk and by Remy[22] to establish the shift in the valence

band of alkali atoms near a metal surface will be used in the present treatment. They considered the interaction in terms of the perturbation on the energy levels caused by the presence of the images of the ion core and electron in the metal.

Consider the diagram of fig. 6.15. An electron at distance d from a metal surface may have its interaction with the surface represented by the classical image potential $-\frac{q^2}{4d}$. Appelbaum and Hamann[23] have shown that the classical image potential is an adequate approximation to the true interaction for distances $\geqslant 2$ Å from the surface. The presence of the ion core in the surface region perturbs the metal and thus alters this interaction. Referring to fig. 6.15, the perturbation on the metal gives rise to a repulsive interaction $+\frac{q^2}{R}$ between the image of the positive ion core and the electron. R is the distance between the electron and the image of the ion core. Further, the electron feels the Coulomb attraction of the alkali ion core $-\frac{q^2}{r}$. The total Hamiltonian of the system, metal plus atom, is given by

$$H_{TOT} = H_A + H_M + H_{INT} \qquad (19)$$

where H_A describes the unperturbed atom, H_M the unperturbed metal and H_{INT} the coupling between the atom and metal. The Born-Oppenheimer approximation is assumed and thus equation (19) is taken as the electron Hamiltonian. Gadzuk has shown that this Hamiltonian may be reduced to the single electron Hamiltonian

$$H = -\frac{\hbar^2}{2m}\nabla^2 - \frac{q^2}{4d} + \frac{q^2}{R} - \frac{q^2}{r} \quad \text{for } \epsilon > s_c \qquad (20)$$

$$H = -\frac{\hbar^2}{2m}\nabla^2 - V_o \quad \text{for } \epsilon < s_c \qquad (21)$$

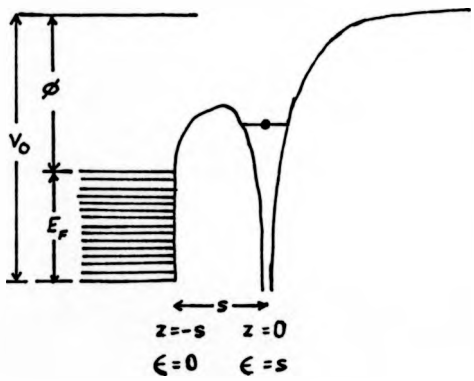

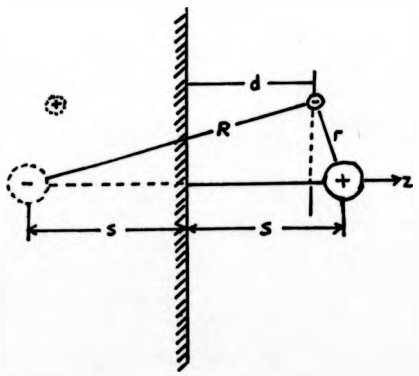

FIG. 6.15

Diagram showing the parameters used in the calculation.

where V_o is given by $(\phi + E_F)$, ϕ being the metal's work function and E_F the energy of its Fermi level measured from the bottom of its conduction band.

For $\epsilon > s_c$, the Hamiltonian may be split into a soluble unperturbed Hamiltonian plus a perturbation

$$H_a = -\frac{\hbar^2}{2m}\nabla^2 - \frac{q^2}{r} \qquad (22)$$

$$H'_{a-M} = -\frac{q^2}{4d} + \frac{q^2}{R} \qquad (23)$$

These equations describe an atomic electron existing as a solution of H_a that is perturbed by the metal through H'_{a-M}. As the atom interacts with the metal, there is a shift in the atomic energy level which, by first order perturbation theory, is given by

$$E = \frac{\langle \psi_{2s} | H' | \psi_{2s} \rangle}{\langle \psi_{2s} | \psi_{2s} \rangle} \qquad (24)$$

ψ_{2s} being the wavefunction of the unperturbed atomic electron. Following Cobas and Lamb, the following function was used for the 2s electron of the excited helium atom

$$\psi_{2s} = \frac{1}{4\sqrt{2\pi}}\left(\frac{Z}{a_o}\right)^{3/2}\left(2 - \frac{Zr}{a_o}\right)e^{-Zr/2a_o} \qquad (25)$$

where a_o is the Bohr radius and Z = 1.19. Thus equation (24) reduces to

$$E = \frac{\int_{-(s-s_c)}^{\infty} dz \left(\frac{q^2}{2s+z} - \frac{q^2}{4(s+z)}\right)\left\{\iint_{-\infty}^{+\infty} dxdy(1-2ar+a^2r^2)e^{-2ar}\right\}}{\int_{-(s-s_c)}^{\infty} dz \left\{\iint_{-\infty}^{+\infty} dxdy(1-2ar+a^2r^2)e^{-2ar}\right\}} \qquad (26)$$

where a is given by $Z/2a_o$. The coordinate system used in this calculation is one with z = 0 at the centre of the ion core and z increasing positively away from the

metal. Further, the integration has been restricted to the region outside the metal ($z > -(s-s_c)$) and R and d have been approximated by 2s+z and s+z respectively, s being the ion's s distance from the surface. Equation (26) has been evaluated by both Gadzuk and Remy yielding

$$E = q^2 \frac{\int_{-(s-s_c)}^{\infty} \frac{1}{2s+z} - \frac{1}{4(s+z)}(4a^3|z|^3 - 2a^2|z|^2 + 2a|z| + 1)e^{-2a|z|}dz}{\int_{-(s-s_c)}^{\infty} (4a^3|z|^3 - 2a^2|z|^2 + 2a|z| + 1)e^{-2a|z|}dz} \qquad (27)$$

As Remy noted, there exists some disagreement in the literature as to the evaluation of this equation and therefore a further evaluation was attempted. The result was in the rather cumbersome form

$$\begin{aligned} E = \frac{q^2 a}{8}\Big(& e^{-2a(s-s_c)}(50a^2s^2 - 26a^2ss_c - 6a^2s_c^2 + 3a(s-s_c) + \tfrac{9}{2}) \\ & + 4e^{-4as}(32a^3s^3 - 8a^2s^2 + 4as - 1)\int_{2a(s+s_c)}^{4as} \frac{e^t}{t}\,dt \\ & - (4a^3s^3 - 2a^2s^2 + 2as + 1)e^{-2as}\int_{2as_c}^{2as} \frac{e^t}{t}\,dt - 4e^{4as}(32a^3s^3 \\ & + 8a^2s^2 + 4as - 1)\int_{4as}^{\infty} \frac{e^{-t}}{t}\,dt + (4a^3s^3 + 2a^2s^2 + 2as - 1)e^{2as}\int_{2as}^{\infty} \frac{e^{-t}}{t}\,dt\Big) \\ & (2 - e^{-2a(s-s_c)}(a^3(s-s_c)^3 + a^2(s-s_c)^2 + \tfrac{3}{2}a(s-s_c) + 1))^{-1} \end{aligned} \qquad (28)$$

Using this equation, values of the shift as a function of distance of the ion from the surface were calculated and plotted in fig. 6.16. Also plotted are the shifts given by Hagstrum's approximation. It will be seen that little advantage was gained from the exercise as at large distances from the surface the two approximations are in fairly good agreement.

With the metastable atom and metal interacting

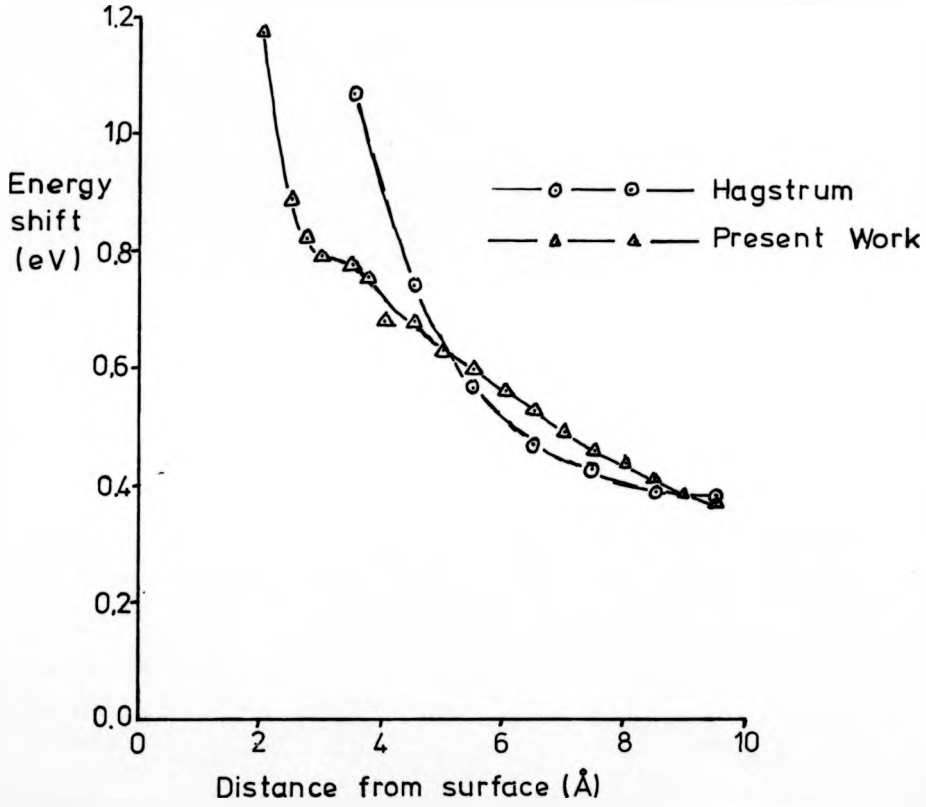

FIG. 6.16

A comparison of the energy shift of the excited level of the helium metastable state near a metal surface as given by the present calculations and by Hagstrum's approximation.

as shown in fig. 6.15, the transition rate w for resonance ionization is given by a modified first order Golden Rule as;

$$w = \sum \frac{2\pi}{\hbar} \rho_k \, T_{if}^{\,2} \qquad (29)$$

where the sum is over all degeneracies of the metal state and the transition matrix element T_{if} is discussed below. Treating the transition process as a re-arrangement collision Gadzuk has shown that both resonance neutralization and resonance ionization may be treated by the same matrix element.

The Hamiltonian of equation (20) may now be divided as

$$H_M = -\frac{\hbar^2}{2m}\nabla^2 - \frac{e^2}{4d} + \frac{e^2}{R} \qquad (30)$$

and $$H'_{M-a} = -\frac{e^2}{r}$$

These equations describe a conduction electron in the surface region in a state which is an eigenfunction of H_M, perturbed by the presence of the ion core through H'_{M-a}. The matrix element for the resonance processes is then written as

$$T_{i,f} = \langle n,s | -\frac{e^2}{r} | u_t \rangle \qquad (31)$$

where $|n,s\rangle$ is the wavefunction of the atomic electron (equation (25) in the present case) and $|u_t\rangle$ is the metallic electron wavefunction for which Gadzuk uses the form

$$u_t = \frac{1}{k_v L^{3/2}} e^{i(k_1 x + k_2 y)} 2k'_3 e^{ik_3 \epsilon} \quad \text{for } \epsilon > 0. \qquad (32)$$

L is the length of the large but finite cubic metal,

and k and k' are the wavenumbers of the electron state measured from the vacuum level and from the bottom of the conduction band. The subscripts 1, 2, and 3 refer to the projections in the x and y directions, parallel to the surface, and the z or ξ direction perpendicular to the surface. The wavenumber k_v is defined by

$$\phi + E_F = \frac{\hbar^2 k_v^2}{2m} \tag{33}$$

The reader is referred to the paper by Gadzuk for the evaluation of the matrix element $T_{i,f}$ where the final form is given by

$$T_{i,f} = \frac{2\sqrt{\pi} e^2 k_v' a^{\frac{1}{2}} s^2 e^{-Fs}}{k_v L^{3/2} F^2} \left(1 + \frac{2}{a^2 sF}(a^2 - F^2)\right) \tag{34}$$

F is given by

$$F^2 = a^2 + k_1^2 + k_2^2$$

and a is the constant defined earlier in the atomic wavefunction.

If the density of states as a function of energy is given by

$$\rho_k = \frac{mkL^3}{\hbar^3 (2\pi)^3} \sin\theta d\theta d\phi \tag{35}$$

then substitution of the matrix element $T_{i,f}$ into equation (29) for the transition rate gives after evaluation of integrals:

$$w = \frac{2a^4 q^2 k' s^3 e^{-2as}}{k_v^2 a_o \hbar} \left(1 - \frac{4}{a^2 s^2} + \frac{8}{a^4 s^4}\right) \tag{36}$$

where $a_o = \hbar^2/mq^2$.

Starting with the transition rate w, it is possible to derive two related probability functions. The probability that a particle in moving with velocity v_o through the element ds at distance s from the surface will undergo transition is given by $^{wds}/_{v_o}$. Then the probability $P_o(s,v_o)$ that the incident particle, starting from infinity and moving towards the metal, will reach the distance s without undergoing transition is given by

$$P_o(s,v_o) = 1 - \int_s^\infty \frac{w\,ds}{v_o} \tag{37}$$

For large distances from the surface this may be approximated by

$$P_o(s,v_o) = \exp\left(-\int_s^\infty \frac{w\,ds}{v_o}\right) \tag{38}$$

The probability that the particle, having started from infinity, will undergo transition in ds at s is then

$$P_t(s,v_o)\,ds = \frac{w\,ds}{v_o} \exp\left(-\int_s^\infty \frac{w\,ds}{v_o}\right) \tag{39}$$

Most authors in the past have assumed that the transition rate w may be expressed in the form

$$w = A \exp(-as) \tag{40}$$

where A and a are constants. However, reference to equation (36) above shows that A is not constant and therefore it was decided that in any evaluation of $P_t(s, v_o)$ the integral in equation (39) would be evaluated as a function of distance from the surface. This then enables $P_t(s, v_o)$ to be written as

$$P_t(s,v_o) = \frac{K(E+\Delta E)^{\frac{1}{2}} s^3 e^{-2as}}{v_o}\left(1 - \frac{4}{a^2s^2} + \frac{8}{a^4s^4}\right) \tag{41}$$

$$\times \exp\left(\frac{K(E+\Delta E)^{\frac{1}{2}}}{v_o} e^{-2as}\left(\frac{s^3}{2a} + \frac{3s}{4a^2} - \frac{5s}{4a^3} - \frac{5}{8a^4}\right)\right.$$

where K is a constant given by

$$K = \frac{2a^4 a^4 m^{\frac{3}{2}} \sqrt{2}}{k_v^2 h^4}$$

E is the energy of the excited electron at infinity referred to the bottom of the conduction band and ΔE is the shift of the excited electron energy level computed by equation (28). $P_t(s, v_o)$ was evaluated at different distances from the surface for a He (2^3S) atom incident on a tungsten surface. The results of this evaluation are shown in fig. 6.17 where it will be seen that the resonance processes have a maximum probability at 5 Å from the surface. This is closer to the surface than the predictions of either Cobas and Lamb or Janev, but it is still a relatively long distance away. The fact that resonance ionization may occur closer to the surface does not seriously alter the conclusions of section 6.3, as Auger neutralization of the ion thus formed will occur at about 2.8 Å as opposed to 2.6 Å.

Thus, from the analysis of this section, it will be seen that there is no obvious reason why resonance ionization should not occur unless some other process has a higher transition rate at large distances from the surface.

6.6 The Possibility of Auger De-excitation

It was shown earlier in section 1.5 of chapter one that if an excited atom Auger de-excites at a surface, the electron in the excited stated will be ejected with energy E_k given by

$$E_k = E_x' - \epsilon \qquad (42)$$

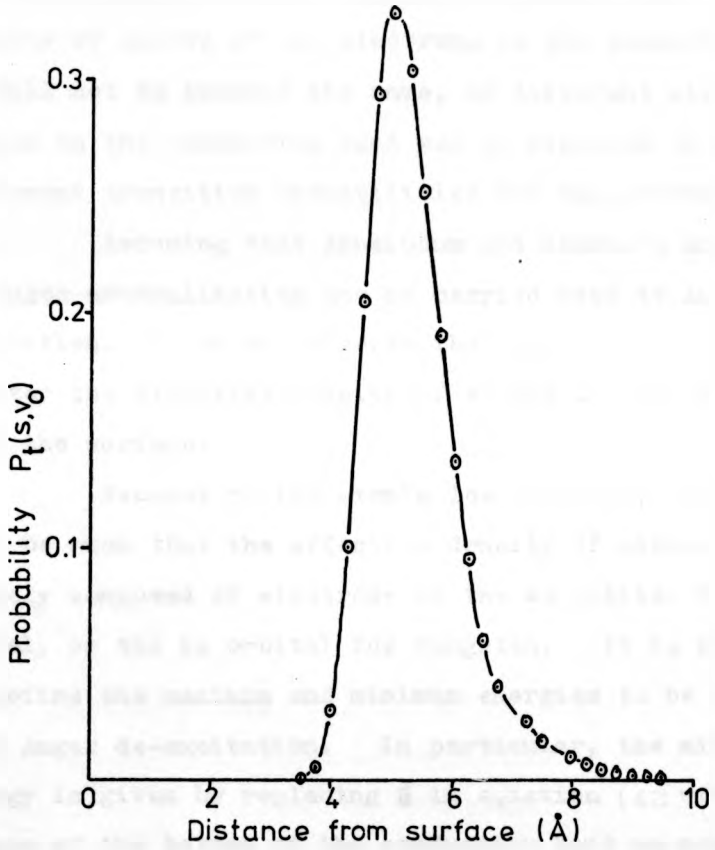

FIG. 6.17

The probability of resonance ionization occurring at different distances from the surface as given by the present calculations.

where E_x' is the effective excitation energy of the atom near the surface and ϵ is the energy of the participating metallic electron, measured from the vacuum level. Examination of equation (42) leads to the conclusion that the external electron energy distribution resulting from such a process should be very similar in form to the actual density of states of the electrons in the conduction band. It will not be exactly the same, as different electron states in the conduction band may be expected to have different transition probabilities for the process.

Assuming that Appelbaum and Hamann's analysis of Auger neutralization may be carried over to Auger de-excitation, it can be inferred that the excited atom will monitor the effective density of states at some distance from the surface.

Because of the atom's low velocity, this distance will be such that the effective density of states is largely composed of electrons in the 4s orbital for nickel, or the 6s orbital for tungsten. It is possible to define the maximum and minimum energies to be expected from Auger de-excitation. In particular, the minimum energy is given by replacing ϵ in equation (42) with the energy of the bottom of the conduction band as measured from the vacuum level. Applying this procedure to the case of a He (2^3S) incident on a Ni (100) surface produces a value of about 6.5 eV for the minimum energy of the ejected electrons. This is clearly a lot higher than anything observed in the present experiments and at first leads to the conclusion that Auger de-excitation does not occur. However, a re-examination of the

electron energy distributions recorded from a clean nickel surface, fig. 4.8, and from a clean tungsten surface, fig. 5.6, shows that these distributions are similar in form to the spectrum of "true secondary" electrons resulting from the impact of electrons on a surface. The spectra of secondary electron distributions resulting from low energy electrons incident on a molybdenum surface[24] are shown in fig. 6.18. It will be seen that the region of these distributions associated with the "true secondaries" is generally peaked at about 2eV; the same was observed for secondary electrons resulting from the impact of metastable atoms on clean surfaces. A possible explanation for the results from a clean surface therefore, is that the excited atom Auger de-excites and the electron released in the transition is preferentially ejected in the direction of the metal surface.

An argument in favour of such preferential ejection is that the metallic electron, in falling to the hole in the groundstate of the atom, leaves behind a hole in the conduction band. This latter hole will be positively charged and may well exert an attractive force on the electron released from the 2s level of the atom. Such an argument would seem to imply that the hole in the 1s level is filled at a distinct time interval before the 2s electron is released, which is incorrect as the two processes will occur simultaneously. However the idea does point to the fact that no regard to final state effects is made in the calculation of a transition rate simply by use of the matrix element

FIG. 6.18

The energy spectra for secondary electrons emitted from polycrystalline molybdenum under bombardment by primary electrons incident along the surface normal. The primary energy is indicated and for convenience the spectra are plotted as a function of energy loss and not emission energy[24].

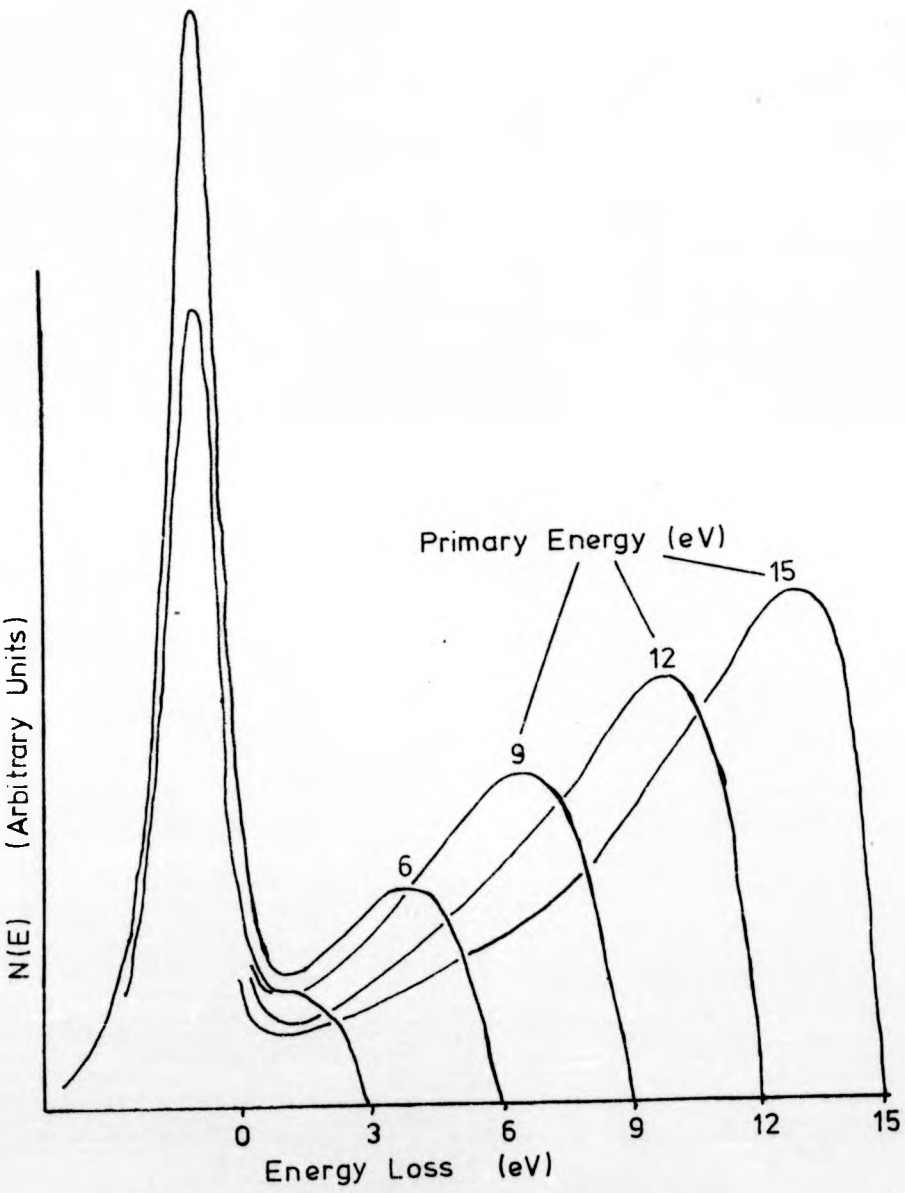
Primary Energy (eV)
15
12
9
6
N(E) (Arbitrary Units)
0
3
6
9
12
15
Energy Loss (eV)

$$U_f^*(\underline{r}_1)U_G^*(\underline{r}_2)\frac{e^2}{r_{12}}U_M(\underline{r}_2)U_E(\underline{r}_1)d\underline{r}_1 d\underline{r}_2 \qquad (43)$$

It is known from many photoelectron experiments that contamination of a surface leads to an increase in the number of secondary electrons[25]. With this fact it is possible to postulate that the excited atom Auger de-excites at the surface and, as a result of the excited electron entering the metal, a number of secondary electrons are allowed to escape from the surface. As the surface contaminates, the number of secondary electrons increases and thus the total yield increases. However it was felt that the total yields were rather high to be explained solely by secondary electrons resulting from the relatively low energy electrons released in the Auger de-excitation process and therefore other mechanisms were explored.

6.7 Other Possible Mechanisms for the Ejection of Electrons

The first mechanism that was examined was done in an attempt to explain the increase in the total yield as the surface contaminates; in particular, the question of why the adsorption of carbon monoxide on tungsten produces a larger increase when the CO was adsorbed in the α state than the β state.

Within the energy range of interest the molecular orbitals of the carbon monoxide molecule are tabulated in Table 1[26]. This table shows the observed experimental photoionization data for the gas phase molecule and also for the molecule adsorbed on the

Gas phase photoionization data.

Energy Level	Measured I.P. (eV)
5σ	14.0
1π	16.5
4σ	19.7

Surface photoionization data.

Energy Level	Binding relative to E_f (ev)	Work Function (eV)	Binding Energy (eV)
CO(1)	8.3	5.0	13.3
CO(2)	~11.4	5.0	16.4

TABLE 1

The measured ionization potentials for the different energy levels of the gas phase CO molecule and for the CO molecule adsorbed in the α-state on a tungsten (100) surface.

Molecular Orbital	<z> (a.u.)	n	Atom
1σ	-1.0657	2	O
2σ	1.0653	2	C
3σ	-0.4841	2	$\sim$O
4σ	-1.0910	2	O
5σ	1.5700	2	C
1π	-0.5572	4	$\sim$O

TABLE 2

The distribution of charge in the carbon monoxide molecule. The origin is at the midpoint between C and O, and C is in the +z direction. The number of electrons, n, occupying each orbital is also shown.

tungsten (100) surface in the α-state. The level labelled CO(1) in the surface work is believed to be derived from overlapping 5σ and 1π CO orbitals. In Table 2, the average distance $\langle z \rangle$ from the centre of the CO molecule is tabulated from the work of Huo[27]; the carbon atom is considered to be in the +ve direction. The atom towards which the charge distribution of each molecular orbital is displaced is also indicated.

As stated earlier, section 5.6, the carbon monoxide molecule adsorbed in the α-state is believed to stand upright on the surface with the carbon atom next to the surface. With this simple picture and the information tabulated in Tables 1 and 2, it can be seen that the incoming excited atom may be expected to interact preferentially with electrons in the 4σ state, for which the binding energy is approximately 16.4 eV. The elctrons released in the initial de-excitation may still be expected to travel towards the metal and may be reflected or lead to the emission of secondary electrons. However, there now exists the possibility that the hole in the 4σ orbital, which will be reasonably localised on the adatom, will be filled by processes analagous to the Auger mechanism for the neutralization of incident ions. Such a process will lead to the release of a number of low energy electrons. Adsorption into the β-state is believed to be dissociative and as such this 4σ molecular orbital will not be seen by the incident metastable atom; therefore the increase in the yield will not be as large.

In order to examine this mechanism in more detail, the computer model used earlier for the Auger neutralization process was modified to give some measure of the total yield to be expected from such a process. The effective ionization energy of the incident ion was replaced by the energy of the 4σ resonance measured from the vacuum level. The internal electron energy distribution $N_i(\epsilon)$ was then calculated but, because of the lower energies involved, it was necessary to restrict the transitions to those which produced an excited electron at an energy ϵ above the Fermi level. This distribution $N_i(\epsilon)$ was normalised to one excited electron per hole in the conduction band and consequently one electron per incident atom. Multiplying this internal distribution by an escape function then gives an external distribution $N_o(\epsilon)$ and the total yield γ can be found simply from the equation

$$\gamma = \int_o^\infty N_o(\epsilon)\,d\epsilon \qquad (44)$$

When modelling a process such as this, it is difficult to know what form to use for the density of states. Should it be the density of states in the top layer of the substrate or the effective density of states centred on the adatom? The eventual form used was thought to be something midway between the two possibilities; however, as no information exists within the literature it cannot be said that this model is thought particularly accurate. The use of the same escape function for this process as that used by Hagstrum[2] for Auger neutralization produces a figure of approximately 0.1 electrons/excited

atom for γ . The external distribution obtained from this mechanism is shown in fig. 6.19. It was felt that the escape function used to derive this distribution might not be appropriate, as it was derived to account for the overlap of the wavefunction of the electron excited in the neutralization process, with the ion outside of the surface. Possibly a more appropriate escape function would be that describing an isotropic distribution for the excited electrons. Such an escape function is given by[2]

$$P(\epsilon_k) = \tfrac{1}{2}(1 - (\epsilon_o/\epsilon_k)^{\frac{1}{2}}) \text{ for } \epsilon_k > \epsilon_o \quad (45)$$
$$= 0 \text{ for } \epsilon_k < \epsilon_o,$$

where ϵ_k and ϵ_o, the vacuum level, are measured from the bottom of the conduction band. The isotropic escape function is compared with that appropriate to the Auger neutralization process in fig. 6.20. The use of the isotropic escape function gave a smaller total yield of approximately 0.01, and the external distribution was now peaked at 4 eV. It could be argued that the hole in the 4σ orbital will remain localised on the oxygen atom and that the use of the Auger neutralization escape function is therefore reasonable. Allison et al[10] measured the angular distribution of the electrons leaving their metal surface as a result of excited atom impact and they found that the low energy electrons tended to have a more marked anisotropy than the higher energy electrons. In fact the direction in which the low energy electrons was emitted tended to be peaked at the normal to the surface. They attempted to explain such

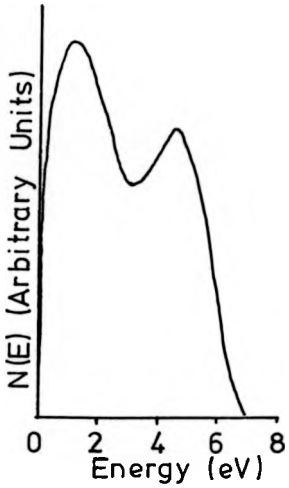

FIG. 6.19

The secondary electron energy distribution produced by the computer in an attempt to account for the increased total yield when CO is adsorbed on a tungsten surface in the α-state.

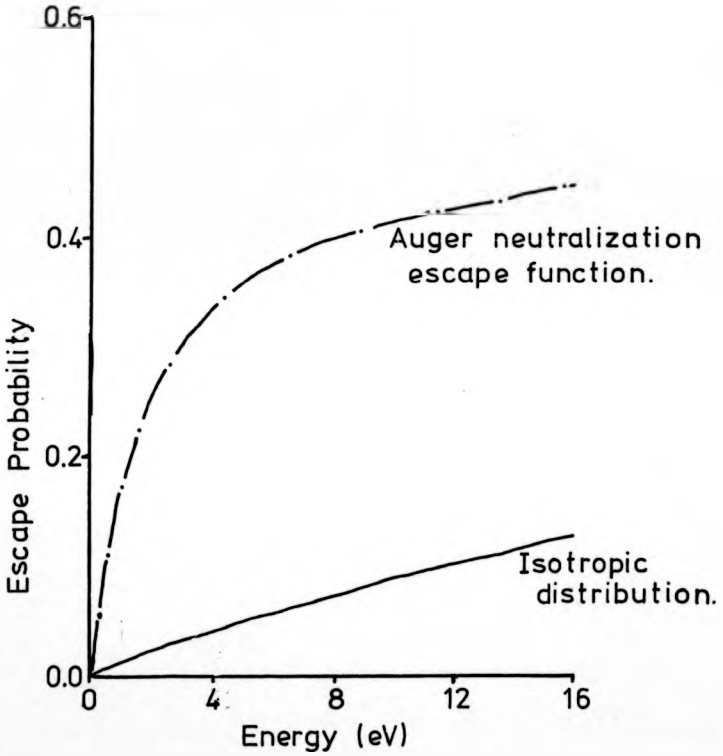

FIG. 6.20

The Auger neutralization escape function is compared with the escape function for an isotropic distribution of the excited electrons. The energy scale refers to the external energy with respect to the vacuum level.

an anisotropy by suggesting that it was a characteristic of isotropic emission from many facets oriented in different directions.

Is it possible to apply such a model to the adsorption of the chalcogens on nickel? Fig. 6.21 shows the densities of states obtained by Hagstrum and Becker[5] using INS for the different chalcogens adsorbed on the Ni (100) surface in the c (2 x 2) structure. Also included in the figure is the density of states taken from a Ni (100) surface that was heavily contaminated with sulphur. In attempting to assign different molecular orbitals to the resonances observed in these distributions, Hagstrum and Becker made reference to the vertical ionization energies observed for the different orbitals in the gaseous hydrogen chalcogenides H_2S, H_2O, and H_2Se. These energies are tabulated in Table 3. When the chalcogens are bonded to a nickel surface it is believed that the bonding orbital $1b_1$ and the non-bonding orbital $1b_2$ are both parallel to the surface. The bonding orbital $3a_1$ is believed to be perpendicular to the surface. Because of their greater breadth the resonances labelled A in fig. 6.21 are associated with the bonding orbitals of the chalcogen; exchange of electrons between the adatom and substrate may be expected to produce a broad resonance. Within this resonance no attempt has been made to assign different areas to different bonding orbitals. However if it is assumed that the two orbitals maintain their same relative binding energies as in the hydrogen chalcogenides, it would seem that the binding energy of the orbital that

	Orbitals		
	$1b_1$	$3a_1$	$1b_2$
H_2O	12.6	14.7	18.3
H_2S	10.5	13.3	15.4
H_2Se	9.9	12.9	14.6

TABLE 3

Vertical ionization energies in electron volts for several orbitals in the free molecules H_2O, H_2S, and H_2Se obtained by molecular photoelectron spectroscopy.

projects from the surface, $3a_1$, is only far enough below the Fermi level to produce an increase in the total yield by the mechanism proposed for the situation of oxygen adsorption. Even for oxygen the increase will be low. Re-examination of fig. 6.21 shows peaks, labelled B, at 9eV below the Fermi level for the sulphur contaminated surface and 8 eV below the Fermi level for the selenium covered surface. No similar peak is observed in UPS measurements from the same surfaces and consequently Hagstrum[28] concludes that this peak is more readily seen by his incoming ion than the photon. He further suggests that this orbital may well have s-character. If the metastable atom interacts preferentially with an orbital such as this, it will lead to an increase in the total yield by the mechanism proposed. The peaks labelled C in fig. 6.21 are believed to be associated with secondary electrons near the vacuum level.

The model proposed for the system of carbon monoxide adsorption on tungsten does not seem so straightforward when applied to the situation of chalcogen adsorption on a nickel surface. Therefore a second mechanism was explored, whereby the incident atom interacted with the adsorbate via the core level immediately below the valence band. If the atom was initially de-excited by an electron falling from a level approximately 18.5eV below the vacuum level, the energy released in this transition would result in an electron with an energy approximately 1eV above the vacuum level. The subsequent occupation of the core hole by electrons falling from the valence band would result in

FIG. 6.21

Overleaf are shown the densities of states measured by Hagstrum and Becker[5] for the chalcogens adsorbed on the Ni(100) surface.

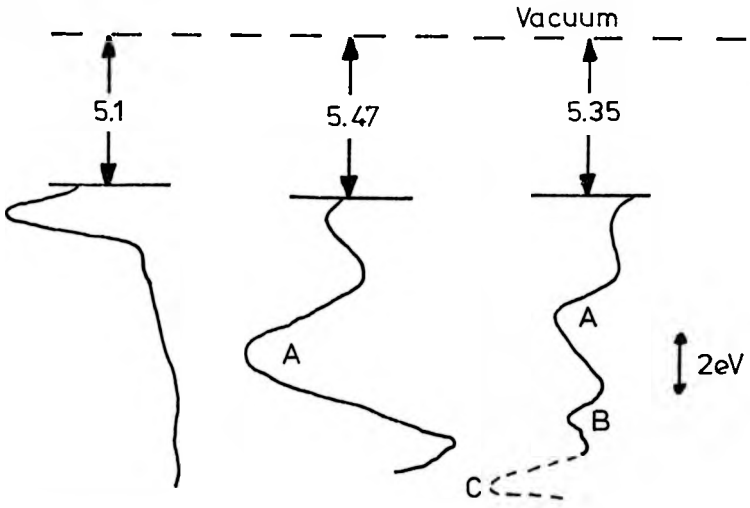

Clean Ni(100) c(2x2)O c(2x2)Se

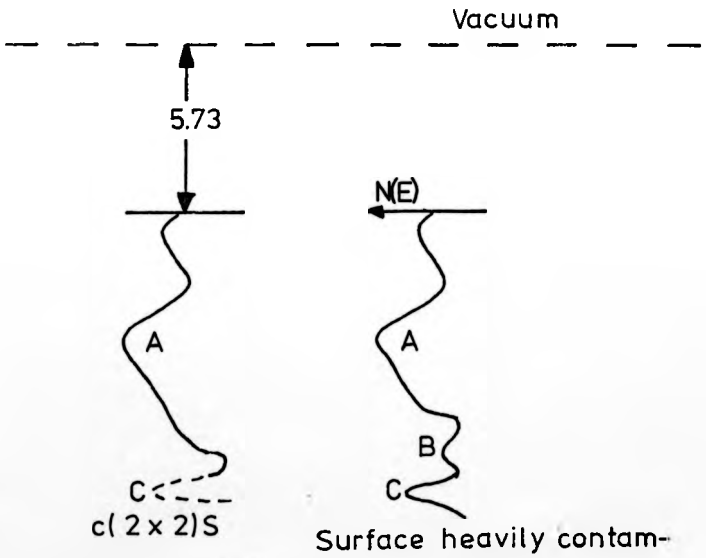

c(2x2)S

Surface heavily contaminated with sulphur.

electrons leaving the metal, via an Auger process, with an energy distribution peaked at about 4 eV. Furthermore, it was felt that the side structure at 1.9eV might well be merely an indication of the percentage of the incident beam in the He (2^1S) state. This would require the incident beam to consist of a large percentage in the He (2^3S) state. This is not unreasonable as it is known that the concentration of the He (2^3S) state in the afterglow of a He discharge remains at a higher level than the concentration of the He (2^1S) level[29].

Using the computer model, the yield from this mechanism is found to be of approximately the right order. If the core level involved were associated with the adatom the increase in the total yield would be linear with coverage. It is difficult to be more specific as, to the author's knowledge, hardly any examination has been made of the core levels of interest in connection with adsorption on surfaces.

Whilst this latter mechanism possibly reproduces the form of the electron energy distribution from a contaminated surface there are one or two points which should be noted. Firstly, it seems unlikely that the relevant core levels of oxygen and sulphur, which in the free atoms have binding energies of 29.15 eV and 20.8 eV respectively, will move to approximately equal binding energies when adsorbed on nickel. Secondly, it is known that core levels may play an important part in the neutralization of ions at surfaces[30], where it is possible, if the level is suitably placed, to have a resonant or quasi-resonant

exchange of an electron between the metallic level and the ground state level of the ion. However, it should be noted that this neutralization process has been observed only in cases where the metallic core level is a d-orbital and further the process is thought to be very short-range. In fact, at low velocities, the Auger neutralization process is the most dominant[31].

6.8 Conclusions

A careful examination of the experimental work detailed in this thesis has led to the conclusion that there is little evidence to support the theory that an excited atom incident on a metal surface will undergo resonance ionization follower by Auger neutralization. Furthermore, a study of the results obtained in experiments performed previously has shown that there is no conclusive evidence to support the theory in these experiments either.

A more formal treatment has been applied to the theory of the resonance process and this has shown that the process would probably occur closer to the surface than has previously been thought. However, without a better treatment of the Auger de-excitation process, which is beyond the scope of this thesis, it is difficult to produce a good reason why the resonance process should not occur.

An attempt has been made to explain the results of the present experiments by Auger de-excitation of the metastable atom with the excited electron being released preferentially in the direction of the metal surface.

The electrons which are then released as secondaries are detected by the spectrometer. It may then be possible that the increase in the total yield as the surface contaminates is related to the fact that more secondaries are produced from contaminated surfaces. However other mechanisms have been examined whereby the incident atom is de-excited by an electron from an orbital localised on the adatom. The most reasonable of these would seem to be a mechanism favouring de-excitation via an orbital, lying near the bottom of the valence band, which projects out from the surface. The subsequent "neutralization" of this hole may then be expected to produce more electrons leaving the metal surface.

A computer model has been used throughout this analysis to examine the different processes. Whilst lacking the rigour of more formal theoretical approaches, this model has been able to give an indication of the shape of the electron energy distribution to be expected and also a measure of the yield of electrons for each incident atom.

References:-

1. A. Cobas and W. E. Lamb, Jr., Phys. Rev. 65, 327 (1944)
2. H. D. Hagstrum, Phys. Rev. 96., 336 (1954).
3. R. K. Janev, J. Phys. B: Atom. Molec. Phys. 7, 1506 (1974).
4. H. D. Hagstrum, Phys. Rev. 104, 1516 (1956).
5. H. D. Hagstrum, J. Chem. Phys. 54, 1015 (1970).
6. J. A. Appelbaum and D. R. Hamann, Phys. Rev. B 12, 5590 (1975).
7. F. Herman and S. Skillman, "Atomic Structure Calculations" (Prentice-Hall, New York, 1963).
8. J. B. Hasted, J. Appl. Phys. 30, 22 (1959).
9. S. Sonkin, Phys. Rev. 43, 788 (1933).
10. W. Allison, F. B. Dunning and A.C.H. Smith, J. Phys. B: Atom. Molec. Phys. 5, 1175 (1972).
11. D. A. Maclennan and T. A. Delchar, J. Chem. Phys. 50, 1772 (1969).
12. T. A. Delchar, D. A. Maclennan and A. M. Landers, J. Chem. Phys. 50, 1779 (1969).
13. N. E. Christensen and B. Feuerbacher, Phys. Rev. B 10, 2349 (1974).
14. H. D. Hagstrum, Rev. Sci. Inst. 24, 1122 (1953).
15. C. Boiziau, V. Dose and J. Roussel, Surf. Sci. 61, 412 (1976).
16. R. N. Varney, Phys. Rev. 175, 98 (1968).
17. H. D. Hagstrum, Phys. Rev. 123, 758 (1961).
18. T. Shibata, T. Hirooka and K. Kuchitsu, Chem. Phys. Lett. 30, 241 (1975).
19. D. W. Bullett, Solid State Comm. 23, 893 (1977).
20. S. Andersson and C. Nyberg, Surf. Sci. 52, 489 (1975).
21. J. W. Gadzuk, Surf. Sci. 6, 133-170 (1967).
22. M. Remy, J. Chem. Phys. 53, 2487 (1969).
23. J. A. Appelbaum and D. R. Hamann, Phys. Rev. B 6, 1122 (1972).

24. M. P. Seah, Ph.D. Thesis, Bristol University (1969).

25. N. Wainfan, W. C. Walker and J. Weissler, J. Appl. Phys. 26, 1366 (1955).

26. E. W. Plummer, B. J. Waclawski, T.V. Vorburger and C. E. Kuyatt, Prog. Surf. Sci. 7, 149 (1976).

27. W. M. Huo, J. Chem. Phys. 43, 624 (1965).

28. H. D. Hagstrum and G. E. Becker, J. Vac. Sci. Tech. 14, 369 (1977).

29. A. V. Phelps, Phys. Rev. 99, 1307 (1955).

30. T. W. Rusch and R. L. Erickson, J. Vac. Sci. Tech. 13, 374 (1976).

31. F. Delannay, P. Bertrand, and J. M. Streydio, Phys. Rev. B 16, 3913 (1977).

APPENDIX I

AUGER ELECTRON SPECTROSCOPY

When a monoenergetic electron beam of energy E_p is directed at a solid, the energy distribution N(E) of the secondary electrons back-scattered from the surface is typically of the form shown in fig. Al.1. N(E) spectra have three distinct regions:

a) a broad maximum near zero energy, consisting of true secondary electrons thought to be produced by cascade processes within the solid.

b) An intermediate region characterised by a slowly varying background superimposed with features mainly due to plasmon excitations, interband transitions and Auger emitted electrons.

c) At E_p a single narrow peak is observed which consists of elastically scattered electrons.

The identification of particular Auger electron peaks is the principal means of establishing the chemical composition of the surface. These peaks consist of electrons which are ejected from the surface atoms as they de-excite following ionization of an inner core level by the incident electron beam. The de-excitation mechanism is best undestood by reference to fig. Al.2 where a particular Auger transition is shown.

The atom is initially ionised by the removal of an electron from the core level $M_{2,3}$. The hole in this shell is then filled by an electron falling from the valence band $M_{4,5}$, and the energy released in this transition is given to a second electron which is released

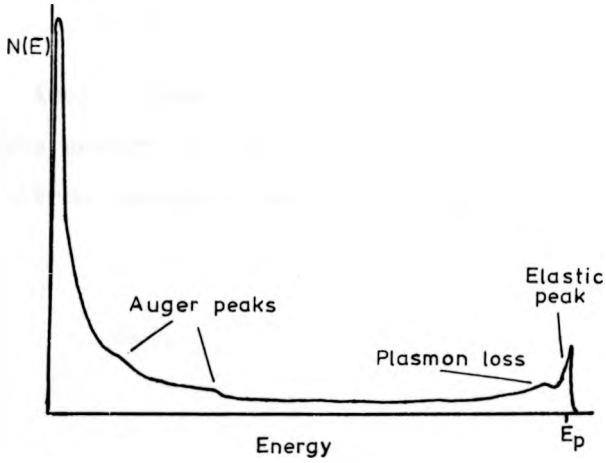

FIG. A1.1

The spectrum of secondary electrons emitted from a solid as a result of primary electron impact. E_p labels the primary energy of the incident electrons.

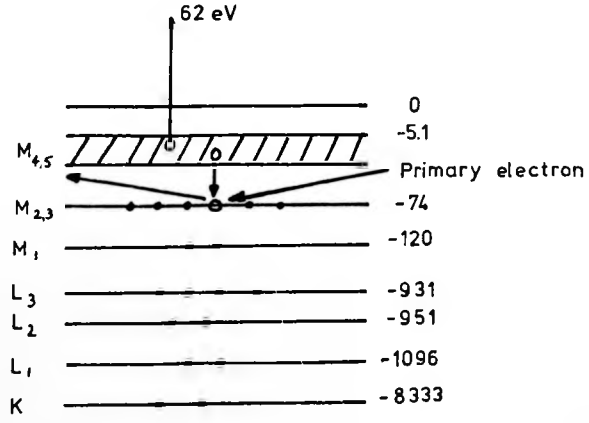

FIG. A1.2

The energy level diagram relating to a particular Auger transition for nickel. The energy levels are labelled using the X-ray notation.

into the vacuum from the valence band. The energy of this Auger electron is approximately

$$E \sim E_{M_{2,3}} - E_{M_{4,5}} - E_{M_{4,5}}$$

Atomic species are individually characterised by discrete energy levels and consequently specific Auger electron energies are associated with each element.

APPENDIX II

CHROMIUM PLATING OF TUNGSTEN

Before attempting to chromium plate, it was found to be essential to clean the tungsten by electro-polishing in a caustic soda bath. The chromium plating solution used consisted of:

Chromic Acid (C_rO_3)	250 grms/litre
Sulphuric Acid (H_2SO_4)	2.5 grms/litre
Distilled Water	1 litre

Specific Gravity 1.17

This solution was placed in a glass bowl which contained a lead anode of approximately the same radius as the tungsten grids. With this bath warmed to approximately 30°C each grid was plated for approximately 6 hrs at $\frac{1}{3}$ amp/sq. in.

APPENDIX III

OPTICAL PYROMETRY

When using an optical pyrometer, there are two main corrections to be made to the observed temperature. These are

1) an emissivity correction due to the fact that a non-black body is being observed and

2) a reflection correction to account for intensity losses as measurements are made through a glass window.

The spectral energy density of a black body is given by Planck's radiation formula

$$w_\lambda = \frac{C_1}{\lambda^5\{e^{C_2/\lambda T} - 1\}} \qquad (1)$$

where C_1 and C_2 are constants and λ refers to the wavelength of the emitted radiation. For a non-black body the spectral energy density w_λ' is given by

$$w_\lambda' = \epsilon_\lambda w_\lambda \qquad (2)$$

where ϵ_λ is the emissivity of the body at wavelength and temperature T.

When taking temperature measurements from this body, the optical pyrometer "sees" a temperature T' corresponding to the real temperature T, so that

$$\frac{\epsilon_\lambda C_1}{\lambda^5\{e^{C_2/\lambda T} - 1\}} = \frac{C_1}{\lambda^5\{e^{C_2/\lambda T'} - 1\}} \qquad (3)$$

This may be rewritten to give

$$\ln \epsilon_\lambda = \frac{C_2}{\lambda}\left(\frac{1}{T} - \frac{1}{T'}\right) \qquad (4)$$

$$\text{or} \quad \frac{1}{T} = \frac{1}{T'} + \frac{\lambda}{C_2} \ln \epsilon_\lambda \qquad (5)$$

At a glass interface so much of the radiant energy will be reflected and the reflection coefficient r is obtained simply from Fresnel's equations

$$r = \left(\frac{n - 1}{n + 1}\right)^2 \qquad (6)$$

where n is the refractive index of the glass window. For a glass window there are 2 interfaces and thus the optical pyrometer "sees" a temperature T'' which is in reality T' such that

$$\frac{C_1}{\lambda^5\left(e^{C_2/\lambda T''} - 1\right)} = \frac{C_1}{\lambda^5\left(e^{C_2/\lambda T'} - 1\right)}(1 - r)^2 \qquad (7)$$

This may be rewritten

$$\frac{C_2}{\lambda}\left(\frac{1}{T'} - \frac{1}{T''}\right) = 2\ln(1 - r) \qquad (8)$$

or

$$\frac{1}{T'} = \frac{1}{T''} + \frac{\lambda}{C_2}2\ln(1 - r) \qquad (9)$$

Combining equations (5) and (9) one obtains

$$\frac{1}{T} = \frac{1}{T''} + \frac{\lambda}{C_2}\left(\ln \epsilon_\lambda + 2\ln(1 - r)\right) \qquad (10)$$

Here T is the actual temperature and T'' is the measured temperature.